IMMISCIBLE POLYMER BLEND MEMBRANES FOR HIGH PRESSURE, HIGH TEMPERATURE H_2/CO_2 SEPARATION

by

Yu Huang

APPROVED BY SUPERVISORY COMMITTEE:

_____

Dr. Inga H. Musselman, Chair

_____

Dr. Kenneth J. Balkus, Jr.

_____

Dr. John P. Ferraris

_____

Dr. Ronald A. Smaldone

IMMISCIBLE POLYMER BLEND MEMBRANES FOR HIGH PRESSURE, HIGH TEMPERATURE H_2/CO_2 SEPARATION

by

YU HUANG, BS

DISSERTATION

Presented to the Faculty of

The University of Texas at Dallas

in Partial Fulfillment

of the Requirements

for the Degree of

DOCTOR OF PHILOSOPHY IN

CHEMISTRY

THE UNIVERSITY OF TEXAS AT DALLAS

December 2016

ACKNOWLEDGMENTS

I am most grateful to my supervisor, Dr. Inga Holl Musselman, for providing a great research opportunity and environment. Her guidance, encouragement, and patience have been invaluable during this accomplishment. I also extend my sincere appreciation to my committee, Dr. John P. Ferraris, Dr. Kenneth J. Balkus, Jr., and Dr. Ronald A. Smaldone for supportive suggestions and guidance. I would like to thank the UTD membrane group and the Musselman research group for all the support throughout my research career, which has facilitated me to fulfill my achievements. And lastly, my special thanks to my wife and my family for supporting me all these years. Without you I would not be able to accomplish what I have accomplished.

<October 2016>

IMMISCIBLE POLYMER BLEND MEMBRANES FOR HIGH PRESSURE, HIGH TEMPERATURE H_2/CO_2 SEPARATION

Publication No. _____

Yu Huang, PhD
The University of Texas at Dallas, 2016

Supervising Professor: Dr. Inga H. Musselman

High pressure and high temperature separation of H_2/CO_2 is of great interest for clean energy generation in processes such as coal gasification. Flat and tubular membranes of polybenzimidazole (PBI)/6FDA-DAM immiscible blends containing colloidal ZIF-8 were prepared. Membranes were tested for the separation of H_2, CO_2, and a H_2/CO_2 gas mixture at various pressures and temperatures. The amount of colloidal ZIF-8 in the blend has a remarkable effect on membrane morphology and gas separation. An increase in the colloidal ZIF-8 loading in the blend resulted in a decrease in the size of the dispersed 6FDA-DAM domains. A higher experimental temperature resulted in higher gas permeance through the membrane, while the gas selectivity remained constant. At 30 atm and 300 °C, a 5% colloidal ZIF-8 PBI/6FDA-DAM membrane exhibited a H_2 permeance of 29.52 GPU (approximately 472 Barrers), a H_2/CO_2 ideal selectivity of 17.4, and a H_2/CO_2 gas mixture selectivity of 12.8. In comparison to other membranes, this polymer blend membrane shows high gas permeance and high gas selectivity and surpasses the upper bound of the 2008 Robeson plot for H_2/CO_2.

TABLE OF CONTENTS

LIST OF FIGURES

LIST OF TABLES

Located in Appendix 2

Located in Appendix 3

Located in Appendix 4

CHAPTER 1

OVERVIEW

Clean energy has gained attention over the last few decades due to the impact of fossil fuels on the environment including global warming. Hydrogen (H_2) is considered a clean source of energy [1], and it has the potential to replace gasoline, diesel fuel, and natural gas in transportation and electricity production [2]. H_2 can be generated from a variety of sources, including fossil fuels, biomass, or even water [3–5]. Coal can be gasified to produce H_2 [6–8]. During the gasification of coal (Figure 1.1), pulverized coal particles react with steam and oxygen under high temperature (900-1800 °C) to produce synthesis gas (syngas), a mixture consisting of H_2, CO, and CO_2 (H_2 = 29%, CO = 39%, and CO_2 = 13%) [9–11]. The CO is then reacted with water in the presence of a catalyst to produce more H_2 and CO_2 in what is known as the water-gas shift (WGS) reaction (Eq. 1.1). The WGS reaction is reversible and exothermic ($\Delta H° = -41.2\ kJ/mol$). Due to its

$$H_2O + CO \overset{\text{Catalyst}}{\rightleftharpoons} H_2 + CO_2 \qquad \Delta H° = -41.2\ kJ/mol \qquad \text{(Eq. 1.1)}$$

exothermicity, the WGS reaction is not thermodynamically favorable at high temperatures, however, elevated temperatures favor the kinetics of this catalytic reaction. The final gas mixture contains approximately 41-55% of H_2 and 31-38% of CO_2 [12]. The separation and sequestration of CO_2 from the H_2/CO_2 gas mixture is necessary in order to provide pure H_2 and to prevent the emission of greenhouse gases into the atmosphere (i.e., CO_2) [13,14]. Furthermore, simultaneous removal of CO_2 during the WGS reaction leads to a shift of the reaction equilibrium towards the products, increasing H_2 production. The gasification of coal is typically performed at 900-1800

°C to reduce char formation [6]. The resulting high pressure (>30 atm) syngas is passed through a reactor where the WGS reaction is performed at 200-400 °C to activate the catalyst [15]. Typically, a gas mixture of H_2 and CO_2 exits the WGS reactor at pressures between 30 and 50 atm and at temperatures higher than 250 °C, depending on the catalyst used [12]. The high pressure and high temperature conditions of the WGS reaction increase the challenges for the methods and materials required to perform this separation.

A variety of processes can be employed to separate H_2 from CO_2 after the WGS process. The most common method is pressure swing adsorption (PSA) in which a gas mixture is separated based on differences in the affinities of various gas species for an adsorbent material at a given pressure [16]. PSA is capable of providing high purity H_2 gas (99.9%) [17]. However, the pressure needs to be increased and decreased alternately during the separation process in order to adsorb and desorb the target gas, making PSA an energy intensive process. Another method used to separate H_2 from CO_2 is temperature swing adsorption (TSA). TSA separates gas mixtures based on the affinity between a gas species and an adsorbent material at various temperatures [18]. Similar to PSA, TSA is based on phase equilibrium and, thus, is also an energy intensive process due to the repeating heating and cooling cycles. In fact, most separation techniques that are based on phase equilibrium, such as cryogenic distillation [19], electric swing adsorption [20], and vacuum swing operations [21], could achieve gas separation effectively and produce gases with high purity. Unfortunately, these processes require repeated changes in phase by means of adjusting either pressure or temperature that lead to complex, high cost, and high energy consumption processes [19].

In contrast to conventional techniques, membrane technology only requires a differential pressure across a membrane to perform the separation without subjecting the mixture to phase changes. Membranes perform gas separation by selectively allowing one gas species to pass through the membrane while retaining another on the high pressure side [22]. Membrane-based gas separation consumes significantly less energy compared to phase equilibrium techniques [23], has low gas production cost, and a small footprint, making it a promising candidate for gas separations [24,25]. Several types of membranes have been used for industrial gas separations including nitrogen separation from air, CO_2 removal from natural gas, and H_2 recovery from purge streams in ammonia production [22–25].

Based on the materials used for their preparation, membranes can be categorized as inorganic or polymeric. Inorganic membranes are made from ceramics [26–31], zeolites [32–39], carbons [40–44], metals [45–47], and hybrid metal-organic frameworks (MOFs) [48–56]. Inorganic membranes exhibit high gas flux and high gas selectivity, however, the complexity of their preparation, poor flexibility, and low mechanical strength limit their use to the laboratory scale. In contrast, the fabrication of polymeric membranes is relatively easy and inexpensive since many polymers exhibit good flexibility and high mechanical strength. Most polymeric materials, however, have glass transition temperatures below 300 °C, which restricts them from high temperature applications. The types of polymers used in gas separations include polyimides [57–59], polysulfones [60,61], polyurethanes [62,63], and polybenzimidazoles [64–66]. Polymeric membranes exhibit a trade-off between permeability and selectivity that has resulted in upper bounds for gas separations [67–69].

Unlike pure polymer membranes, polymer blend membranes are prepared by mixing miscible or immiscible polymers to strategically combine the desired characteristics or properties of the individual components. For example, a thermally stable polymer could be blended with a mechanically strong polymer to simultaneously increase the thermal stability and mechanical strength. Blending a highly selective polymer with a highly permeable polymer to increase both selectivity and permeability beyond that of the individual polymers is also a good strategy. Although polymer blend membranes possess attractive characteristics and properties, their gas separation performances are strongly affected by their morphologies that are governed by the miscibility and compatibility of the blended polymers [70]. For a polymer blend membrane at a fixed polymer composition, different morphologies, such as layer-by-layer, matrix-droplet, and co-continuous, result in different gas transport properties. Therefore, different models, including series, parallel, Maxwell, and the equivalent box, were developed to predict gas transport properties for each case [71].

Another type of membrane known as a mixed-matrix membrane (MMM) is prepared by dispersing additives in a polymeric matrix. MMMs with improved gas separation properties over pure polymers have been reported in the open literature. These MMMs are generally made of one polymer combined with silica [72–74], zeolite [75–77], carbon nanotube [78,79], MOF [80–83], or zeolitic imidazolate framework (ZIF) [84–86] additives. This combination allows for MMMs to display enhanced gas permeabilities and selectivities, good flexibility and mechanical strength, easy processability, and low cost, properties that make them attractive materials for industrial gas separations. While MMMs show great potential in gas separations, their actual performance relies on the matching of the intrinsic permeability and selectivity of the additive and polymer matrix

[87,88] as well as their interaction and compatibility, similar to the performance limitation of the polymer blend.

The research presented herein focuses on H_2/CO_2 separations using MMMs under industrially relevant conditions of pressure and temperature. As described earlier, efficient H_2/CO_2 separations could have a significant impact on clean energy production and greenhouse gas sequestration by reducing energy consumption and costs associated with the process. Separating H_2 from CO_2 is challenging due to the similarities in kinetic diameters (H_2 = 2.89 Å, CO_2 = 3.30 Å). Furthermore, the H_2/CO_2 gas mixture produced in industrial processes is at high pressure and high temperature (30 atm and 300 °C) [12], raising the technological demands in terms of the thermal, chemical, and mechanical stability of the membranes. Many membranes have been fabricated, characterized, and tested at low pressure and low temperature at laboratory scale, showing promising results for H_2/CO_2 separations [66,85,89–95]. Several membranes have been tested at high temperature (>230 °C) but low pressure (2-8 atm) [66,84,89,96–98]. In most cases, however, the true separation performances of the membranes were not measured under industrially relevant conditions.

In order to thoroughly evaluate the performance of a membrane under real world conditions, a high pressure, high temperature (HPHT) permeameter was constructed to simulate the industrial conditions of the WGS reaction and to determine H_2 and CO_2 permeance through flat and tubular membranes at pressures up to 30 atm and temperatures up to 300 °C. The construction, calibration, and testing of the permeameter is described in Chapter 2. A polybenzimidazole (PBI) membrane coated on a microporous zirconia layer deposited on a porous SS-316 tubular support, as well as flat membranes of PBI, were tested to calibrate and evaluate the performance of the

permeameter. In Chapter 3, methods for coating polymeric membranes (e.g., PBI and Matrimid®) on a microporous zirconia layer deposited on a porous SS-316 tubular support were developed. Different coating techniques, such as spray-coating and dip-coating, were used to develop an effective method for the fabrication of polymeric tubular membranes. The fabricated tubular membranes were also tested in the HPHT permeameter for H_2/CO_2 separations at high pressure and high temperature. In Chapter 4, flat and tubular MMMs, containing different weight percentages of colloidal ZIF-8 in 50/50 PBI/6FDA-DAM polymer blends, were fabricated and tested for H_2/CO_2 separations with pure H_2 and CO_2 and a 50/50 H_2/CO_2 mixture at 30 atm and 300 °C. Their thermal stability and morphology were studied, and models for the calculation of gas permeation in polymer blends were evaluated based on membrane morphology. The results showed that the MMMs were thermally and mechanical stable at the testing conditions and that they exhibited improvements in gas selectivity as compared to most polymeric membranes using the Robeson's plot [69].

APPENDIX 1 FIGURE

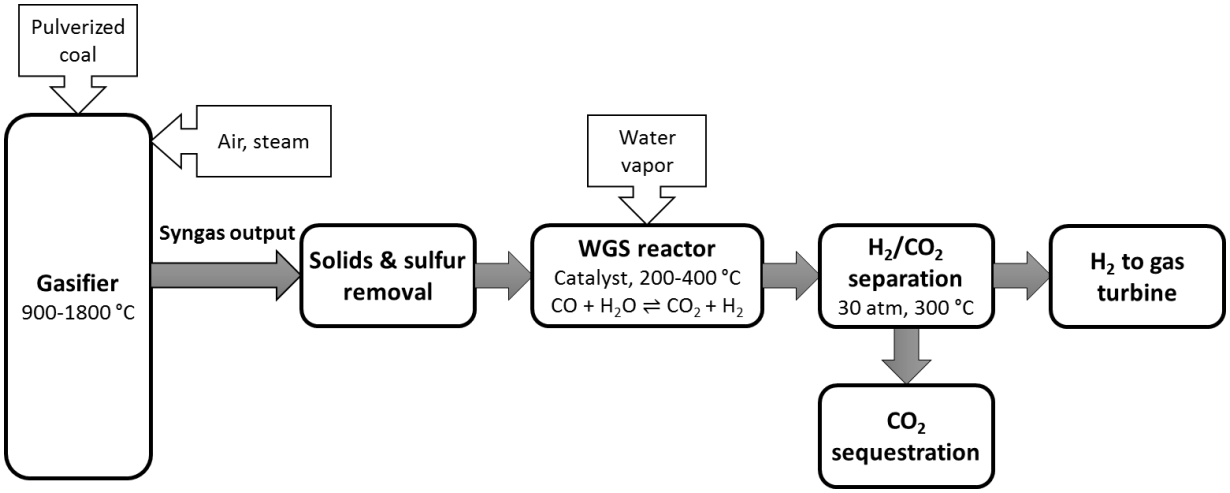

Fig 1.1. Industrial coal gasification process and generation of H_2 and CO_2 through the WGS reaction followed by H_2/CO_2 separation.

REFERENCES

[1] S.E. Hosseini, M.A. Wahid, Hydrogen production from renewable and sustainable energy resources: Promising green energy carrier for clean development, *Renew. Sustain. Energy Rev.* **2016**, *57*, 850–866.

[2] A. Zuttel, A. Remhof, A. Borgschulte, O. Friedrichs, Hydrogen: The future energy carrier, *Philos. Trans. R. Soc. A Math. Phys. Eng. Sci.* **2010**, *368*, 3329–3342.

[3] C.W. Forsberg, Future hydrogen markets for large-scale hydrogen production systems, *Int. J. Hydrogen Energy* **2007**, *32*, 431–439.

[4] J.D. Holladay, J. Hu, D.L. King, Y. Wang, An overview of hydrogen production technologies, *Catal. Today* **2009**, *139*, 244–260.

[5] I.K. Kapdan, F. Kargi, Bio-hydrogen production from waste materials, *Enzyme Microb. Technol.* **2006**, *38*, 569–582.

[6] A.J. Minchener, Coal gasification for advanced power generation, *Fuel* **2005**, *84*, 2222–2235.

[7] E. Shoko, B. McLellan, A.L. Dicks, J.C.D. da Costa, Hydrogen from coal: Production and utilization technologies, *Int. J. Coal Geol.* **2006**, *65*, 213–222.

[8] G.J. Stiegel, M. Ramezan, Hydrogen from coal gasification: An economical pathway to a sustainable energy future, *Int. J. Coal Geol.* **2006**, *65*, 173–190.

[9] R. Xiao, M. Zhang, B. Jin, Y. Huang, H. Zhou, High-temperature air/steam-blown gasification of coal in a pressurized spout-fluid bed, *Energy and Fuels* **2006**, *20*, 715–720.

[10] P. Mondal, G.S. Dang, M.O. Garg, Syngas production through gasification and cleanup for downstream applications - Recent developments, *Fuel Process. Technol.* **2011**, *92*, 1395–1410.

[11] D. Parsley, R.J. Ciora, D.L. Flowers, J. Laukaitaus, A. Chen, P.K.T. Liu, J. Yu, M. Sahimi, A. Bonsu, T.T. Tsotsis, Field evaluation of carbon molecular sieve membranes for the separation and purification of hydrogen from coal- and biomass-derived syngas, *J. Membr. Sci.* **2014**, *450*, 81–92.

[12] D. Driscoll, B. Morreale, L. Headley, NETL test protocol testing of hydrogen separation membranes, *DOE/NETL – 2008/1335*. **2008**, 14.

[13] D.W. Keith, Why capture CO2 from the atmosphere?, *Science* **2009**, *325*, 1654–1655.

[14] S.W. Lee, J.S. Park, C.B. Lee, D.W. Lee, H. Kim, H.W. Ra, S.H. Kim, S.K. Ryi, H_2 recovery and CO_2 capture after water-gas shift reactor using synthesis gas from coal gasification, *Energy*. **2014**, *66*, 635–642.

[15] N. Schumacher, A. Boisen, S. Dahl, A.A. Gokhale, S. Kandoi, L.C. Grabow, J.A. Dumesic, M. Mavrikakis, I. Chorkendorff, Trends in low-temperature water-gas shift reactivity on

transition metals, *J. Catal.* **2005**, *229*, 265–275.

[16] C.A. Grande, Advances in pressure swing adsorption for gas separation, *ISRN Chem. Eng.* **2012**, *2012*, 1–13.

[17] S. Sircar, T.C. Golden, Purification of hydrogen by pressure swing adsorption, *Sep. Sci. Technol.* **2000**, *35*, 667–687.

[18] R. Kumar, T.C. Golden, Thermal swing adsorption process for removing trace impurities from a multi-component gas mixture: (Landfill gas), *Gas Sep. Purif.* **1991**, *5*, 21–24.

[19] W.J. Koros, R. Mahajan, Pushing the limits on possibilities for large scale gas separation: Which strategies?, *J. Membr. Sci.* **2001**, *181*, 141.

[20] C.A. Grande, A.E. Rodrigues, Electric Swing Adsorption for CO_2 removal from flue gases, *Int. J. Greenh. Gas Control* **2008**, *2*, 194–202.

[21] R. Kumar, Vacuum swing adsorption process for oxygen production–-A historical perspective, *Sep. Sci. Technol.* **1996**, *7*, 877.

[22] W.J. Koros, G.K. Fleming, Membrane-based gas separation, *J. Membr. Sci.* **1993**, *83*, 1–80.

[23] R.W. Baker, Future directions of membrane gas separation technology, *Ind. Eng. Chem. Res.* **2002**, *41*, 1393–1411.

[24] K. Ghosal, B.D. Freeman, Gas separation using polymer membranes: An overview, *Polym. Adv. Technol.* **1994**, *5*, 673–697.

[25] P. Bernardo, E. Drioli, G. Golemme, Membrane gas separation: A review/state of the art, *Ind. Eng. Chem. Res.* **2009**, *48*, 4638–4663.

[26] S.S. Hashim, A.R. Mohamed, S. Bhatia, Oxygen separation from air using ceramic-based membrane technology for sustainable fuel production and power generation, *Renew. Sustain. Energy Rev.* **2011**, *15*, 1284–1293.

[27] Y. Wei, W. Yang, J. Caro, H. Wang, Dense ceramic oxygen permeable membranes and catalytic membrane reactors, *Chem. Eng. J.* **2013**, *220*, 185–203.

[28] S. Koonaphapdeelert, K. Li, Preparation and characterization of hydrophobic ceramic hollow fibre membrane, *J. Membr. Sci.* **2007**, *291*, 70–76.

[29] H.H. Han, S.H. Ryu, S. Nakao, Y.T. Lee, Gas permeation properties and preparation of porous ceramic membrane by CVD method using siloxane compounds, *J. Membr. Sci.* **2013**, *431*, 72–78.

[30] N.C. Nwogu, M. Kajama, E. Gobina, A study of gas diffusion characteristics on a micro porous composite silica ceramic membrane, *Compos. Struct.* **2015**, *134*, 1044–1050.

[31] K.M. McGrath, Ceramic membrane technologies for oxygen separation, *Adv. Mater.* **2001**, *13*, 993–996.

[32] J. Caro, M. Noack, Zeolite membranes - Recent developments and progress, *Microporous Mesoporous Mater.* **2008**, *115*, 215–233.

[33] T. Tomita, K. Nakayama, H. Sakai, Gas separation characteristics of DDR type zeolite membrane, *Microporous Mesoporous Mater.* **2004**, *68*, 71–75.

[34] Q. Liu, T. Wang, C. Liang, B. Zhang, S. Liu, Y. Cao, J. Qiu, Zeolite married to carbon: A new family of membrane materials with excellent gas separation performance, *Chem. Mater.* **2006**, *18*, 6283–6288.

[35] Y. Zhang, Z. Wu, Z. Hong, X. Gu, N. Xu, Hydrogen-selective zeolite membrane reactor for low temperature water gas shift reaction, *Chem. Eng. J.* **2012**, *197*, 314–321.

[36] G.R. Gavalas, Zeolite Membranes for Gas and Liquid Separations, in: Mater. Sci. Membr. Gas Vap. Sep., **2006**: pp. 307–336.

[37] T. Muñoz, K.J. Balkus, Jr., Preparation of oriented zeolite UTD-1 membranes via pulsed laser ablation, *J. Am. Chem. Soc.* **1999**, *121*, 139–146.

[38] D. Coutinho, K.J. Balkus, Jr., Preparation and characterization of zeolite X membranes via pulsed-laser deposition, *Microporous Mesoporous Mater.* **2002**, *52*, 79–91.

[39] K.J. Balkus, Jr., G. Gbery, Z. Deng, Preparation of partially oriented zeolite MCM-22 membranes via pulsed laser deposition, *Microporous Mesoporous Mater.* **2002**, *52*, 141–150.

[40] C. Liang, G. Sha, S. Guo, Carbon membrane for gas separation derived from coal tar pitch, *Carbon N. Y.* **1999**, *37*, 1391–1397.

[41] A.B. Fuertes, Adsorption-selective carbon membrane for gas separation, *J. Membr. Sci.* **2000**, *177*, 9–16.

[42] W.N.W. Salleh, A.F. Ismail, T. Matsuura, M.S. Abdullah, Precursor selection and process conditions in the preparation of carbon membrane for gas separation: A Review, *Sep. Purif. Rev.* **2011**, *40*, 261–311.

[43] S.M. Saufi, A.F. Ismail, Fabrication of carbon membranes for gas separation - A review, *Carbon N. Y.* **2004**, *42*, 241–259.

[44] W.N.W. Salleh, A.F. Ismail, Carbon membranes for gas separation processes: Recent progress and future perspective, *J. Membr. Sci. Res.* **2015**, *1*, 2–15.

[45] S.K. Ryi, J.S. Park, S.H. Kim, S.H. Cho, D.W. Kim, K.Y. Um, Characterization of Pd-Cu-Ni ternary alloy membrane prepared by magnetron sputtering and Cu-reflow on porous nickel support for hydrogen separation, *Sep. Purif. Technol.* **2006**, *50*, 82–91.

[46] Y. Bi, H. Xu, W. Li, A. Goldbach, Water–gas shift reaction in a Pd membrane reactor over $Pt/Ce_{0.6}Zr_{0.4}O_2$ catalyst, *Int. J. Hydrogen Energy* **2009**, *34*, 2965–2971.

[47] A.E. Lewis, D.C. Kershner, S.N. Paglieri, M.J. Slepicka, J.D. Way, Pd-Pt/YSZ composite

membranes for hydrogen separation from synthetic water-gas shift streams, *J. Membr. Sci.* **2013**, *437*, 257–264.

[48] Y. Yoo, Z. Lai, H.K. Jeong, Fabrication of MOF-5 membranes using microwave-induced rapid seeding and solvothermal secondary growth, *Microporous Mesoporous Mater.* **2009**, *123*, 100–106.

[49] Y. Li, F. Liang, H. Bux, W. Yang, J. Caro, Zeolitic imidazolate framework ZIF-7 based molecular sieve membrane for hydrogen separation, *J. Membr. Sci.* **2010**, *354*, 48–54.

[50] K. Tao, C. Kong, L. Chen, High performance ZIF-8 molecular sieve membrane on hollow ceramic fiber via crystallizing-rubbing seed deposition, *Chem. Eng. J.* **2013**, *220*, 1–5.

[51] D.J. Lee, Q. Li, H. Kim, K. Lee, Preparation of Ni-MOF-74 membrane for CO_2 separation by layer-by-layer seeding technique, *Microporous Mesoporous Mater.* **2012**, *163*, 169–177.

[52] A. Huang, W. Dou, J. Caro, Steam-stable zeolitic imidazolate framework ZIF-90 membrane with hydrogen selectivity through covalent functionalization, *J. Am. Chem. Soc.* **2010**, *132*, 15562–15564.

[53] A. Huang, H. Bux, F. Steinbach, J. Caro, Molecular-sieve membrane with hydrogen permselectivity: ZIF-22 in LTA topology prepared with 3-aminopropyltriethoxysilane as covalent linker, *Angew. Chemie - Int. Ed.* **2010**, *49*, 4958–4961.

[54] N. Wang, Y. Liu, Z. Qiao, L. Diestel, J. Zhou, A. Huang, J. Caro, Polydopamine-based synthesis of a zeolite imidazolate framework ZIF-100 membrane with high H_2/CO_2 selectivity, *J. Mater. Chem. A.* **2015**,.

[55] A. Huang, Y. Chen, N. Wang, Z. Hu, J. Jiang, J. Caro, A highly permeable and selective zeolitic imidazolate framework ZIF-95 membrane for H_2/CO_2 separation, *Chem. Commun.* **2012**, *48*, 10981.

[56] Y. Zhang, I.H. Musselman, J.P. Ferraris, K.J. Balkus, Jr., Gas permeability properties of Matrimid membranes containing the metal-organic framework Cu-BPY-HFS, *J. Membr. Sci.* **2008**, *313*, 170–181.

[57] L.S. White, T.A. Blinka, H.A. Kloczewski, I. Wang, Properties of a polyimide gas separation membrane in natural gas streams, *J. Membr. Sci.* **1995**, *103*, 73–82.

[58] Y. Kase, Gas separation by polyimide membranes, in: Adv. Membr. Technol. Appl., **2008**: pp. 581–598.

[59] H. Kawakami, K. Nakajima, H. Shimizu, S. Nagaoka, Gas permeation stability of asymmetric polyimide membrane with thin skin layer: Effect of polyimide structure, *J. Membr. Sci.* **2003**, *212*, 195–203.

[60] C. Camacho-Zuñiga, F.A. Ruiz-Treviño, S. Hernández-López, M.G. Zolotukhin, F.H.J. Maurer, A. González-Montiel, Aromatic polysulfone copolymers for gas separation membrane applications, *J. Membr. Sci.* **2009**, *340*, 221–226.

[61] M.A. Aroon, A.F. Ismail, M.M. Montazer-Rahmati, T. Matsuura, Morphology and permeation properties of polysulfone membranes for gas separation: Effects of non-solvent additives and co-solvent, *Sep. Purif. Technol.* **2010**, *72*, 194–202.

[62] M. Sadeghi, M.A. Semsarzadeh, M. Barikani, B. Ghalei, Study on the morphology and gas permeation property of polyurethane membranes, *J. Membr. Sci.* **2011**, *385–386*, 76–85.

[63] K.H. Hsieh, C.C. Tsai, S.M. Tseng, Vapor and gas permeability of polyurethane membranes. Part I. Structure-property relationship, *J. Membr. Sci.* **1990**, *49*, 341–350.

[64] J.S. Young, G.S. Long, B.F. Espinoza, Cross-linked polybenzimidazole membrane for gas separation, *US Pat. 6,946,015*. **2006**, *A1*, 12. http://www.google.com/patents/US6946015.

[65] S.H. Han, J.E. Lee, K.J. Lee, H.B. Park, Y.M. Lee, Highly gas permeable and microporous polybenzimidazole membrane by thermal rearrangement, *J. Membr. Sci.* **2010**, *357*, 143–151.

[66] K.A. Berchtold, R.P. Singh, J.S. Young, K.W. Dudeck, Polybenzimidazole composite membranes for high temperature synthesis gas separations, *J. Membr. Sci.* **2012**, *415–416*, 265–270.

[67] L.M. Robeson, Correlation of separation factor versus permeability for polymeric membranes, *J. Membr. Sci.* **1991**, *62*, 165–185.

[68] L.M. Robeson, Polymer membranes for gas separation, *Curr. Opin. Solid State Mater. Sci.* **1999**, *4*, 549–552.

[69] L.M. Robeson, The upper bound revisited, *J. Membr. Sci.* **2008**, *320*, 390–400.

[70] L.M. Robeson, *Polymer blends: A comprehensive review*, Hanser Gardner Publications: Cincinnati, OH, **2007**.

[71] L.M. Robeson, Polymer blends in membrane transport processes, *Ind. Eng. Chem. Res.* **2010**, *49*, 11859–11865.

[72] J. Ahn, W.J. Chung, I. Pinnau, M.D. Guiver, Polysulfone/silica nanoparticle mixed-matrix membranes for gas separation, *J. Membr. Sci.* **2008**, *314*, 123–133.

[73] B. Zornoza, C. Téllez, J. Coronas, Mixed matrix membranes comprising glassy polymers and dispersed mesoporous silica spheres for gas separation, *J. Membr. Sci.* **2011**, *368*, 100–109.

[74] J. Ahn, W.J. Chung, I. Pinnau, J. Song, N. Du, G.P. Robertson, M.D. Guiver, Gas transport behavior of mixed-matrix membranes composed of silica nanoparticles in a polymer of intrinsic microporosity (PIM-1), *J. Membr. Sci.* **2010**, *346*, 280–287.

[75] A.L. Khan, A. Cano-Odena, B. Guti??rrez, C. Minguill??n, I.F.J. Vankelecom, Hydrogen separation and purification using polysulfone acrylate-zeolite mixed matrix membranes, *J. Membr. Sci.* **2010**, *350*, 340–346.

[76] M.G. Suer, N. Bac, L. Yilmaz, Gas permeation characteristics of polymer-zeolite mixed matrix membranes, *J. Membr. Sci.* **1994**, *91*, 77–86.

[77] T.W. Pechar, M. Tsapatsis, E. Marand, R. Davis, Preparation and characterization of a glassy fluorinated polyimide zeolite-mixed matrix membrane, *Desalination* **2002**, *146*, 3–9.

[78] M. Nour, K. Berean, S. Balendhran, J.Z. Ou, J. Du Plessis, C. McSweeney, M. Bhaskaran, S. Sriram, K. Kalantar-zadeh, CNT/PDMS composite membranes for H_2 and CH_4 gas separation, *Int. J. Hydrogen Energy* **2013**, *38*, 10494–10501.

[79] A. Sharma, S. Kumar, B. Tripathi, M. Singh, Y.K. Vijay, Aligned CNT/Polymer nanocomposite membranes for hydrogen separation, *Int. J. Hydrogen Energy* **2009**, *34*, 3977–3982.

[80] E. V. Perez, K.J. Balkus, Jr., J.P. Ferraris, I.H. Musselman, Mixed-matrix membranes containing MOF-5 for gas separations, *J. Membr. Sci.* **2009**, *328*, 165–173.

[81] S. Basu, A. Cano-Odena, I.F.J. Vankelecom, MOF-containing mixed-matrix membranes for CO_2/CH_4 and CO_2/N_2 binary gas mixture separations, *Sep. Purif. Technol.* **2011**, *81*, 31–40.

[82] T.H. Bae, J.S. Lee, W. Qiu, W.J. Koros, C.W. Jones, S. Nair, A high-performance gas-separation membrane containing submicrometer-sized metal-organic framework crystals, *Angew. Chemie - Int. Ed.* **2010**, *49*, 9863–9866.

[83] J. Hu, H. Cai, H. Ren, Y. Wei, Z. Xu, H. Liu, Y. Hu, Mixed-matrix membrane hollow fibers of $Cu_3(BTC)_2$ MOF and polyimide for gas separation and adsorption, *Ind. Eng. Chem. Res.* **2010**, *49*, 12605–12612.

[84] T. Yang, G.M. Shi, T.S.C. Chung, Symmetric and asymmetric zeolitic imidazolate frameworks (ZIFs)/Polybenzimidazole (PBI) nanocomposite membranes for hydrogen purifi cation at high temperatures, *Adv. Energy Mater.* **2012**, *2*, 1358–1367.

[85] M.J.C. Ordoñez, K.J. Balkus, Jr., J.P. Ferraris, I.H. Musselman, Molecular sieving realized with ZIF-8/Matrimid mixed-matrix membranes, *J. Membr. Sci.* **2010**, *361*, 28–37.

[86] C. Zhang, Y. Dai, J.R. Johnson, O. Karvan, W.J. Koros, High performance ZIF-8/6FDA-DAM mixed matrix membrane for propylene/propane separations, *J. Membr. Sci.* **2012**, *389*, 34–42.

[87] C.M. Zimmerman, A. Singh, W.J. Koros, Tailoring mixed matrix composite membranes for gas separations, *J. Membr. Sci.* **1997**, *137*, 145–154.

[88] R. Mahajan, W.J. Koros, Factors controlling successful formation of mixed-matrix gas separation materials, *Ind. Eng. Chem. Res.* **2000**, *39*, 2692–2696.

[89] T. Yang, T.-S. Chung, High performance ZIF-8/PBI nano-composite membranes for high temperature hydrogen separation consisting of carbon monoxide and water vapor, *Int. J.*

Hydrogen Energy **2013**, *38*, 229–239.

[90] L. Shao, C.H. Lau, T.S. Chung, A novel strategy for surface modification of polyimide membranes by vapor-phase ethylenediamine (EDA) for hydrogen purification, *Int. J. Hydrogen Energy* **2009**, *34*, 8716–8722.

[91] S.S. Hosseini, M.M. Teoh, T.S. Chung, Hydrogen separation and purification in membranes of miscible polymer blends with interpenetration networks, *Polymer* **2008**, *49*, 1594–1603.

[92] L. Shao, B.T. Low, T.S. Chung, A.R. Greenberg, Polymeric membranes for the hydrogen economy: Contemporary approaches and prospects for the future, *J. Membr. Sci.* **2009**, *327*, 18–31.

[93] O.C. David, D. Gorri, A. Urtiaga, I. Ortiz, Mixed gas separation study for the hydrogen recovery from $H_2/CO/N_2/CO_2$ post combustion mixtures using a Matrimid membrane, *J. Membr. Sci.* **2011**, *378*, 359–368.

[94] T.-H. Weng, H.-H. Tseng, M.-Y. Wey, Preparation and characterization of PPSU/PBNPI blend membrane for hydrogen separation, *Int. J. Hydrogen Energy* **2008**, *33*, 4178–4182.

[95] L. Kong, X. Zhang, Y. Liu, S. Li, H. Liu, J. Qiu, K.L. Yeung, In situ fabrication of high-permeance ZIF-8 tubular membranes in a continuous flow system, *Mater. Chem. Phys.* **2014**, *148*, 10–16.

[96] S.C. Kumbharkar, Y. Liu, K. Li, High performance polybenzimidazole based asymmetric hollow fibre membranes for H_2/CO_2 separation, *J. Membr. Sci.* **2011**, *375*, 231–240.

[97] D.R. Pesiri, B. Jorgensen, R.C. Dye, Thermal optimization of polybenzimidazole meniscus membranes for the separation of hydrogen, methane, and carbon dioxide, *J. Membr. Sci.* **2003**, *218*, 11–18.

[98] X. Li, R.P. Singh, K.W. Dudeck, K.A. Berchtold, B.C. Benicewicz, Influence of polybenzimidazole main chain structure on H_2/CO_2 separation at elevated temperatures, *J. Membr. Sci.* **2014**, *461*, 59–68.

CHAPTER 2

GAS PERMEAMETER FOR MEASUREMENT OF FLAT AND TUBULAR MEMBRANES AT HIGH PRESSURE AND HIGH TEMPERATURE

ABSTRACT

A permeameter was constructed to test gas permeation at high pressure and high temperature. Membrane cells were custom-made to house both flat and tubular membranes. Fittings and parts for the permeameter were selected to match the high pressure and high temperature requirements. A virtual instrument (VI) computer program was developed in LabVIEW to control the instrument and acquire data. To test the instrument, flat and tubular polybenzimidazole membranes were tested at 30 atm and 300 °C with pure H_2 and CO_2 gases and a 50:50 H_2/CO_2 gas mixture. The permeation results show that PBI membranes are suitable for H_2/CO_2 separations under water-gas shift reaction conditions (e.g., 30 atm and 300 °C). The flat membrane exhibits H_2/CO_2 ideal selectivities of 24 (10 atm) and 26 (30 atm) at 300 °C, whereas the tubular membrane showed H_2/CO_2 ideal selectivities of 22 (10 atm) and 23 (30 atm) and a mixed gas selectivity of 17.8 (30 atm), all at 300 °C. The H_2 and CO_2 permeabilities of tubular membranes are slightly less than those for flat membranes, which may result from the thickness of the tubular membrane being thicker than its estimated value. The permeation results also indicate that the permeameter is suitable for measuring gas transport properties of a membrane at high pressure, high temperature, especially for those highly permeable membranes. Additionally, the design of the permeameter permits it to conduct fast measurements with various pressures at constant temperature using different geometries of the membranes.

2.1. INTRODUCTION

The demand for clean energy has increased in recent years due to environmental pollution and global warming, making H_2 a good source of energy compared to traditional fossil fuels [1]. Because H_2 is considered a clean energy source, its industrial generation through the gasification of coal and the water-gas shift (WGS) reaction has become more important in recent years [2–4]. One of the major by-products of H_2 production from the WGS reaction is the greenhouse gas CO_2, which plays a major role in global warming. Consequently, for environmental protection, separating H_2 from CO_2 is a critical and necessary step during the H_2 production process. In industry, pressure swing adsorption [5] and cryogenic distillation [6] have been applied to separate H_2 from CO_2, however, these processes are energy intensive and increase the operating costs.

An alternative solution for gas separation is to use membrane technology [6,7]. A membrane separates gases by selectively passing some gas molecules, while reducing the diffusion of others. Compared to conventional methods, membrane technology exhibits several major advantages, such as lower energy consumption, lower cost, a smaller footprint, and less environmental impact [6–8]. In recent years, membrane technology has been well studied, and membranes have been developed and tested at the laboratory scale, showing promising properties for H_2/CO_2 separations [9–16]. The majority of gas permeation experiments, however, have been conducted at temperatures below 50 °C and at pressures less than 10 atm. Very few experiments have been conducted under industrial conditions of pressure (30-60 atm) and temperature (250-400 °C) [17,18] due to the limitations of existing testing instruments.

Several membranes have been tested at high temperature and low pressure [9–11,19–23] or at high pressure and low temperature [24,25]. Most of the instruments capable of testing at high

temperature and low pressure were constructed based on the concept of constant-volume, variable-pressure in which the downstream volume of the instrument remains constant while the increased pressure from permeate in this volume is recorded. Depending on the resolution of the downstream pressure transducer, an instrument based on this concept typically provides accurate results for a membrane that has low gas permeability or a small membrane area, and the solubility and diffusivity coefficients are determined from the time-lag in the plot of downstream pressure versus time. However, in order to obtain an accurate measurement, a sufficient evacuation is required to degas the instrument and membrane between experiments, which lengthens the experimental period. Additionally, this design may not be suitable for testing highly permeable membrane materials, in which the high flux can easily saturate the downstream volume and over pressurize the downstream pressure transducer. Instruments for measurement at high pressure and low temperature normally employ the concept of variable-volume, constant-pressure in which the downstream pressure remains at atmospheric pressure while the flow rate of the permeate is measured. An instrument based on this design is apt to test highly permeable membrane materials and, since no evacuation is required between experiments, it can conduct gas permeation tests quickly. However, it is not suitable for testing low permeable membrane materials or a membrane with a small area for which the flow rate of the permeate can be too small to detect.

The limitations of performing gas permeation experiments at industrially relevant pressure and temperature arise from different aspects. One common barrier results from the limited thermal stability or mechanical strength of membrane materials to high pressures and high temperatures [26,27]. For example, the WGS reaction produces a gas mixture at 30 atm and 300 °C that is typically streamed to a gas separator that also operates at these conditions. A polymeric membrane

in this unit would not only be subjected to high pressure that may cause membrane tearing, but also to high temperature that may decompose the polymeric material. Another restraint comes from limited thermal stability and mechanical strength of seals or parts used on the instrument. In a high pressure and high temperature environment, sealing the low pressure side from the high pressure side is difficult to achieve and hence becomes a major concern because leaks could invalidate results or, even worse, result in a catastrophic mechanical failure. As described previously, instruments were designed and constructed to measure pressure of permeate at a constant volume [9,10] are suitable for measuring slightly permeable membranes. For highly permeable membranes, or when operating at high pressure and high temperature, it is more advantageous to measure permeate flow rate at a constant pressure with mass flow meters. In this work, a high pressure, high temperature (HPHT) permeameter was designed and constructed to test membranes under industrially relevant conditions of feed, pressure, and temperature. The HPHT permeameter is capable of handling high flux measurement for both flat and tubular membranes. The construction of the instrument is described in detail, and the testing of high performance flat and tubular polybenzimidazole (PBI) membranes at high pressure and high temperature was accomplished using pure H_2 and CO_2 and their 50:50 mixture.

2.2. DESIGN AND ASSEMBLY

2.2.1 Theory and Design

The HPHT permeameter is designed to measure the gas permeance through a membrane by measuring gas flux at constant downstream pressure. Given the permeate flow rate, J, the differential pressure across the membrane, Δp, and the active membrane area, A, the gas permeance Q is calculated using Eq. (2.1). With a known membrane thickness, l, the gas permeability of a

membrane, P, is calculated using Eq. (2.2). The membrane selectivity, α, is then determined by calculating the ratio of the gas permeances of two different gas species, Q_a/Q_b.

$$Q = \frac{J}{A\,\Delta p} \quad \text{(Eq. 2.1)}$$

$$P = Q \times l \quad \text{(Eq. 2.2)}$$

The HPHT permeameter was designed to monitor and record gas flow to the feed side, gas flow from the retentate in order to adjust the stage cut, and gas flow to the permeate side to measure the permeance for pure gases and gas mixtures (Fig. 2.1). The flow of the high pressure feed to the upstream side of the membrane is regulated by a metering valve and measured with a pressure transducer. To avoid damage of the instrument components by excessive pressurization, a check valve and a back pressure regulator were installed on the upstream side to ensure the pressure does not exceed a set level. To minimize thermal losses during permeability experiments at high temperatures, the feed gas is preheated to 100 °C before it enters the high temperature furnace where the membrane cell is located. In the furnace, the membrane is exposed to the feed gas heated to the desire temperature. The pressure on the downstream side of the membrane is controlled by a back pressure regulator set to 1 atm and monitored with a pressure transducer (5 atm) to ensure that constant pressure is maintained during permeability experiments. The mass flow meter installed on the downstream side measures the permeate flow rate, J, when gas diffuses through the membrane, providing a direct measurement of the total gas flux across the membrane. Type K thermocouples were installed on the upstream and downstream sides and in the furnace to monitor, adjust, and record the temperatures of the feed, retentate, permeate, and the membrane. For wet gas mixtures, condensers were installed on both the upstream and downstream sides to

prevent excess water from entering the GC columns when the composition of the feed, retentate, and permeate are analyzed. The HPHT permeameter design permits the measurement of gas permeabilities of membranes for H_2, CO_2, and their mixture at various temperatures and pressures.

2.2.2 Components and Hardware Assembly

2.2.2.1 Components

Considering the required mechanical strength against high pressure, thermal stability, and corrosion resistance, only stainless steel (SS-316) fittings and tubing with proper operating temperature and pressure ranges were used in the construction of the HPHT permeameter. Stainless steel 316 tubing with ODs of 1/8 inch (SS-T2-S-028-20) and 1/4 inch (SS-T4-S-065-20), high pressure bellow valves (SS-HBV51-C and SS-HBVS4-C), adjustable check valves (SS-4CA-350 and SS-4CA-3), metering valves (SS-SS4-VH), back pressure regulators (KBP1J0D4D5E20000RD and KBP1F0D4D5E20000OG), and fittings rated up to 60.0 MPa were purchased from Swagelok™. Solenoid valves (SY114-5LOZ) to actuate pneumatic valves were purchased from SMC Corporation. Two-stage brass pressure regulators (Y12-244F), rated up to 250 psi, used to adjust pressure from 30 atm to 2 atm from the feed and retentate sides to the GC were purchased from Airgas®. The upstream pressure transducer (UNIK 5000) with a range from 70 mbar to 700 bar was purchased from General Electric Company. The downstream pressure transducer (Baratron® 127) with a range up to 1000 torr, the mass flow controllers (MKS-1179B) with ranges from 500 to 2000 sccm, and the mass flow meters (MKS-179B) with ranges from 500 to 1000 sccm were purchased from MKS Instruments. To detect small flow rates on the downstream side, a 5 sccm mass flow meter (UFC-8100) was purchased from Unit Instruments. Temperature controllers (CN-7500) and thermocouples type K were purchased from Omega

Engineering. A gas chromatograph (SRI-8610C) equipped with a TCD detector, a molecular sieve column (MOL SIEVE 13X), and a polymer column (HAYESEP D) were purchased from SRI instruments and calibrated with H_2, CO_2, and H_2/CO_2 mixture standards using He and N_2 as carrier gases for CO_2 and H_2, respectively.

2.2.2.2 Membrane Cells

For the testing of flat membranes at high temperature and high pressure, a permeation cell was made of two CF flanges (MDC-130008 and MDC-110008 Conflat™ style, 7.0 cm OD) that sandwich and compress the membrane between high temperature aluminum tape (3M) and graphite gaskets to seal the membrane [17] (Fig. 2.2). A copper gasket was used to contain leaks should the graphite gasket fail. On the feed side flange, an additional set of glands (SS-2-VCR-3) was welded to allow the removal of the retentate and to control the stage cut of the membrane. On the inner side of the downstream flange, a 1/2-inch stainless steel porous disk (1000-.500-.125-2-A, Mott Corporation) was embedded to provide a support for the membrane. The diameter of this porous support defines the membrane diameter to exactly 1/2 inch.

For the testing of tubular membranes, a cell made of a CF type full nipple (MKS-100883055) and two CF type flanges (MKS-100883054) was made (Fig. 2.3). On the downstream flange, a set of 1/4-inch gland (316L-4-VCR-3A) and 1/4-inch female VCR nut (SS-4-HVCR-1) was welded to the inner side to connect the tubular membrane support (AccuSep®) that was obtained from Pall Corporation. The porous stainless steel 316 tubular support (Fig. 2.4) was coated with a thin layer of zirconia with an area of 13.8 cm^2. Similar to the flat membrane cell, a set of glands (SS-2-VCR-3) and nuts (SS-2-HVCR-4) was also welded to the flange to allow the removal of the retentate.

2.2.2.3 Hardware Assembly

The HPHT permeameter (Fig 2.5) was assembled following the design shown in Fig. 2.1. The bending, cutting, welding, and assembling of the stainless steel tubing and fittings were completed according to the manufacturers' recommendations [28]. The cracking pressure of the upstream check valves was adjusted to 525 psi, and the downstream check valves were adjusted to 45 psi to prevent excess pressure build-up and damage to the pressure transducers. The backpressure regulators of the upstream and downstream sides were adjusted to 450 psi and 30 psi, respectively, in order to maintain the feed and permeate pressures. The two-stage pressure regulators that lower the pressure from the upstream and downstream sides to the GC were adjusted to 20 psi to prevent damage to the GC components. To prevent the accumulation of leaks from the membrane cell and fittings in the furnace, a flow of N_2 continuously purged the furnace during permeability experiments.

2.2.3 Electronics and Software

2.2.3.1 Controller

The HPHT permeameter controls and monitors the experiments through data acquisition units (DAQ) that also serve as interfaces to communicate with a PC. A NI-USB-6009 16 bit USB 2.0 analog/digital converter, a 24 bit MCC DAQ USB-2408 series USB 2.0 analog/digital converter with built-in cold-junction compensation for direct measurements of different types of thermocouples, and a LabJack PS12DC relay module attached to a LabJack U3HV DAQ with digital I/O channels to control the solenoid valves were purchased. All the pressure transducers, thermocouples, mass flow meters, mass flow controllers, and solenoid valves were connected to the DAQs using shielded cables to minimize noise in the signals. Typical signal voltages for

pressure transducers ranged from 0 to 10 V and from 0 to 5 V for mass flow controllers and flow meters. To control the temperature of the heater and furnace, solid state relays with attached heat sinks were used to deliver the high power required by the heaters. The relays were connected to temperature controllers and to the PC through RS-232 serial interfaces, allowing for the PC to control the temperature of the heaters.

2.2.3.2 Software

Figure 2.6 shows the front panel of the HPHT LabVIEW VI developed using LabVIEW 2012 (National Instruments). This VI controls and monitors the HPHT transducers, thermocouples, mass flow meters, and valves connected to the DAQs and presents the data to the operator in real time. The VI also allows the operator to have full control of the instrument through the digital interface, which has a layout similar to the front panel of the controller on the HPHT permeameter. The experimental data, including time, pressures, temperatures, and flow rates, are written to a text file on the PC's hard drive.

2.3. EXAMPLES OF APPLICATION

2.3.1 Flat PBI Membranes

Polymer membranes with high H_2/CO_2 selectivities that are mechanically, thermally, and chemically stable at 300 °C and 30 atm are sought for their application in the WGS reaction. Polybenzimidazole (PBI) is a polymer with a tensile strength of 160 MPa and a T_g of 427 °C [29], making it a promising membrane material for H_2 separations under WGS conditions. Previous permeability tests conducted in our lab at 35 °C and 3 atm using flat PBI membranes (annealed at 250 °C) showed a H_2 permeability of 1.37 Barrers and a H_2/CO_2 ideal selectivity of 27.4. It was previously shown that gas permeation in polymers increased with increasing temperature while

retaining selectivity [17]. It was anticipated that at 300 °C, PBI membranes would exhibit enhanced H_2 permeability without significant decrease in H_2/CO_2 selectivity.

Flat PBI membranes were prepared from a 26 wt% PBI solution containing 1.5 wt% LiCl (PBI Performance Products Inc.). The casting solution was prepared by diluting 192 mg of the 26 wt% PBI dope with 3 mL of *N*,*N*-dimethylacetamide (Aldrich) while stirring at 80 °C for 1 d. After a homogeneous solution was formed, the excess solvent was evaporated to obtain a 15 wt% PBI solution. The solution was cast onto a glass substrate using an automatic film applicator (Sheen 1133N) with an adjustable doctor blade. The membrane was dried for 4 h in a chamber that was heated at 50 °C and purged with N_2. The membrane was then placed in a vacuum oven to anneal at 80 °C for 1 d, 150 °C for 12 h, 200 °C for 12 h, and 250 °C for 1 d. A piece of the flat PBI membrane with a thickness of 25 μm and an exposed area of 1.27 cm^2 was mounted in the flat membrane cell (Fig. 2.2).

Single gas permeation experiments with H_2 and CO_2 were performed at 300 °C with feed pressures ranging from 10 to 30 atm. In a typical permeation experiment, the temperature of the membrane was kept constant for 6 h before measurement began. Then, the upstream was pressurized to 30 atm with either H_2 or CO_2 while data from the temperature and pressure transducers and the mass flow meters were recorded. Once steady state flow in the downstream was achieved, the duration of the experiment was extended at least 5 min. Immediately after the data were acquired at this pressure, the feed pressure was dropped to 20 atm and then to 10 atm following the same experimental procedure for data acquisition. At the end of the experiments, the upstream pressure was reduced to atmospheric pressure to obtain the response of the flow

meters for baseline correction. Permeability data for H_2 and CO_2 in PBI at 35 °C and at 300 °C are shown in Table 2.1.

Table 2.1 shows that the permeability of H_2 increased approximately 37 times from 1.37 Barrers at 35 °C and 3 atm to 51.25 Barrers at 300 °C and 30 atm. For CO_2, the permeability increased approximately 40 times from 0.05 Barrers at 35 °C and 3 atm to 2.01 Barrers at 300 °C and 30 atm. Because the permeability of CO_2 increased slightly more than the permeability of H_2 when the temperature was increased, the H_2/CO_2 ideal selectivity exhibited a minor decrease from 27.4 at 35 °C to 25.5 at 300 °C. Table 2.1 also shows that at 300 °C, the permeabilities of H_2 and CO_2 did not change significantly when the pressure was increased from 10 to 30 atm (permeability of H_2 = 50.26 Barrers at 10 atm; H_2 = 51.25 Barrers at 30 atm, CO_2 = 2.13 Barrers at 10 atm; CO_2 = 2.01 Barrers at 30 atm). Due to increased thermal motion of the polymer chains at elevated temperature, additional free volume was likely created in the membrane, leading to an enhancement in gas permeability and a decrease in H_2/CO_2 selectivity [9]. The H_2 permeability for our PBI membrane (51.25 Barrers), tested at 30 atm and 300 °C, is similar to that for a PBI membrane (58 Barrer) that was tested at 3 atm and 250 °C [9]. However, the H_2/CO_2 selectivity for our flat PBI membrane (25.5) is lower than that for the tubular PBI membrane (43), which may be due to the difference in testing temperature.

2.3.2 Tubular PBI Membranes

Tubular membranes present several advantages over flat membranes. For example, tubular membranes allow for larger membrane areas, resulting in larger flow rates. Tubular membranes also offer better mechanical strength than flat membranes because the membranes are coated directly onto the tubular support facilitating the measurement of the gas transport properties of thin

membranes at high pressures and high temperatures. Another benefit of using tubular supports is that they provide more reliable sealing of the low and high pressure sides than typical flat membrane cells. The major drawback of tubular membranes is that the thickness of the membrane cannot be measured accurately due to the unevenness of the coating and due to polymer diffusion into the pores of the support. Hence, gas permeance is used to evaluate the permeation properties of tubular membranes.

Formation of a continuous thin membrane on a tubular support can be realized by comparing the gas flux before and after coating the membrane on the tubular support. Therefore, it is important to perform a blank test using the bare tubular support to determine the gas flux of the support at the conditions the membrane would be tested. For this test, the temperature was set to 300 °C and the support was pressurized with N_2 at 5 atm. The gas flow rate on the downstream was measured by the MFMs to determine the N_2 permeance through the tubular support, which was found to be 14755 GPU. It was, therefore, anticipated that a defect-free, coated membrane would reduce the gas flow rate of the bare tubular support and exhibit a gas selectivity higher than Knudsen selectivity.

Tubular PBI membranes with areas up to 13.8 cm^2 were coated on the tubular support. The tubular PBI membrane was fabricated by dipping the tubular support into an 8 wt% PBI solution obtained from the dilution of a 26 wt% dope with *N*,*N*-dimethylacetamide. The tubular support was rotated axially at 60 rpm during the coating process in which it was slowly immersed in the 8 wt% PBI solution and then removed at the same speed. The tubular membrane was left rotating at room temperature for 2 h and then transferred to a heated drying table at 50 °C for 4 h while purging with N_2. The drying protocol for the tubular membrane was the same as for the flat

membrane. The resulting tubular membrane exhibited an estimated thickness of 16 ± 1 μm measured with a micrometer.

The membrane was tested at 300 °C and 30 atm with H_2, CO_2, and a 50:50 H_2/CO_2 mixture using the HPHT permeameter. Single gas permeation experiments with the tubular PBI membrane were carried out following the same procedure used for flat PBI membranes. For gas mixture experiments, a H_2/CO_2 mixture at 30 atm was introduced into the upstream side once the temperature of the membrane was equilibrated for at least 1 h. After steady state was reached, the permeate was directed to the GC to determine its composition. Due to similar thermal conductivities between H_2 and He, N_2 was used as carrier gas for the measurement of H_2, and He was used for the measurement of CO_2. The H_2 and CO_2 compositions were alternately measured 7 times, and the average was used to calculate the H_2/CO_2 ideal selectivity of the membrane. The GC's columns were purged between analyses with the carrier gas to flush the previous samples from the columns. The gas permeation results for the tubular PBI membrane at 300 °C and 30 atm for H_2, CO_2, and the H_2/CO_2 mixture are shown in Table 2.

Kumbharkar, et al. [23] measured the gas permeance of PBI hollow fibers between 300 and 400 °C at 5 to 8 atm. Their work showed their PBI hollow fibers exhibited H_2 and CO_2 permeances of 2.60 and 0.096 GPU, respectively, with a H_2/CO_2 ideal selectivity of 27.3. These results are similar to those measured for the tubular PBI membrane in this work (Table 2). Using Eq. (2.2) and the estimated thickness of the tubular membrane (16 μm), the gas permeability for H_2 and CO_2 were estimated and compared to those obtained for the flat membrane. The results indicated that the tubular membrane was slightly less permeable for H_2 and CO_2 than the flat membranes at 10 to 30 atm and 300 °C, which possibly results from a difference between the

estimated and actual thickness of the tubular membrane. The tubular membrane might be thicker than the estimation due to the diffusion of polymer solution into the pores of the support during coating. The ideal gas selectivities of the flat membrane (23.6 to 25.5 at 10 to 30 atm and 300 °C) and tubular membrane (22.1 to 23.1 at 10 to 30 atm and 300 °C) are similar. The measurement of gas mixture selectivity at 30 atm and 300 °C showed a reduction in H_2/CO_2 selectivity from 23.1 (ideal) to 17.8 at a stage cut of 0.2. Gas mixture selectivity drops from ideal selectivities have been observed before and are attributed to the increased concentration of CO_2 in the feed competing with H_2 for diffusion pathways in the membrane [15]. It should be noted that the accumulation of the retentate (CO_2) on the upstream side is reduced by purging the feed from the surface of the membrane at a rate low enough to provide a maximum selectivity (stage cut of the membrane). In the HPHT permeameter, this is accomplished by connecting a piece of tubing at the opposite end of the feed on the upstream side and lowering the temperature and pressure of this line to room temperature and 2 atm. Purging rates are controlled with mass flow controllers based on the permeation rate across the membrane.

From the permeation results, it can be seen that the HPHT permeameter in this work is capable of testing the H_2/CO_2 separation of a membrane at industrially relevant pressure and temperature, which is superior to most instruments [9,10,12,19,23–25] that can only test a membrane at high pressure or high temperature. Compared to the existing instrument in our lab for measuring gas permeation at high pressure, high temperature [17], the HPHT permeameter in this work exhibits several advantages. First, the HPHT permeameter is better in measuring membranes with high gas permeability. As described previously, at high temperature, polymeric membranes tend to be more permeable due to the thermal motion of the polymer chains, leading

to a significant increase in gas diffusivity. The HPHT permeameter was designed based on the concept of variable-volume, constant-pressure, which implies that the flux will not build up on the downstream side of the membrane. Therefore, the HPHT permeameter can handle high flux measurements better than instruments based on the concept of constant-volume, variable-pressure. Due to this feature, the HPHT permeameter is also suitable for testing inorganic membranes that normally exhibit high gas permeability. Second, the variable-volume, constant-pressure design does not require the evacuation of the downstream side of the membrane, which simplifies the testing procedure and enables fast measurement at various pressures. And last, the HPHT permeameter is versatile to membrane geometry, capable of measuring flat, tubular, and other membrane geometries.

2.4. CONCLUSION

The HPHT permeameter was designed and assembled to measure gas permeance through a membrane under industrially relevant conditions of feed, pressure, and temperature. The design of the HPHT permeameter involved means to regulate the flow of high pressure gas. For the assembly, all the fittings and parts were carefully selected and assembled according to specifications to ensure the instrument can properly handle gases at high pressures and high temperatures. Because of the wide range of the MFMs (0.005 to 5 sccm, 0.5 to 500 sccm, 1 to 1000 sccm) and MFCs (2 to 2000 sccm, 5 to 5000 sccm), the HPHT permeameter is capable of measuring flow rates up to 2000 sccm, making it suitable for measuring the gas transport properties of highly permeable membranes. The results obtained with PBI membranes show that the HPHT permeameter can provide reliable gas permeance results for flat or tubular membranes using single gas or gas mixtures under industrial conditions. Compared to other systems for gas permeation

measurement, the HPHT permeameter exhibits several features and advantages that make it more suitable for high pressure, high temperature applications.

APPENDIX 2 FIGURES AND TABLES

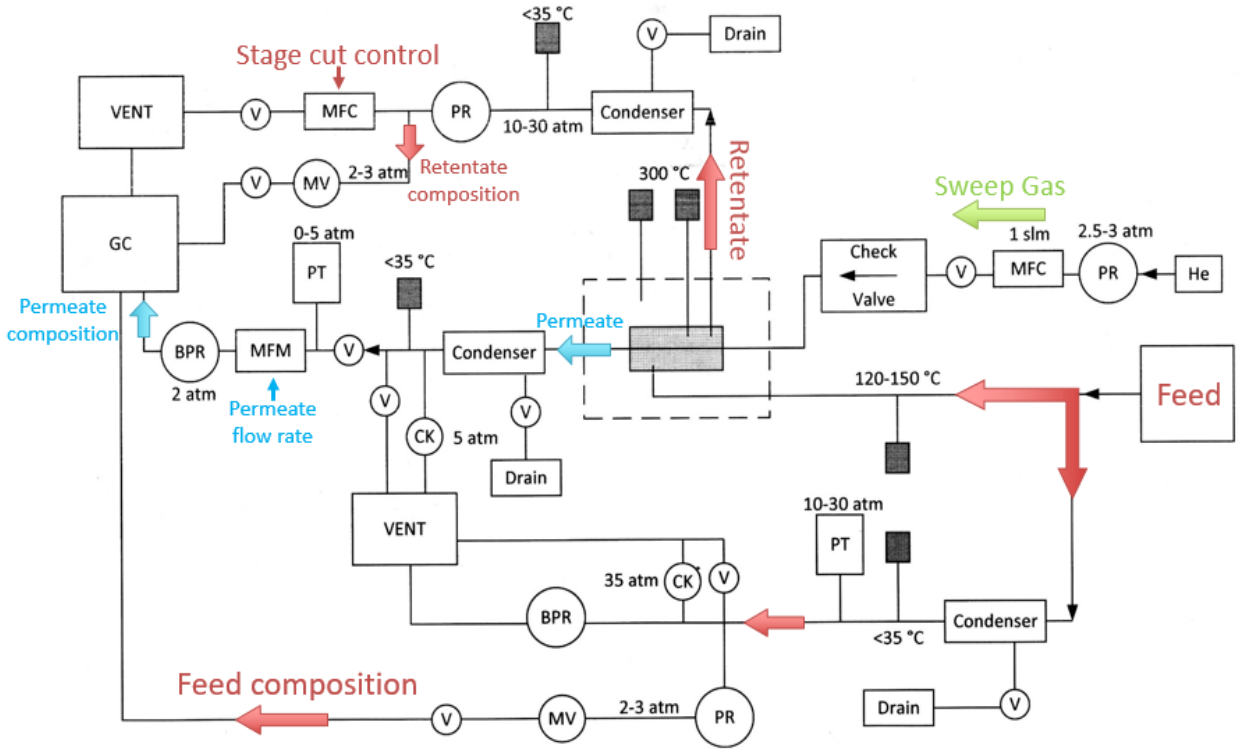

Fig 2.1. Schematic diagram of the HPHT permeameter. V = high pressure bellow valve, BPR = back pressure regulator, PR = pressure regulator, MV = metering valve, CK = check valve, PT = pressure transducer, MFM = mass flow meter, and MFC = mass flow controller.

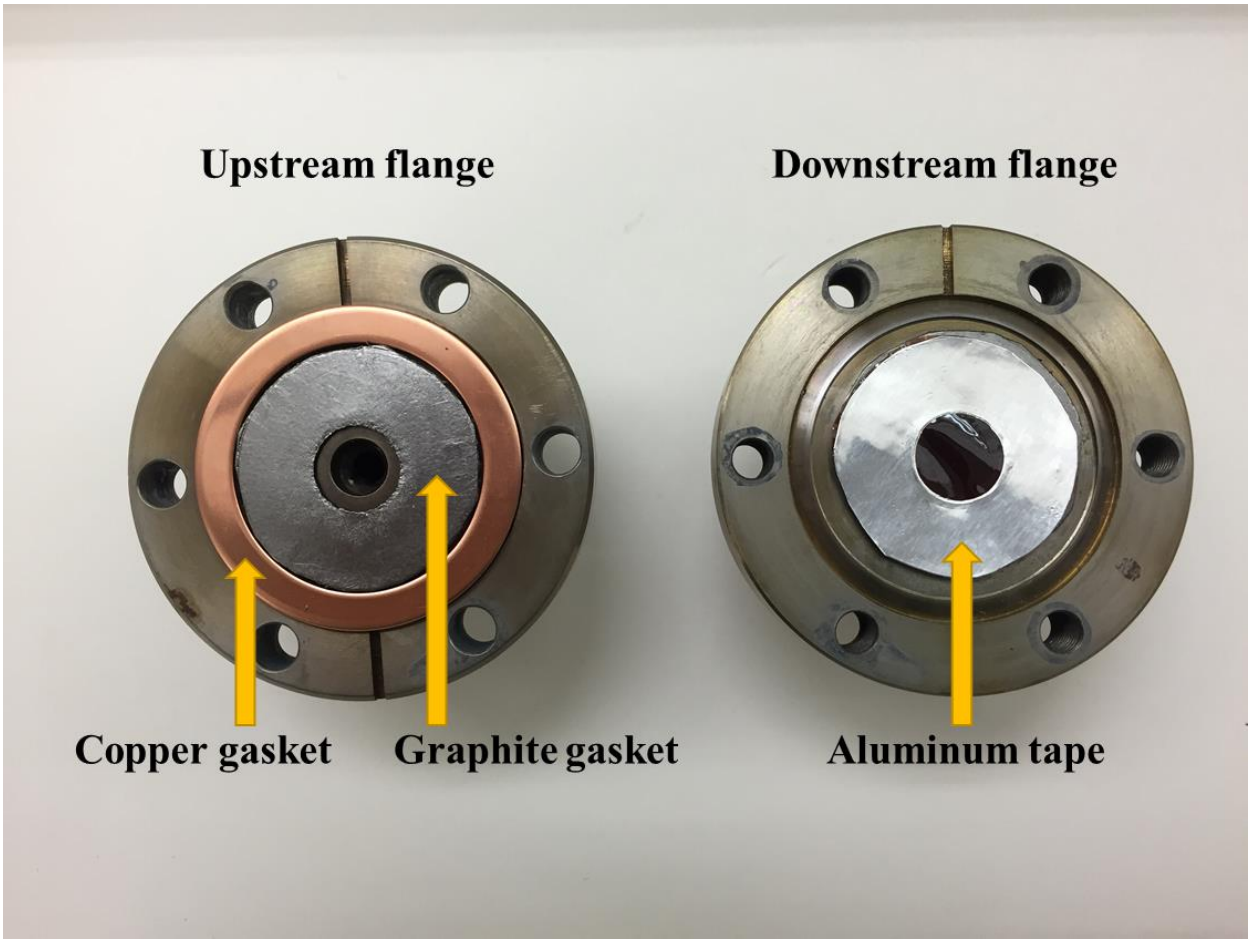

Fig 2.2. Optical image of a flat membrane cell for high pressure, high temperature gas permeation measurements.

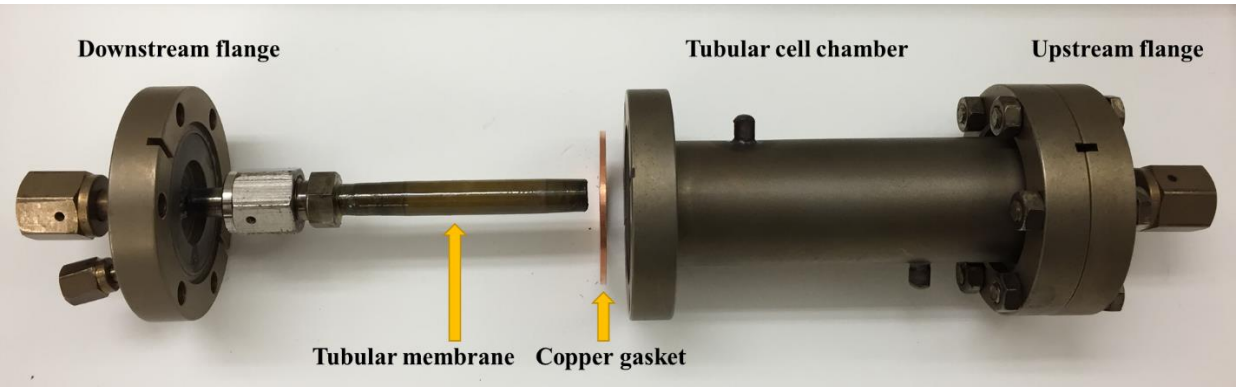

Fig 2.3. Optical image of a tubular membrane cell.

Fig 2.4. Optical image of a zirconia-coated stainless steel tubular support.

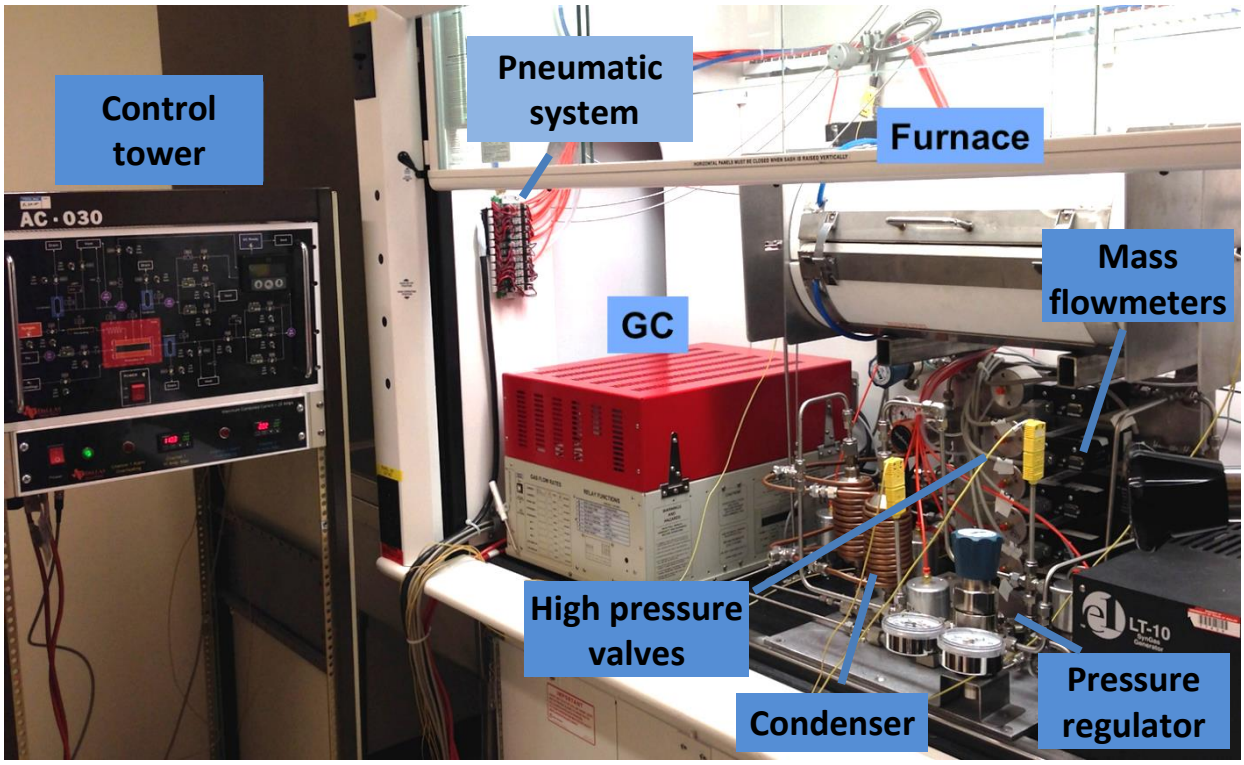

Fig 2.5. Optical image of the assembled HPHT permeameter located in a fume hood.

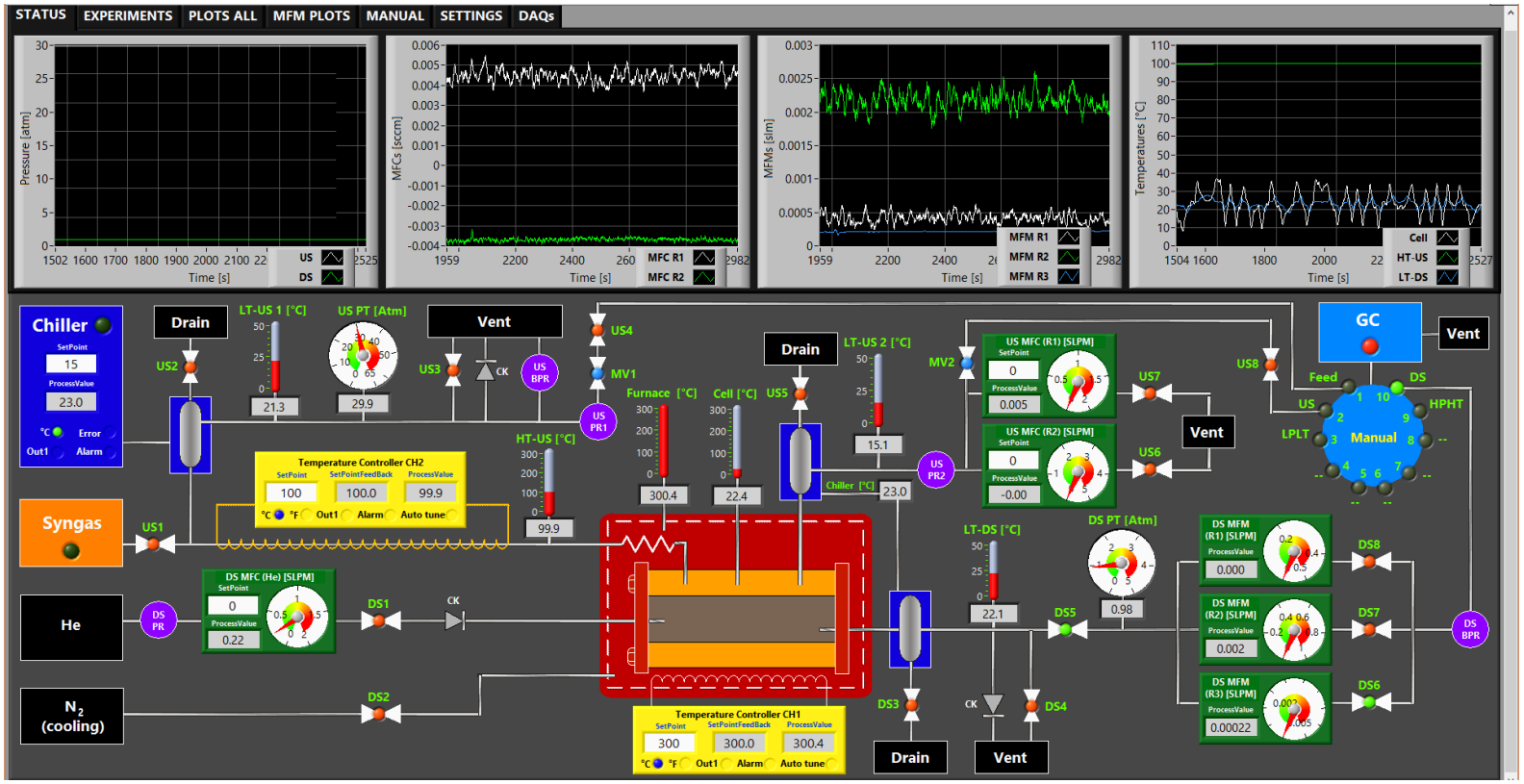

Fig 2.6. LabVIEW front panel of the HPHT permeameter.

Table 2.1. Permeability (Barrer) of H_2 and CO_2 and H_2/CO_2 ideal selectivity in a flat PBI membrane at various temperatures and pressures.

Temperature (°C)	35	300	300	300
Pressure (atm)	3	10	20	30
H_2 permeability (Barrer)	1.37	50.26	50.53	51.25
CO_2 permeability (Barrer)	0.05	2.13	2.15	2.01
H_2/CO_2 ideal selectivity	27.4	23.6	23.5	25.5

1 Barrer = 1×10^{-10} $cm^3_{(STP)}$ cm^{-2} s^{-1} $cmHg^{-1}$

Table 2.2. Permeance, permeability*, and selectivity of a tubular PBI membrane for H_2 and CO_2 at high pressure and high temperature.

Temperature (°C)	300	300	300
Pressure (atm)	10	20	30
H_2 permeance (GPU)	2.55	2.52	2.52
CO_2 permeance (GPU)	0.12	0.11	0.11
H_2 permeability (Barrer)	39.34	38.75	38.84
CO_2 permeability (Barrer)	1.93	1.92	1.82
H_2/CO_2 ideal selectivity	20.4	20.2	21.3
H_2/CO_2 mixed gas selectivity	-	-	17.8

1 GPU = 1×10^{-6} $cm^3_{(STP)}$ cm^{-2} s^{-1} $cmHg^{-1}$

* 16 ± 1 μm for membrane thickness

REFERENCES

[1] S.E. Hosseini, M.A. Wahid, Hydrogen production from renewable and sustainable energy resources: Promising green energy carrier for clean development, *Renew. Sustain. Energy Rev.* **2016**, *57*, 850–866.

[2] E. Shoko, B. McLellan, A.L. Dicks, J.C.D. da Costa, Hydrogen from coal: Production and utilization technologies, *Int. J. Coal Geol.* **2006**, *65*, 213–222.

[3] G.J. Stiegel, M. Ramezan, Hydrogen from coal gasification: An economical pathway to a sustainable energy future, *Int. J. Coal Geol.* **2006**, *65*, 173–190.

[4] P. Mondal, G.S. Dang, M.O. Garg, Syngas production through gasification and cleanup for downstream applications - Recent developments, *Fuel Process. Technol.* **2011**, *92*, 1395–1410.

[5] C.A. Grande, Advances in pressure swing adsorption for gas separation, *ISRN Chem. Eng.* **2012**, *2012*, 1–13.

[6] R.W. Baker, Future directions of membrane gas separation technology, *Ind. Eng. Chem. Res.* **2002**, *41*, 1393–1411.

[7] P. Bernardo, E. Drioli, G. Golemme, Membrane gas separation: A review/state of the art, *Ind. Eng. Chem. Res.* **2009**, *48*, 4638–4663.

[8] W.J. Koros, G.K. Fleming, Membrane-based gas separation, *J. Membr. Sci.* **1993**, *83*, 1–80.

[9] K.A. Berchtold, R.P. Singh, J.S. Young, K.W. Dudeck, Polybenzimidazole composite membranes for high temperature synthesis gas separations, *J. Membr. Sci.* **2012**, *415–416*, 265–270.

[10] T. Yang, T.S. Chung, High performance ZIF-8/PBI nano-composite membranes for high temperature hydrogen separation consisting of carbon monoxide and water vapor, *Int. J. Hydrogen Energy* **2013**, *38*, 229–239.

[11] X. Li, R.P. Singh, K.W. Dudeck, K.A. Berchtold, B.C. Benicewicz, Influence of polybenzimidazole main chain structure on H_2/CO_2 separation at elevated temperatures, *J. Membr. Sci.* **2014**, *461*, 59–68.

[12] R.P. Singh, G.J. Dahe, K.W. Dudeck, C.F. Welch, K.A. Berchtold, High temperature polybenzimidazole hollow fiber membranes for hydrogen separation and carbon dioxide capture from synthesis gas, *Energy Procedia* **2014**, *63*, 153–159.

[13] L.M. Robeson, *Polymer blends: A comprehensive review*, Hanser Gardner Publications: Cincinnati, OH, **2007**.

[14] L.M. Robeson, Polymer membranes for gas separation, *Curr. Opin. Solid State Mater. Sci.* **1999**, *4*, 549–552.

[15] M.J.C. Ordoñez, K.J. Balkus, Jr., J.P. Ferraris, I.H. Musselman, Molecular sieving realized

with ZIF-8/Matrimid mixed-matrix membranes, *J. Membr. Sci.* **2010**, *361*, 28–37.

[16] N.P. Panapitiya, S.N. Wijenayake, D.D. Nguyen, Y. Huang, I.H. Musselman, K.J. Balkus, Jr., J.P. Ferraris, Gas separation membranes derived from high-performance immiscible polymer blends compatibilized with small molecules, *ACS Appl. Mater. Interfaces* **2015**, *7*, 18618–18627.

[17] E. V Perez, K.J. Balkus, Jr., J.P. Ferraris, I.H. Musselman, Instrument for gas permeation measurements at high pressure and high temperature., *Rev. Sci. Instrum.* **2013**, *84*, 65107.

[18] D. Driscoll, B. Morreale, L. Headley, NETL test protocol testing of hydrogen separation membranes, *DOE/NETL – 2008/1335*. **2008**, 14.

[19] E.R. Geus, H. van Bekkum, W.J.W. Bakker, J.A. Moulijn, High-temperature stainless steel supported zeolite (MFI) membranes: Preparation, module construction, and permeation experiments, *Microporous Mater.* **1993**, *1*, 131–147.

[20] S.I. Semenova, H. Ohya, T. Higashijima, Y. Negishi, Dependence of permeability through polyimide membranes on state of gas, vapor, liquid and supercritical fluid at high temperature, *J. Membr. Sci.* **1992**, *67*, 29–37.

[21] J.C.S. Wu, D.F. Flowers, P.T.K. Liu, High-temperature separation of binary gas mixtures using microporous ceramic membranes, *J. Membr. Sci.* **1993**, *77*, 85–98.

[22] J.C.S. Wu, H. Sabol, G.W. Smith, D.L. Flowers, P.K.T. Liu, Characterization of hydrogen-permselective microporous ceramic membranes, *J. Membr. Sci.* **1994**, *96*, 275–287.

[23] S.C. Kumbharkar, Y. Liu, K. Li, High performance polybenzimidazole based asymmetric hollow fibre membranes for H_2/CO_2 separation, *J. Membr. Sci.* **2011**, *375*, 231–240.

[24] S. Damle, W.J. Koros, Permeation equipment for high-pressure gas separation membranes, *Ind. Eng. Chem. Res.* **2003**, *42*, 6389–6395.

[25] S.A. Stern, S.M. Fang, R.M. Jobbins, Permeation of gases at high pressures, *J. Macromol. Sci. Part B.* **1971**, *5*, 41–69.

[26] L. Shao, C.H. Lau, T.S. Chung, A novel strategy for surface modification of polyimide membranes by vapor-phase ethylenediamine (EDA) for hydrogen purification, *Int. J. Hydrogen Energy* **2009**, *34*, 8716–8722.

[27] Y. Li, F. Liang, H. Bux, W. Yang, J. Caro, Zeolitic imidazolate framework ZIF-7 based molecular sieve membrane for hydrogen separation, *J. Membr. Sci.* **2010**, *354*, 48–54.

[28] F.J. Callahan, *Tube Fitter's Manual (Swagelok, Solon, Ohio)*, **1993**.

[29] G.S. Copeland, M. Gruender, J.M. Pettit, J.C. Moore, Thermal resistant coatings using PBI resin, *Soc. Adv. Mater. Process Eng. Conf. Balt. MD*. **2012**, 1–8.

CHAPTER 3

COMPARISON OF FLAT AND TUBULAR POLYMERIC MEMBRANES FOR H_2/ CO_2 SEPARATION

ABSTRACT

Tubular Matrimid® and PBI membranes were fabricated using the dip-coating technique. The application time and polymer solution concentration were varied to determine the optimal coating conditions to obtain defect-free membranes. The dip-coating technique, using an 8 wt% polymer solution, provided defect-free polymer membranes on tubular supports with thicknesses of 16 to 18 μm. The H_2/CO_2 separation performance of the flat and tubular polymeric membranes were compared from 3 atm and 35 °C to 30 atm and 300 °C. The tubular Matrimid® membranes exhibited H_2 permeability of 32.5 Barrers and H_2/CO_2 ideal selectivity of 3.8, which is similar to the reported H_2 permeability (28.9 Barrers) and H_2/CO_2 ideal selectivity (3.0) of the flat Matrimid® membranes that were tested at the same conditions. The flat PBI membranes exhibited H_2 permeability of 51.3 Barrers and H_2/CO_2 ideal selectivity of 25.5, whereas the tubular membranes exhibited H_2 permeability of 38.8 Barrers and H_2/CO_2 ideal selectivity of 21.3, both tested at 30 atm and 300 °C. The gas permeability and selectivity of the flat membranes are similar to those for tubular membranes tested under the same conditions, indicating that the dip-coating technique provides defect-free tubular membranes.

3.1 INTRODUCTION

Membrane technology has been widely investigated and developed for several decades due to its economic merits. Compared to conventional methods for gas separations, such as pressure swing adsorption [1] and cryogenic distillation [2], membrane-based separations leave a smaller footprint, require less maintenance, and consume less energy [2–4]. Due to these advantages, several types of membranes have been utilized in industrial processes for separating gas pairs such as O_2 from N_2 in O_2 production [5–7], CO_2 from N_2 in flue gas from coal plants [8–11], H_2 from purge streams in ammonia production [12–14], and H_2 from CO_2 in the water-gas shift (WGS) reaction [15–17].

The two major parameters used to evaluate the gas separation performance of a membrane are permeability and selectivity. Permeability is the product of gas flux and membrane thickness, while selectivity is the ratio of the permeabilities of two gases. Membranes with high permeability, high gas flux, and high selectivity are typically desired. While permeability and selectivity are intrinsic properties of a membrane material, gas flux can be increased by increasing the membrane area or decreasing the membrane thickness. The fabrication of flat membranes with large areas is achievable, yet the low surface area to volume ratio requires large membrane cells for housing and sealing, which limits their applications. For industrial applications, modules of tubular [18–20], spiral wound [21,22], and hollow fiber [23–25] membranes are preferred due to their high surface area to volume ratio that reduces the size of the membrane cells and lowers the manufacturing cost.

Tubular membranes exhibit many advantages compared to flat membranes, especially in high pressure and temperature applications, such as the recovery of H_2 in ammonia production and

the WGS reaction [14,26]. As mentioned previously, tubular membranes offer a higher surface area to volume ratio than flat membranes. In addition, the sealing for tubular membranes is easier to achieve than for flat membranes. In a typical flat membrane cell, the membrane sample sits on a permeable support, and sealants or O-rings are used to seal or tightly compress the membrane to prevent leaks. During the sealing and mounting process, the membranes are subjected to compressive forces that can damage the membrane. Furthermore, under high pressure and high temperature conditions, the sealant or O-rings tend to leak or fail, which could result in a catastrophic mechanical failure. In the case of the tubular membranes, the stainless steel tubular supports do not require any sealant or O-rings and, thus, can safely be used under corrosive conditions and in high pressure and high temperature applications. The most attractive feature of tubular membranes is the mechanical support they provide to the membranes under harsh conditions. Membranes made of brittle materials, such as zeolites [27–29], metal-organic frameworks [30], zeolitic imidazolate frameworks [31,32], and carbon molecular sieves [18,20,33], are normally prepared on tubular supports and exhibit excellent mechanical strength in high pressure and high temperature environments. Hollow fiber membranes also possess high surface area to volume ratios, however, the sealing capacity is limited by the sealants, which normally are epoxy resins that may decompose at higher temperatures [34,35]. Spiral wound modules formed from flat membranes require spacers in between the layers [21,36,37], which adds complexity and cost to the assembly for high pressure and high temperature applications.

Most tubular membranes are made of inorganic materials, but a few polymeric materials have also been reported for low temperature and low pressure applications. High performance polymers, such as polyimides [38–42] and polybenzimidazole (PBI) [43–45], have emerged in the

past few decades, finding use in membrane fabrication due to their low manufacturing cost and processability. Tubular polymeric membranes of high performance polymers could find use in gas separations at high pressures and high temperatures if the fabrication of defect-free thin films can be achieved. However, optimal fabrication conditions for tubular polymeric membrane have not been well discussed, and the gas separation performance of flat and tubular polymeric membranes has not been compared. In this chapter, flat and tubular membranes were fabricated using a polyimide (Matrimid® 5218) and PBI (Fig. 3.1 A-B). For the tubular membranes, different coating techniques and coating parameters were studied to determine the optimal fabricating conditions. Using H_2, CO_2, and their 50:50 mixture, the gas transport properties of the flat and tubular membranes were measured at various pressure and temperature ranges and compared.

3.2 EXPERIMENTAL

3.2.1 Materials

All chemicals and solvents were used as received unless otherwise noted. Anhydrous dimethylacetamide (DMAc, 99.8% purity) and chloroform ($CHCl_3$, 99% purity) were purchased from EMD Chemicals and Fisher Scientific, respectively. All organic solvents were dried prior to their use using activated 4A type molecular sieves. Polybenzimidazole (PBI) S26 solution was purchased from PBI Performance Products, Inc. (26 wt% PBI and 1.5 wt% LiCl in DMAc, $M_w \sim 30{,}000$) and used as received. Matrimid® 5218 was purchased from Huntsman Advance Materials Americas, Inc. and was dried in a vacuum oven at 120 °C for 12 h prior to use. Zirconia-coated (10 μm layer) 316 stainless steel porous tubular supports (AccuSep®, Fig. 3.2) were received from Pall Corporation. The zirconia layer had a pore size of 0.1 μm and an area of

13.8 cm^2. For gas permeation experiments, H_2, CO_2, N_2, He, and a certified H_2/CO_2 (50:50) mixture were purchased from Airgas, Inc. The purities of all the gases were greater than 99.99%.

3.2.2 Membrane Fabrication

3.2.2.1 Flat PBI Membrane Fabrication

Flat PBI membranes were fabricated from a casting solution that was prepared by diluting 192 mg of the 26 wt% PBI dope with 3 mL of *N*,*N*-dimethylacetamide (Aldrich) while stirring at 80 °C for 1 d. After a homogeneous solution was formed, the excess solvent was slowly evaporated until a 15 wt% PBI solution was obtained. The solution was cast onto a glass substrate using an automatic film applicator (Sheen 1133N) with an adjustable doctor blade. The membrane was then transferred to a heated chamber purged with N_2 at 50 °C to dry for 4 h. The membrane was then placed in a vacuum oven to anneal at 80 °C for 1 d, 150 °C for 12 h, 200 °C for 12 h, and 250 °C for 1 d. A piece of the flat PBI membrane with a thickness of 22 μm and exposed area of 1.27 cm^2 was used for gas permeation measurements.

3.2.2.2 Tubular PBI and Matrimid® Fabrication by Dip-coating

Solutions of 5, 8, and 12 wt% PBI in DMAc were prepared by diluting the PBI S26 solution with DMAc. Matrimid® solutions with the same concentrations were prepared by dissolving Matrimid® in chloroform. During coating, the tubular supports were rotated at 60 rpm, held vertically, immersed into the polymer solution, and then withdrawn (Fig. 3.3). The freshly coated supports were oriented horizontally and rotated at 60 rpm in air at 25 °C for 12 h to form a uniform film on the support. The tubular PBI membranes were dried and annealed following the protocol used for the flat PBI membranes. The tubular Matrimid® membranes were annealed in a vacuum

oven at 240 °C for 12 h. The fabricated tubular Matrimid® and PBI membranes were shown in Fig. 3.4.

3.2.3 Gas Permeation

Gas permeation measurements at pressures ranging from 3 to 30 atm and at temperatures of 35 and 300 °C were conducted on a custom-built high pressure, high temperature (HPHT) gas permeameter [Chapter 2]. The HPHT permeameter was designed to measure gas permeance based on the permeate flow rate at constant downstream pressure. Custom-made stainless steel flat and tubular permeation cells were used to house the flat and tubular membranes. Permeation experiments were conducted by pressurizing the upstream side after the experimental temperature had been reached. As the permeate gas diffused through the membrane and entered the downstream side, the permeate flow rate (J) was measured using a mass flow meter. The gas permeance (Q) in GPU (1 GPU = 1×10^{-6} $cm^3_{(STP)}$ cm^{-2} s^{-1} $cmHg^{-1}$) was calculated using Equation (3.1), where Δp is the differential pressure across the membrane and A is the effective membrane area.

$$Q = \frac{J}{A\,\Delta p} \qquad \text{(Eq. 3.1)}$$

If the membrane thickness, l, can be measured accurately, then the gas permeability (P) of the pure polymer membranes can be calculated using Equation (3.2):

$$P = Q \times l \qquad \text{(Eq. 3.2)}$$

For mixed gas permeability measurements at 30 atm and 300 °C, a 50:50 H_2/CO_2 gas mixture was used as the feed. The stage cut, which is the ratio of permeate flow to feed flow, was maintained at 0.2 by venting the upstream of the permeation cell through a mass flow controller to keep the feed composition constant. The permeate composition was determined using an SRI gas chromatograph (8610C) equipped with a molecular sieve column (MOL SIEVE 13X), a polymer column (HAYESEP D), and a TCD detector. N_2 for H_2 and He for CO_2 were used as carrier gases to measure the concentration of H_2 and CO_2 in the permeate. For each tubular polymeric membrane type (PBI and Matrimid®), two separately prepared membranes were tested and their gas permeance was measured a minimum of six times each.

3.3 RESULTS AND DISCUSSION

3.3.1 PBI and Matrimid® Membranes Fabricated by Dip-coating

From Equation 1, it can be inferred that higher gas fluxes across the membrane can be achieved by decreasing the thickness of the membrane. Thinner (<18 μm) tubular membranes were obtained by dip-coating the tubular supports into polymer solutions having lower polymer concentrations. Although the 5 wt% polymer solution provided the thinnest membrane, the lowest polymer concentration that could be used to form a defect free tubular membrane was 8 wt%, which resulted in a 16 to 18 μm thick membrane. Multiple coatings of the tubular support cannot be applied in this technique because the excess solvent in the polymer solution re-dissolves the previously coated polymer membrane on the tubular support. Therefore, all of the tubular membranes tested for gas permeation were fabricated by dipping the tubular supports only once into 8 wt% polymer solutions. The Matrimid® and PBI tubular membranes are shown in Fig 3.4.

3.3.2 Gas Permeation

3.3.2.1 Low Pressure, Low Temperature Gas Permeation

Single gas and gas mixture permeation experiments at 3 atm and 35 °C were conducted for tubular Matrimid® membranes. Owing to PBI's low permeability at ambient conditions, PBI membranes were not tested for gas permeation at 3 atm and 35 °C. Using a micrometer with a resolution of 1 μm, the membrane thickness was estimated by averaging the thicknesses at 9 spots on the tubular support before (bare support) and after coating the membrane. The estimated thickness, based on two tubular Matrimid® membranes, was 18 ± 3 μm. Using this thickness value and Equation 2, the gas permeability and the H_2/CO_2 ideal selectivity were calculated (Table 3.1). Percent errors of 13, 9, 27, and 4%, were found for the H_2 and CO_2 permeabilities and the H_2/CO_2 ideal and gas mixture selectivities when comparing the tubular Matrimid® membranes to the reported values for flat Matrimid® membranes [46]. The gas permeation properties for tubular and flat membranes were similar, indicating that the coating procedure deposited a defect-free Matrimid® membrane on the porous support.

3.3.2.2 High Pressure, High Temperature Gas Permeation Tests

The gas permeances of the flat and tubular PBI membranes were measured at 300 °C and at pressures ranging from 10 to 30 atm. Using Equation 2 and the estimated thickness based on two tubular PBI membranes (16 ± 1 μm), the H_2 and CO_2 permeabilities and the H_2/CO_2 ideal selectivities for the flat and tubular PBI membranes were calculated (Table 3.2). The results indicated that the tubular membrane was 22-24% and 9-11% less permeable for H_2 and CO_2, respectively, than the flat membrane. This variation in permeability could result from deviations between the true and the estimated thickness of the tubular membrane that arise from the variations

in the thickness of the PBI layer on the tubular support. The similar H_2/CO_2 ideal selectivities of the flat membranes (H_2/CO_2 = 23.6 at 10 atm and 300 °C and H_2/CO_2 = 25.5 at 30 atm and 300 °C) and the tubular membranes (H_2/CO_2 = 20.4 at 10 atm and 300 °C and H_2/CO_2 = 21.3 at 30 atm and 300 °C) also support the possibility that the discrepancies in gas permeability between the tubular and the flat membranes arise from the estimation of the thickness and not from defects in the membranes. The H_2/CO_2 (50:50) gas mixture separation of the tubular PBI membrane at 30 atm and 300 °C showed that, despite using a stage cut of 0.20 (20% H_2 recovery), the H_2/CO_2 selectivity dropped from 21.3 (ideal) to 17.8. The decreased selectivity of membranes to gas mixtures is generally attributed to the limited effectiveness that purging the retentate has on disrupting the accumulation of CO_2 in the feed. The effectiveness of the purging rate depends largely on the design of the cell [47–49].

Tubular Matrimid® membranes tested at 300 °C and at pressures that ranged from 10 to 30 atm (Table 3.3) showed that the polymer retained its H_2/CO_2 ideal selectivity at temperatures close to its glass transition temperature (T_g = 305 °C [50]). In the open literature, most of the Matrimid®-based membranes were tested at either low pressures or ambient temperatures, and none have been tested at temperatures close to the T_g of the polymer. From Table 3.3, it can be observed that the gas permeabilities for H_2 and CO_2 increased significantly from 35 °C (H_2 = 32.53 Barrers and CO_2 = 8.65 Barrers) to 300 °C (H_2 = 488 Barrers and CO_2 = 94 Barrers), while the H_2/CO_2 selectivity increased moderately from 3.8 (35 °C) to 5.2 (300 °C). The increased gas permeability for polymeric membranes resulting from elevated temperatures has been observed before and was attributed to the increased free volume that resulted from the increased thermal motion of the polymer chains as the temperature was increased [45]. Gas mixture selectivity for this membrane

(H_2/CO_2 = 4.2) was also lower than the H_2/CO_2 ideal selectivity (5.9) at 300 °C and 30 atm as in the case of PBI membranes, presumably due to the reduced effectiveness of the purging rate in disrupting the CO_2 accumulation in the feed. As the feed pressure increased from 10 to 30 atm at 300 °C, the H_2/CO_2 ideal selectivities of tubular Matrimid® membranes remained relatively constant (5.2-5.9), indicating that the membrane was holding well at elevated pressure. The permeation results of tubular Matrimid® membranes at 30 atm and 300 °C suggest that the tubular geometry may perform better than the flat geometry in the high pressure, high temperature environment.

3.4 CONCLUSION

Tubular PBI and Matrimid® membranes, fabricated using the dip-coating technique with an 8 wt% polymer solution, provided defect-free membranes on tubular supports with relatively thin membrane thicknesses (16 μm for PBI and 18 μm for Matrimid®). Gas permeation results showed no significant differences in gas separation properties between the flat and tubular Matrimid® membranes at 3 atm and 35 °C or between the flat and tubular PBI membranes at 30 atm and 300 °C, indicating the dip-coating technique provided defect-free membranes. The tubular Matrimid® membrane also permitted the measurement of the H_2/CO_2 gas permeation properties of this polymer at temperatures close to its T_g and at pressures up to 30 atm. The results showed significant enhancement in gas permeability and a slight increase in H_2/CO_2 selectivity from 3.8 (35 °C) to 5.2 (300 °C). The permeation results suggest that the tubular membrane can provide better sealing and may be more suitable than the flat membrane for high pressure, high temperature gas measurement.

APPENDIX 3 FIGURES AND TABLES

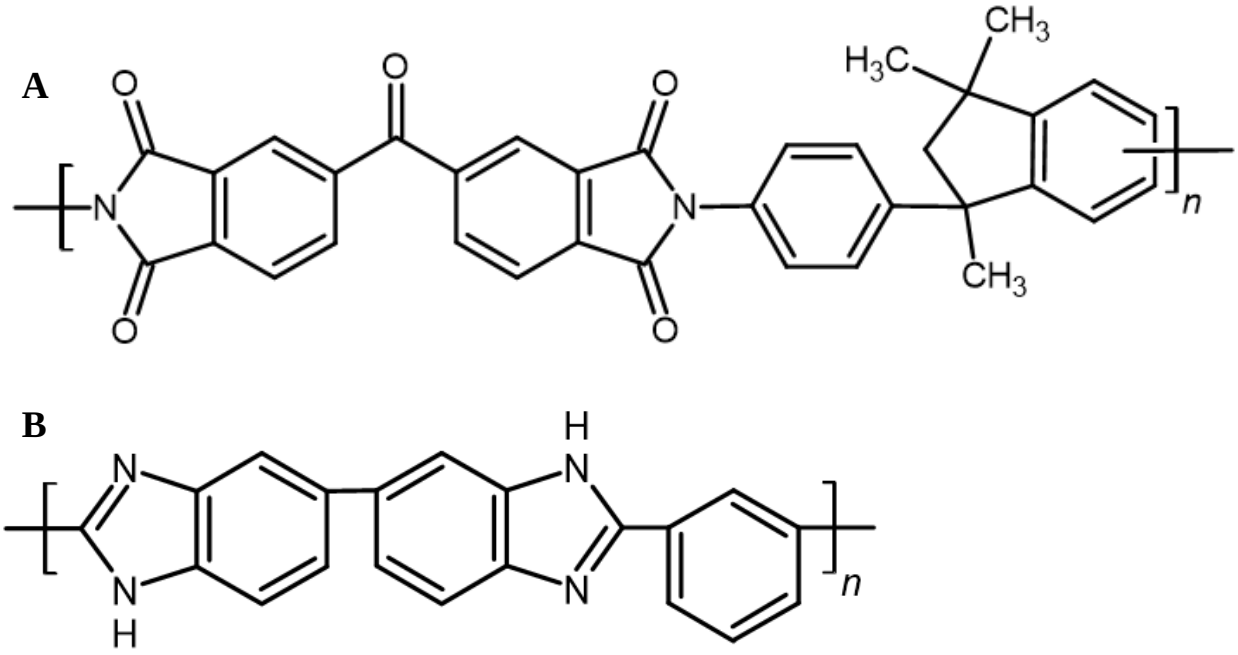

Fig 3.1. Structures of (A) Matrimid® and (B) PBI.

Fig 3.2. Optical image of a zirconia-coated stainless steel tubular support.

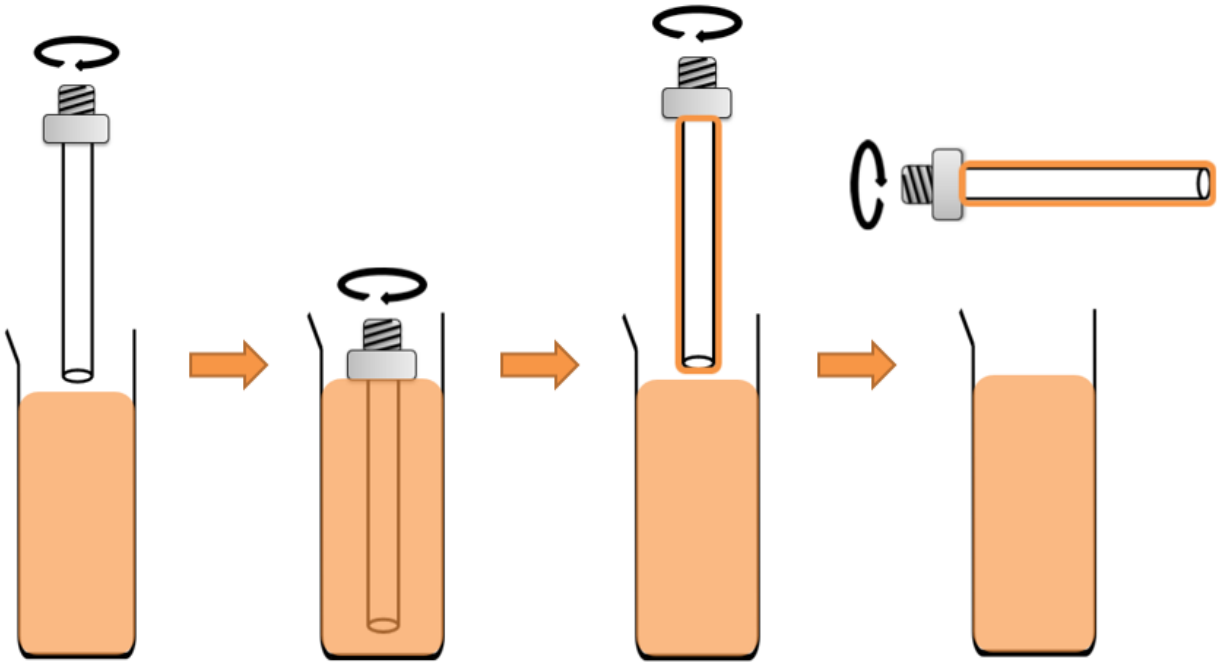

Fig 3.3. Schematic of dip-coating technique for tubular support.

A

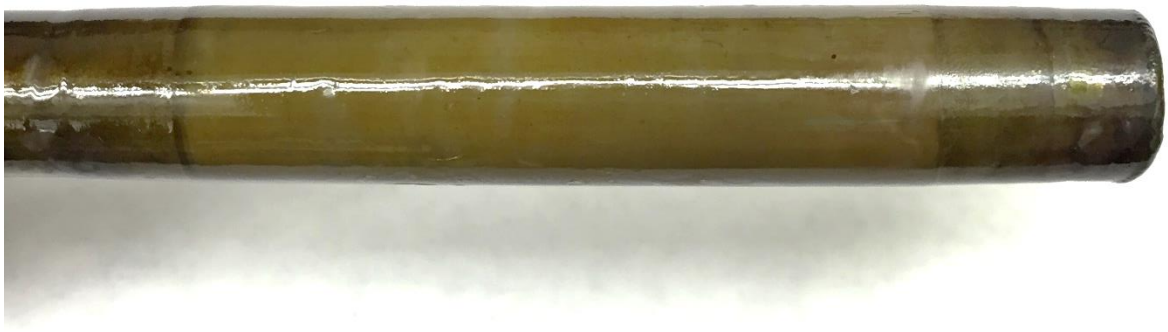

B

Fig 3.4. Optical images of tubular polymeric membranes: (A) Matrimid® and (B) PBI.

Table 3.1. Pure gas and mixed gas permeability and selectivity for flat and tubular Matrimid® membranes measured at 35 °C and 3 atm.

	Tubular	Flat [67]
H_2 permeance (GPU)	1.81	-
CO_2 permeance (GPU)	0.48	-
H_2 permeability (Barrer)	*32.53 ± 0.03	28.88
CO_2 permeability (Barrer)	8.65 ± 0.02	9.52
H_2/CO_2 ideal selectivity	3.8	3.0
H_2/CO_2 mixed gas selectivity	2.5	2.6

*Average of 2 membranes
1 Barrer = 1×10^{-10} $cm^3_{(STP)}$ cm cm^{-2} s^{-1} $cmHg^{-1}$

Table 3.2. Pure gas and mixed gas permeability and selectivity for flat and tubular PBI membranes measured at 300 °C and at various pressures.

Temperature (°C)	300	300	300
Pressure (atm)	10	20	30
Flat PBI			
H_2 permeance (GPU)	3.14	3.16	3.20
CO_2 permeance (GPU)	0.13	0.13	0.13
H_2 permeability (Barrer)	*50.26 ± 0.21	50.53± 0.26	51.25± 0.28
CO_2 permeability (Barrer)	2.13± 0.04	2.15± 0.04	2.01± 0.05
H_2/CO_2 ideal selectivity	23.6	23.5	25.5
Tubular PBI			
H_2 permeance (GPU)	2.46	2.42	2.43
CO_2 permeance (GPU)	0.12	0.12	0.11
H_2 permeability (Barrer)	39.34 ± 0.11	38.75 ± 0.12	38.84 ± 0.11
CO_2 permeability (Barrer)	1.93 ± 0.02	1.92 ± 0.02	1.82 ± 0.02
H_2/CO_2 ideal selectivity	20.4	20.2	21.3
H_2/CO_2 mixed gas selectivity	-	-	17.8

*Average of 2 membranes
1 Barrer = 1×10^{-10} $cm^3_{(STP)}$ cm cm^{-2} s^{-1} $cmHg^{-1}$

Table 3.3. Pure gas and mixed gas permeability and selectivity for tubular Matrimid® membranes measured at 300 °C and at various pressures.

	10 atm	20 atm	30 atm
H_2 permeance (GPU)	27.1	27.8	30.5
CO_2 permeance (GPU)	5.24	5.36	5.20
H_2 permeability (Barrer)	487.82	500.61	548.81
CO_2 permeability (Barrer)	94.32	96.43	93.66
H_2/CO_2 ideal selectivity	5.2	5.2	5.9
H_2/CO_2 mixed gas selectivity	-	-	4.2

1 Barrer = 1×10^{-10} $cm^3_{(STP)}$ cm cm^{-2} s^{-1} $cmHg^{-1}$

REFERENCES

[1] S. Sircar, T.C. Golden, Purification of hydrogen by pressure swing adsorption, *Sep. Sci. Technol.* **2000**, *35*, 667–687.

[2] P. Bernardo, E. Drioli, G. Golemme, Membrane gas separation: A review/state of the art, *Ind. Eng. Chem. Res.* **2009**, *48*, 4638–4663.

[3] L.M. Robeson, *Polymer Blends: A Comprehensive Review*, Hanser Gardner Publications: Cincinnati, OH, **2007**.

[4] A.F. Ismail, L.I.B. David, A review on the latest development of carbon membranes for gas separation, *J. Membr. Sci.* **2001**, *193*, 1–18.

[5] A.F. Ismail, R.A. Rahim, W.A. Rahman, Characterization of polyethersulfone/Matrimid 5218 miscible blend mixed matrix membranes for O_2/N_2 gas separation, *Sep. Purif. Technol.* **2008**, *63*, 200–206.

[6] F. Aziz, A.F. Ismail, Preparation and characterization of cross-linked Matrimid membranes using para-phenylenediamine for O_2/N_2 separation, *Sep. Purif. Technol.* **2010**, *73*, 421–428.

[7] W.F. Yong, F.Y. Li, Y.C. Xiao, T.S. Chung, Y.W. Tong, High performance PIM-1/Matrimid hollow fiber membranes for CO_2/CH_4, O_2/N_2 and CO_2/N_2 separation, *J. Membr. Sci.* **2013**, *443*, 156–169.

[8] T.C. Merkel, H. Lin, X. Wei, R. Baker, Power plant post-combustion carbon dioxide capture: An opportunity for membranes, *J. Membr. Sci.* **2010**, *359*, 126–139.

[9] C.E. Powell, G.G. Qiao, Polymeric CO_2/N_2 gas separation membranes for the capture of carbon dioxide from power plant flue gases, *J. Membr. Sci.* **2006**, *279*, 1–49.

[10] T.E. Rufford, S. Smart, G.C.Y. Watson, B.F. Graham, J. Boxall, J.C. Diniz da Costa, E.F. May, The removal of CO_2 and N_2 from natural gas: A review of conventional and emerging process technologies, *J. Pet. Sci. Eng.* **2012**, *94–95*, 123–154.

[11] P. Shao, M.M. Dal-Cin, M.D. Guiver, A. Kumar, Simulation of membrane-based CO_2 capture in a coal-fired power plant, *J. Membr. Sci.* **2013**, *427*, 451–459.

[12] R. Harmon, W.H. Isalski, Purge gas purification and recovery in ammonia plants., *Ammon. Plant Saf. Relat. Facil.* **1981**, *23*, 39–43.

[13] P. Petit, Hydrogen recovery from ammonia synthesis plant., *Indian J. Cryog.* **1982**, *7*, 155–161.

[14] M.R. Rahimpour, A. Asgari, Production of hydrogen from purge gases of ammonia plants in a catalytic hydrogen-permselective membrane reactor, *Int. J. Hydrogen Energy* **2009**, *34*,

5795–5802.

[15] S.W. Lee, J.S. Park, C.B. Lee, D.W. Lee, H. Kim, H.W. Ra, S.H. Kim, S.K. Ryi, H_2 recovery and CO_2 capture after water-gas shift reactor using synthesis gas from coal gasification, *Energy* **2014**, *66*, 635–642.

[16] A.E. Lewis, D.C. Kershner, S.N. Paglieri, M.J. Slepicka, J.D. Way, Pd-Pt/YSZ composite membranes for hydrogen separation from synthetic water-gas shift streams, *J. Membr. Sci.* **2013**, *437*, 257–264.

[17] Y. Bi, H. Xu, W. Li, A. Goldbach, Water–gas shift reaction in a Pd membrane reactor over $Pt/Ce_{0.6}Zr_{0.4}O_2$ catalyst, *Int. J. Hydrogen Energy* **2009**, *34*, 2965–2971.

[18] D. Parsley, R.J. Ciora, D.L. Flowers, J. Laukaitaus, A. Chen, P.K.T. Liu, J. Yu, M. Sahimi, A. Bonsu, T.T. Tsotsis, Field evaluation of carbon molecular sieve membranes for the separation and purification of hydrogen from coal- and biomass-derived syngas, *J. Membr. Sci.* **2014**, *450*, 81–92.

[19] A Harale, H. Hwang, P. Liu, M. Sahimi, T. Tsotsis, Experimental studies of a hybrid adsorbent-membrane reactor (HAMR) system for hydrogen production, *Chem. Eng. Sci.* **2007**, *62*, 4126–4137.

[20] P.S. Lee, D. Kim, S.E. Nam, R.R. Bhave, Carbon molecular sieve membranes on porous composite tubular supports for high performance gas separations, *Microporous Mesoporous Mater.* **2016**, *224*, 332–338.

[21] J. Schwinge, P.R. Neal, D.E. Wiley, D.F. Fletcher, A.G. Fane, Spiral wound modules and spacers: Review and analysis, *J. Membr. Sci.* **2004**, *242*, 129–153.

[22] K. Ramasubramanian, M. Song, W.S.W. Ho, Spiral-wound water-gas-shift membrane reactor for hydrogen purification, *Ind. Eng. Chem. Res.* **2013**, *52*, 8829–8842.

[23] H. Jiang, H. Wang, S. Werth, T. Schiestel, J. Caro, Simultaneous production of hydrogen and synthesis gas by combining water splitting with partial oxidation of methane in a hollow-fiber membrane reactor, *Angew. Chemie - Int. Ed.* **2008**, *47*, 9341–9344.

[24] O.C. David, D. Gorri, K. Nijmeijer, I. Ortiz, A. Urtiaga, Hydrogen separation from multicomponent gas mixtures containing CO, N_2 and CO_2 using matrimid asymmetric hollow fiber membranes, in: Procedia Eng., **2012**: pp. 1117–1118.

[25] N. Peng, N. Widjojo, P. Sukitpaneenit, M.M. Teoh, G.G. Lipscomb, T.S. Chung, J.Y. Lai, Evolution of polymeric hollow fibers as sustainable technologies: Past, present, and future, *Prog. Polym. Sci.* **2012**, *37*, 1401–1424.

[26] H. Li, J.W. Dijkstra, J.A.Z. Pieterse, J. Boon, R.W. Van Den Brink, D. Jansen, WGS-mixture

separation and WGS reaction test in a bench-scale multi-tubular membrane reactor, *Energy Procedia* **2011**, *4*, 666–673.

[27] E. Piera, C.A.M. Brenninkmeijer, J. Santamaría, J. Coronas, Separation of traces of CO from air using MFI-type zeolite membranes, *J. Membr. Sci.* **2002**, *201*, 229–232.

[28] H. Kalipcilar, T.C. Bowen, R.D. Noble, J.L. Falconer, Synthesis and separation performance of SSZ-13 zeolite membranes on tubular supports, *Chem. Mater.* **2002**, *14*, 3458–3464.

[29] M.P. Bernal, E. Piera, J. Coronas, M. Menéndez, J. Santamaría, Mordenite and ZSM-5 hydrophilic tubular membranes for the separation of gas phase mixtures, *Catal. Today* **2000**, *56*, 221–227.

[30] S. Aguado, C.-H. Nicolas, V. Moizan-Baslé, C. Nieto, H. Amrouche, N. Bats, N. Audebrand, D. Farrusseng, Facile synthesis of an ultramicroporous MOF tubular membrane with selectivity towards CO_2, *New J. Chem.* **2011**, *35*, 41.

[31] X. Zhang, Y. Liu, L. Kong, H. Liu, J. Qiu, W. Han, L.-T. Weng, K.L. Yeung, W. Zhu, A simple and scalable method for preparing low-defect ZIF-8 tubular membranes, *J. Mater. Chem. A*. **2013**, *1*, 1063510638.

[32] L. Kong, X. Zhang, Y. Liu, S. Li, H. Liu, J. Qiu, K.L. Yeung, In situ fabrication of high-permeance ZIF-8 tubular membranes in a continuous flow system, *Mater. Chem. Phys.* **2014**, *148*, 10–16.

[33] S.M. Saufi, A.F. Ismail, Fabrication of carbon membranes for gas separation - A review, *Carbon* **2004**, *42*, 241–259.

[34] N. Muruganandam, Composite cellulose acetate/poly blend gas separation membranes, *Polymer* **1994**, *94*, 313–328.

[35] S.C. Kumbharkar, K. Li, Structurally modified polybenzimidazole hollow fibre membranes with enhanced gas permeation properties, *J. Membr. Sci.* **2012**, *415–416*, 793–800.

[36] F. Li, W. Meindersma, A.B. De Haan, T. Reith, Optimization of commercial net spacers in spiral wound membrane modules, *J. Membr. Sci.* **2002**, *208*, 289–302.

[37] A.I. Radu, M.S.H. van Steen, J.S. Vrouwenvelder, M.C.M. Van Loosdrecht, C. Picioreanu, Spacer geometry and particle deposition in spiral wound membrane feed channels, *Water Res.* **2014**, *64*, 160–176.

[38] W. Qiu, L. Xu, C.-C. Chen, D.R. Paul, W.J. Koros, Gas separation performance of 6FDA-based polyimides with different chemical structures, *Polymer* **2013**, *54*, 6226–6235.

[39] Y. Kase, *Gas separation by polyimide membranes*, in: Adv. Membr. Technol. Appl., John Wiley & Sons, Inc., Hoboken, NJ, USA., **2008**: pp. 581–598.

[40] H. Kawakami, K. Nakajima, H. Shimizu, S. Nagaoka, Gas permeation stability of asymmetric polyimide membrane with thin skin layer: Effect of polyimide structure, *J. Membr. Sci.* **2003**, *212*, 195–203.

[41] C. Zhang, Y. Dai, J.R. Johnson, O. Karvan, W.J. Koros, High performance ZIF-8/6FDA-DAM mixed matrix membrane for propylene/propane separations, *J. Membr. Sci.* **2012**, *389*, 34–42.

[42] L. Shao, C.H. Lau, T.S. Chung, A novel strategy for surface modification of polyimide membranes by vapor-phase ethylenediamine (EDA) for hydrogen purification, *Int. J. Hydrogen Energy* **2009**, *34*, 8716–8722.

[43] T. Yang, T.-S. Chung, High performance ZIF-8/PBI nano-composite membranes for high temperature hydrogen separation consisting of carbon monoxide and water vapor, *Int. J. Hydrogen Energy* **2013**, *38*, 229–239.

[44] S.H. Han, J.E. Lee, K.J. Lee, H.B. Park, Y.M. Lee, Highly gas permeable and microporous polybenzimidazole membrane by thermal rearrangement, *J. Membr. Sci.* **2010**, *357*, 143–151.

[45] K.A. Berchtold, R.P. Singh, J.S. Young, K.W. Dudeck, Polybenzimidazole composite membranes for high temperature synthesis gas separations, *J. Membr. Sci.* **2012**, *415–416*, 265–270.

[46] M.J.C. Ordoñez, K.J. Balkus, Jr., J.P. Ferraris, I.H. Musselman, Molecular sieving realized with ZIF-8/Matrimid mixed-matrix membranes, *J. Membr. Sci.* **2010**, *361*, 28–37.

[47] T. Brinkmann, J. Pohlmann, U. Withalm, J. Wind, T. Wolff, Theoretical and experimental investigations of flat sheet membrane module types for high capacity gas separation applications, *Chemie-Ingenieur-Technik*. **2013**, *85*, 1210–1220.

[48] T. Brinkmann, C. Naderipour, J. Pohlmann, J. Wind, T. Wolff, E. Esche, D. Müller, G. Wozny, B. Hoting, Pilot scale investigations of the removal of carbon dioxide from hydrocarbon gas streams using poly (ethylene oxide)-poly (butylene terephthalate) PolyActive^{TM}) thin film composite membranes, *J. Membr. Sci.* **2015**, *489*, 237–247.

[49] W.H. Chen, W.Z. Syu, C.I. Hung, Y.L. Lin, C.C. Yang, Influences of geometry and flow pattern on hydrogen separation in a Pd-based membrane tube, *Int. J. Hydrogen Energy* **2013**, *38*, 1145–1156.

[50] R. Mahajan, W.J. Koros, Mixed matrix membrane materials with glassy polymers. Part 2, *Polym. Eng. Sci.* **2002**, *42*, 1432–1441.

CHAPTER 4

ZIF-8/(PBI/6FDA-DAM) IMMISCIBLE POLYMER BLEND MEMBRANES FOR HIGH PRESSURE, HIGH TEMPERATURE H_2/CO_2 SEPARATION

ABSTRACT

In this work, 50:50 PBI/6FDA-DAM immiscible polymer blend membranes were fabricated with various loadings of ZIF-8 nanoparticles to form mixed-matrix membranes. The ZIF-8 nanoparticles control the shape and size of the dispersed 6FDA-DAM domains. The membranes were tested for the separation of H_2/CO_2 under industrially relevant conditions of composition, pressure, and temperature. The membrane morphologies were found to have a significant impact on gas permeability and H_2/CO_2 selectivity. With a 50:50 H_2/CO_2 mixture at 30 atm and 300 °C, the membranes exhibited a high H_2 permeability of 358 Barrers and a H_2/CO_2 selectivity of 12.8, which surpasses the Robeson upper bound for H_2/CO_2 separations. This work shows for the first time that polymer blend mixed-matrix membranes can be used for H_2/CO_2 separations at pressures up to 30 atm and temperatures up to 300 °C, exhibiting promising results for the production of clean fuel.

.

4.1 INTRODUCTION

Clean energy has grown in importance as environmental pollution and climate deterioration increases. H_2 is a high energy density carrier that only generates water after combustion and is considered a clean energy resource that can be used in gas turbines for the generation of electricity and in fuel cells for energy production [1–3]. H_2 is also consumed in large quantities in processes such as crude oil refining [4], fertilizer production [5], and metal processing [6]. H_2 is becoming a major commodity chemical, and the clean production of H_2 has become an important technological challenge.

H_2 is produced industrially via the steam reforming of natural gas, gasoline, or diesel, or via gasification processes using biomass or coal [7–9]. Both processes operate at high temperature in the presence of water to produce synthesis gas (syngas), a mixture consisting of 25-30% H_2, 30-60% CO, and 5-15% CO_2 [10]. Depending on the type of catalyst employed, the water-gas shift (WGS) reaction is subsequently performed to generate more H_2 from the syngas by reacting CO with water at 200 to 300 °C (low temperature catalyst) or at 300 to 400 °C (high temperature catalyst) [11]. While H_2 is generated through this two-step process, a significant amount of CO_2 is simultaneously generated that must be separated from H_2, not only because CO_2 is a greenhouse gas, but also because H_2 purification is required before transport to prevent pipeline corrosion by CO_2. Conventionally, processes based on phase equilibria, such as pressure swing adsorption [12,13] and cryogenic distillation [14], are used for gas separations. Nevertheless, major drawbacks, including a large footprint, high cost, and high energy consumption, limit the effectiveness of these processes [15]. In contrast, membrane technology for gas separations does not require phase change and, hence, is more economical and less energy intensive [16]. Moreover,

membranes have a smaller footprint, less environmental impact, are easier to operate, and require less maintenance than conventional methods [14,17].

For H_2/CO_2 separations at industrially relevant conditions, sustaining the mechanical and chemical stability of the membranes at high pressure (30-60 atm) and high temperature (200-400 °C) is the primary challenge for selecting the membrane materials. Polybenzimidazole (PBI, Fig. 4.1A) is a high performance polymer that exhibits high thermal and chemical stability. PBI's glass transition temperature (T_g) is above 400 °C, and its rigid structure makes it resilient even at temperatures above 300 °C [18]. Additionally, PBI is mechanically robust and easy to process, which is desirable for membrane fabrication. PBI membranes exhibit high selectivity for H_2 over CO_2 at high temperature (H_2/CO_2 = 43 at 250 °C) [19], however, its H_2 permeability (58 Barrers at 250 °C) is relatively low due to its rigid structure. In order to enhance the gas permeability, and hence the gas flux, various permeable materials have been added to PBI to form composite membranes. For example, hybrid organic-inorganic materials, such as zeolitic imidazolate frameworks (e.g., ZIF-7 and ZIF-8), were added to PBI to form mixed-matrix membranes (MMMs) [20–22]. Polymeric materials, such as Matrimid®, were also combined with PBI to form polymer blend membranes [23]. These composite membranes exhibited a significant increase in H_2 permeability, while maintaining H_2/CO_2 selectivity as compared to pure PBI.

While most PBI-based membranes with additives exhibit improved gas transport properties, concern still remains regarding the performance of PBI-based membranes under high pressure and high temperature. In the open literature, most PBI-based composite membranes have been tested at either low pressure (2-5 atm) or ambient temperature at the lab scale. Several PBI-based membranes have been tested at higher temperatures that range from 230 to 400 °C, but only at

pressures ranging from 2 to 8 atm [18,19,24]. None has been tested under both high pressure (>30 atm) and high temperature (> 300 °C) conditions, which would truly reflect the performance of these membranes. In this study, PBI-based membranes with different loadings of additives were fabricated, characterized, and tested for H_2 and CO_2 gas permeation at low pressure and low temperature as well as at high pressure and high temperature. A high performance and highly permeable polymer, 6FDA-DAM (Fig. 4.1B), was blended with PBI to improve the gas permeability while maintaining the high H_2/CO_2 selectivity of PBI. 6FDA-based polymers exhibit T_g values above 300 °C [25], which are suitable for high temperature applications. They have been used in polymer blend membranes and have shown significant enhancements in gas permeability [26]. The 50:50 PBI/6FDA-DAM immiscible polymer blend in this work was compatibilized by introducing small amounts (5, 10, and 20 wt%) of ZIF-8 nanoparticles to form MMMs. ZIF-8 is a hybrid framework material consisting of Zn atoms and 2-methylimidazolate linkers. ZIF-8 has the sodalite-type topology (Fig. 4.1C) with a pore aperture of 3.4 Å and a cage diameter of 11.1 Å. ZIF-8 is well known for its exceptional chemical and thermal stability [27]. ZIF-8 has been widely used in membranes to enhance gas separation properties [28–33]. It has also been reported that ZIF-8 nanoparticles can control the microstructure in an immiscible polymer blend by reducing the polymer interfacial surface tension and limiting the coalescence of the dispersed phase, thus forming membranes with better uniformity [34]. Due to the high thermal stability of the individual components, PBI, 6FDA-DAM, and the fabricated ZIF-8/(PBI/6FDA-DAM) MMMs were tested for H_2/CO_2 separations at 30 atm and 300 °C using pure H_2 and CO_2 as well as an equimolar mixture.

4.2 EXPERIMENTAL

4.2.1 Materials

All chemicals and solvents were used as received unless otherwise noted. Anhydrous *N,N*-dimethyl acetamide (DMAc, 99.8% purity) and methanol (MeOH, 98% purity) were purchased from EMD Chemicals, Inc. and Fisher Scientific, respectively. Anhydrous 1-methyl-2-pyrrolidone (NMP, 99.8% purity), tetrahydrofuran (THF), and 2-methylimidazole (Hmim) were purchased from Sigma-Aldrich. All organic solvents were dried using activated type 4A molecular sieves prior to use. 4,4-(Hexafluoroisopropylidene) diphthalic anhydride (6FDA, >99% purity) was purchased from Akron Polymer Systems, Inc. and was dried under vacuum at 150 °C prior to use. 2,4,6-Trimethyl-1,3-phenylenediamine (DAM, >97% purity) was purchased from TCI America and purified by vacuum sublimation. Zinc nitrate hexahydrate ($Zn(NO_3)_2 \cdot 6H_2O$, 98% purity) was purchased from EMD Chemicals Inc. Polybenzimidazole (PBI) S26 solution (26% (w/w) in DMAc, 1.5% (w/w) LiCl, $M_w \sim 30{,}000$) was purchased from PBI Performance Products, Inc. and used as received. For gas permeation experiments, H_2, CO_2, N_2, He, and a certified H_2/CO_2 (50:50) mixture were purchased from Airgas, Inc. The purities of all the gases were greater than 99.99%. Tubular supports (AccuSep®) coated with a 10 μm thick zirconia layer (pore size of 0.1 μm and a total area of 13.8 cm^2) on top of the tubular 316L stainless steel porous supports were obtained from Pall Corporation.

4.2.2 Synthesis of ZIF-8

Colloidal ZIF-8 was synthesized following a reported procedure [35]. In a typical ZIF-8 synthesis, a solution of $Zn(NO_3)_2 \cdot 6H_2O$ (1.467 g, 4.94 mmol) in 100 mL of methanol was added to a solution of Hmim (3.245 g, 39.52 mmol) in 100 mL of methanol. The mixture was stirred for

1 h, and the resulting ZIF-8 particles were separated by centrifugation. Then, the ZIF-8 particles were washed three times with methanol and three times with DMAc. A portion of the ZIF-8 particles was dried at 150 ºC under vacuum for 1 d for characterization, and the remaining was stored in DMAc as a colloidal suspension.

4.2.3 Synthesis of 6FDA-DAM

6FDA-DAM was synthesized using a reported procedure [36,37]. 6FDA and DAM were purified by vacuum sublimation before the polymer synthesis. The polymerization was accomplished at 25 °C in a 100 mL 3-necked round bottomed flask under a nitrogen atmosphere. 6FDA (2.00 g, 4.5 mmol) was dissolved in 7.5 mL of NMP and added dropwise into a 3.0 mL solution of 0.68 g of DAM (4.5 mmol) in NMP. The mixture was stirred for 26 h and then 1.7 mL (18.0 mmol) of acetic anhydride and 2.6 mL (18.0 mmol) of trimethylamine were added to the flask to induce imidization of the polyamic acid. After 26 h, the polyimide was precipitated into methanol, separated by vacuum filtration, and dried in a vacuum oven at 120 °C for 48 h. The weight average molecular weight and PDI of the synthesized 6FDA-DAM were 75,000 Da and 1.64, respectively, determined using a gel permeation chromatograph (Viscotek GPCmax, VE2001) equipped with a Viscotek TDA 302 Triple Array Detector and two ViscoGEL I-Series (I-MBHMW 3078, Viscotek) columns.

4.2.4 Membrane Fabrication

4.2.4.1 Polymer Blend Membrane Fabrication

To fabricate a 50:50 (w/w) PBI/6FDA-DAM polymer blend membrane, 2 wt% solutions of PBI in DMAc and 6FDA-DAM in DMAc were stirred separately at 80 °C for 1 d. The 6FDA-

DAM solution was added to the PBI solution and the mixture was stirred at 80 °C for 2 h. The mixture was then concentrated to 15 wt% by evaporating excess DMAc at 80 °C and then cast onto a glass substrate using a Sheen Automatic Film Applicator (1133N) equipped with an adjustable blade forming a flat membrane. The formed membranes were then dried in a N_2-purged heated drying table at 50 °C for 4 h, peeled off the glass substrate, and annealed following a reported protocol in a vacuum oven at 80 °C for 1d, 150 °C for 12 h, 200 °C for 12 h, and 250 °C for 1d [34].

4.2.4.2 MMM Fabrication

Flat 5, 10, and 20 wt% ZIF-8/(PBI/6FDA-DAM) MMMs were fabricated in the same fashion as the polymer blend membranes maintaining the composition of the polymers at 50:50 (w/w). The colloidal ZIF-8 nanoparticles were added to the PBI solution and stirred at 80 °C for 12 h in a capped vial. Then, the 6FDA-DAM solution was added to the ZIF-8/PBI mixture and stirred at 80 °C for 2 h after which the solution was concentrated to 15 wt% by evaporating excess DMAc at 80 °C. The casting, drying, and annealing of the MMMs were performed following the same protocols used for the polymer blend membranes.

4.2.4.3 Tubular Membrane Fabrication

Tubular membranes of PBI, PBI/6FDA-DAM, and 5 and 10 wt% ZIF-8/(PBI/6FDA-DAM) MMMs were prepared by dip-coating the tubular supports. The coating solutions were prepared following the procedures described for the polymer blends and the MMMs, except that the solutions were concentrated to 8 wt%. The tubular support was immersed and removed from the coating solution at 1 cm/s and then rotated at 60 rpm at room temperature for 4 h. The drying and

annealing of the tubular membranes were performed following the same protocol used for the polymer blend membranes.

4.2.5 Characterization

4.2.5.1 Characterization of ZIF-8 and Membranes

Samples of the as-synthesized ZIF-8 nanoparticles, 50:50 PBI/6FDA-DAM polymer blend membrane, and 5, 10, and 20 wt% ZIF-8/(PBI/6FDA-DAM) MMMs were characterized by X-ray diffraction (XRD), scanning electron microscopy (SEM), and thermogravimetric analysis (TGA). XRD patterns were obtained using a Rigaku Ultima III diffractometer with Cu K_α X-ray radiation. The patterns were acquired from 5 to 40° 2θ at a rate of 1°/min. A LEO 1530 VP ultra-high-resolution SEM equipped with a field emission gun operated at 10 keV was used to acquire secondary electron images to determine the morphology and particle size of the ZIF-8 nanoparticles as well as the morphologies and thicknesses of the membranes. Cross-sections of the membranes were prepared by freeze-fracture in liquid nitrogen. Prior to imaging, the samples were sputter-coated with Au/Pd using a Denton Vacuum Desk II sputter coater. A Perkin-Elmer Pyris-1 TGA instrument was used to determine the thermal stability of the samples under N_2. The temperature was increased from 100 to 700 °C at a rate of 5 °C/min and then from 700 to 1000 °C at 10 °C/min. In addition, a long term thermal stability analysis was conducted by loading a 5 wt% ZIF-8/(PBI/6FDA-DAM) MMM in the TGA to monitor the weight loss at 300 °C for 1 d.

4.2.5.2 Gas Permeation

Single gas permeation measurements at 35 °C and 3 atm were performed using a custom-built gas permeameter described previously [38]. A stainless steel permeation cell was used to

house the flat membrane that separated the system into an upstream and a downstream side with constant volumes. Before experiments started, the permeameter was evacuated for 12 h after which the leak rate of the instrument in the downstream side was measured. In a typical experiment, the permeameter exposed the upstream side of the membrane to a constant feed pressure, e.g., 3 atm, and then measured the gas flux through the membrane as pressure increments in the downstream side until the steady state was achieved. The duration of the experiments was 6 h. Two separately fabricated membranes were tested a minimum of four times each with H_2 and CO_2.

Gas permeation measurements at 300 °C and at pressures ranging from 5 to 30 atm were conducted using a custom-built high pressure, high temperature (HPHT) gas permeameter equipped with mass flow meters on the downstream side, mass flow controllers to purge the retentate on the upstream side, and pressure transducers on both the upstream and downstream sides. The HPHT permeameter was designed to measure the gas flow rate across the membrane at a constant downstream pressure of 1 atm. A stainless steel tubular permeation cell was used to house the tubular membrane (Fig. 4.2). Permeability experiments were conducted by pressurizing the upstream side volume to a set pressure after the membrane reached the experimental temperature. As the gases permeated through the membrane and entered the downstream side, the permeate flow rate was measured and recorded with mass flow meters. The permeability, P, expressed in Barrers (1 Barrer = 1×10^{-10} $cm^3_{(STP)}$ cm cm^{-2} s^{-1} $cmHg^{-1}$) can be calculated using Equation (4.1) with the measured flow rate J, the membrane thickness l, the differential pressure across the membrane ΔP, and the exposed membrane area A. In practice, however, when the constant volume method to measure gas permeation is used, Equation (4.2) can be used to calculate permeability by incorporating experimental parameters and constants like the downstream

pressure gradient at the steady state *dp/dt*, the volume of the downstream side V_{cell}, the operating temperature *T*, the average feed pressure $\overline{USP}$, the molar volume of gas V_m, and the gas constant *R*. Alternatively, if the membrane thickness cannot be measured accurately, the gas permeance *Q*, expressed in GPU (1 GPU = 1×10^{-6} $cm^3_{(STP)}$ cm^{-2} s^{-1} $cmHg^{-1}$), can be calculated using Equation (4.3):

$$P = \frac{J \cdot l}{\Delta P \cdot A} \quad \text{(Eq. 4.1)}$$

$$P = \frac{V_m \cdot V_{cell} \cdot l \cdot dp/dt}{R \cdot T \cdot A \cdot \overline{USP}} \quad \text{(Eq. 4.2)}$$

$$Q = \frac{P}{l} \quad \text{(Eq. 4.3)}$$

For 50:50 H_2/CO_2 mixed gas permeability measurements at 300 °C and 30 atm, the stage cut of the membrane (% recovery) was maintained at 0.2 (20%) by purging the retentate through a mass flow controller to keep the feed composition constant. The permeate composition was determined using a SRI gas chromatograph (8610C) equipped with a molecular sieve column (MOL SIEVE 13X), a polymer column (HAYESEP D), and a TCD detector. N_2 and He were used as the carrier gases to measure the concentrations of H_2 and CO_2, respectively. For each tubular membrane composition, two separately coated membranes were tested a minimum of six times each with H_2 and CO_2.

4.3 RESULTS AND DISCUSSION

4.3.1 Characterization of ZIF-8

The experimental XRD pattern of the synthesized ZIF-8 nanoparticles confirmed the material was ZIF-8 since the 2θ° positions of the peaks and the ratios of the peak intensities are

consistent with the theoretical XRD pattern (Fig. 4.3) [39]. The positions of the main peaks of the synthesized ZIF-8 match those in the theoretical pattern at 2θ = 7.3°,12.7°, and 18.0°. The SEM image in Fig. 4.4 shows that the ZIF-8 particles have diameters ranging from 30 to 80 nm with a cubic morphology that represents the sodalite-related framework [40]. The ZIF-8 nanoparticles synthesized using methanol in this work are smaller than those synthesized using dimethylformamide (50-150 nm) [33] as well as the commercially available Basolite® Z1200 (200 nm) [32]. Since the ZIF-8 nanoparticles were incorporated into the 50:50 PBI/6FDA-DAM blend in the colloidal form, they were expected to have better dispersion and less aggregation in the membrane when compared to ZIF-8 added in the dried form [33]. The TGA plot for the synthesized ZIF-8 in Fig. 4.5 shows no weight loss from 100 to 200 °C, a 10% weight loss from 200 to 500 °C that resulted from the removal of residual solvent and guest molecules trapped in the pores, and a significant weight loss beyond 500 °C due to the decomposition of ZIF-8 [27].

4.3.2 Membrane Characterization

4.3.2.2 Thermal Stability

PBI and 6FDA-DAM are high performance polymers that have high T_g (PBI T_g = 425 °C, 6FDA-DAM T_g = 395 °C) and thermal stability. Thermogravimetric analysis of the polymers (Fig. 4.5) shows that PBI and 6FDA-DAM are thermally stable up to 450 °C. PBI exhibited a 6% weight loss from 100 to 170 °C due to the removal of moisture and residual DMAc solvent (boiling point: 165 °C), and reached a plateau up to 300 °C. A similar weight loss of up to 6% was observed for the 50:50 PBI/6FDA-DAM blend and for the ZIF-8 compatibilized MMMs at temperatures up to 300 °C that was also attributed to the removal of moisture and residual solvent. For the MMMs, the major weight loss occurred above 480 °C signaling the decomposition of the materials.

Thermal analysis of the 5 wt% ZIF-8/(PBI/6FDA-DAM) MMM (Fig. 4.6) showed the MMM did not lose weight over a period of 1 d at a constant temperature of 300 °C, confirming the resilience of the MMMs at 300 °C over this timeframe.

4.3.2.3 Membrane Morphology

SEM images of the freeze-fractured membrane cross-sections (Fig. 4.7) show the size, shape, and continuity of the dispersed phase in the membranes. For the 50:50 PBI/6FDA-DAM immiscible blend membranes (Fig. 4.7A), a matrix-droplet structure with ellipsoidal dispersed domains embedded in a continuous matrix was observed. By selectively extracting 6FDA-DAM with THF, the continuous and dispersed phases were identified. The SEM image of the THF-extracted 50:50 PBI/6FDA-DAM membrane (Fig. 4.7B) and the histogram (Fig. 4.7C) confirmed that PBI was the continuous phase and 6FDA-DAM was the dispersed phase with an average domain size of 6.9 ± 7.4 μm^2. The addition to the polymer blend of ZIF-8 nanoparticles as a compatibilizer significantly reduced both the size and the size distribution of the 6FDA-DAM domains in the MMMs (Fig. 4.7D, 7G). As shown in the SEM image of the THF-extracted cross-section of the 5 wt% ZIF-8/(PBI/6FDA-DAM) MMM (Fig. 4.7E) and its corresponding histogram (Fig. 4.7F), the domain sizes of the 6FDA-DAM phase were more uniform and smaller (0.89 ± 0.40 μm^2) than those in the 50:50 PBI/6FDA-DAM blend. As the loading of the ZIF-8 nanoparticles in the polymer blend increased, the domain sizes became even smaller and more uniform. The SEM images of the cross-sections of the 10 and 20 wt% ZIF-8/(PBI/6FDA-DAM) MMMs (Fig. 4.7G and 4.7J, respectively), the THF-extracted cross-sections (Fig. 4.7H and 4.7K, respectively), and their corresponding histograms (Fig. 4.7I and 4.7L, respectively) showed further reductions of the domain sizes, from 0.29 ± 0.16 μm^2 (10 wt% ZIF-8 loading) to 0.13 ± 0.11 μm^2

(20 wt% ZIF-8 loading), with increased ZIF-8 loadings. Compatibilization of a PBI/6FDA-DAM-DABA immiscible blend membrane using ZIF-8 particles revealed a similar size reduction for the dispersed phase [34].

The reduction of the domain size of the dispersed phase in the MMMs could be the result of improved compatibility between the two polymers in the blend in the presence of ZIF-8 nanocrystals. In emulsion chemistry, some additives can compatibilize immiscible polymers by impeding coalescence, leading to a more uniform distribution of the dispersed phase in the continuous phase [41]. During phase separation in the PBI/6FDA-DAM blend, the 6FDA-DAM tends to coalesce in order to reduce interfacial tension, leading to a non-uniform distribution of domain sizes. When ZIF-8 particles are added to the polymer blend, they migrate to the interface of the polymers thereby lowering the interfacial tension between the polymers. The low interfacial tension enhances the compatibility between the polymers and restricts the coalescence, hence, forming small and uniform dispersed domains. It is important to note that at 50:50 PBI/6FDA-DAM blend composition, the compatibilization effect of the ZIF-8 nanoparticles in the blend is high since the domain sizes are reduced from 6.9 ± 7.4 μm^2 for the polymer blend to 0.13 ± 0.11 μm^2 for the 20 wt% ZIF-8/(PBI/6FDA-DAM) MMM.

Similar size reductions of the dispersed 6FDA-DAM domains in PBI with ZIF-8 were observed for the tubular membranes. Due to the good adherence of the membranes to the tubular supports, only part of each tubular membrane was removed for analysis by SEM. The morphologies of the cross-sections (Fig. 4.8) also showed 6FDA-DAM as the dispersed phase and PBI as the continuous phase, indicating that the geometry of the membrane does not affect the membrane's morphology. Additionally, it can be seen that the sizes of 6FDA-DAM domains in

the tubular PBI/6FDA-DAM (6.0 ± 3.2 μm^2) and ZIF-8/(PBI/6FDA-DAM) MMM (0.76 ± 0.28 μm^2) membranes (Fig. 4.8A and 4.8B, respectively) are similar to those observed in the flat membranes (Fig. 4.7A and 4.7D, respectively).

4.3.3 Gas Permeation

4.3.3.2 Low Pressure, Low Temperature Gas Permeation

Low pressure (3 atm) and low temperature (35 °C) H_2 and CO_2 permeabilities in flat PBI, 6FDA-DAM, 50:50 PBI/6FDA-DAM, and the MMMs of the blend with 5, 10, and 20 wt% ZIF-8 loadings are summarized in Table 4.1. The 50:50 PBI/6FDA-DAM blend membrane exhibited a significant 393% increase in H_2 permeability from 1.37 Barrers (PBI) to 6.76 Barrers (blend), which stems from the incorporation of the highly permeable and less selective 6FDA-DAM polymer into the membrane, thereby reducing the effective membrane thickness and introducing more efficient diffusional paths. Compared to the pure PBI membrane, however, the 50:50 PBI/6FDA-DAM blend membrane exhibited a 44% decrease in H_2/CO_2 selectivity, from 27.4 to 15.2. Since the 50:50 PBI/6FDA-DAM blend was not compatibilized, the decrease in H_2/CO_2 selectivity may have resulted from the formation of voids at the interface of PBI and 6FDA-DAM due to poor interaction and large interfacial tension [26].

Compared to 50:50 PBI/6FDA-DAM blend membranes, the 5 wt% ZIF-8/(PBI/6FDA-DAM) MMMs exhibited a 36% decrease in H_2 permeability from 6.76 to 4.30 Barrers, but their selectivities (H_2/CO_2 = 25.2) were similar to PBI (H_2/CO_2 = 27.4) and higher than the 50:50 PBI/6FDA-DAM blend (H_2/CO_2 = 15.2). This increase in H_2/CO_2 selectivity may be due to the compatibilizing effect provided by ZIF-8 nanoparticles. The SEM image in Figure 4.4D shows that, when a small amount of ZIF-8 (e.g., 5 wt%) is present in the polymer blend membrane, the

ZIF-8 nanoparticles migrate to the polymer interface and enhance the compatibility and interaction between the polymers, lowering the surface tension between the polymers by reducing the size of the 6FDA-DAM domains, and consequently reducing the formation of voids at the interface [26,34]. Although the reduction of voids cannot be observed by SEM images, the high H_2/CO_2 selectivity of the 5 wt% ZIF-8/(PBI/6FDA-DAM) MMMs suggests that they have less voids than the 50:50 PBI/6FDA-DAM blend membranes. The presence of ZIF-8 nanoparticles in the polymer blends may also have acted as a barrier that mitigated the percolation effect by inducing the formation of discrete domains. This could explain the decreased gas permeability and improved H_2/CO_2 selectivity of the 5 wt% ZIF-8/(PBI/6FDA-DAM) MMMs compared to the 50:50 PBI/6FDA-DAM blend membranes (Table 4.1).

Although the presence of 5 wt% ZIF-8 in the polymer blend improved the separation properties of the membranes, ZIF-8 loadings above 5 wt% resulted in increased permeabilities and decreased H_2/CO_2 selectivities (Table 4.1). Compared to the 5 wt% ZIF-8/(PBI/6FDA-DAM) MMMs, the 10 wt% ZIF-8/(PBI/6FDA-DAM) MMMs exhibited an increase in permeability for H_2, from 4.30 Barrers to 7.52 Barrers, and an increase in permeability for CO_2, from 0.18 Barrers to 0.48 Barrers. Compared to the 5 wt% membranes, the 20 wt% ZIF-8/(PBI/6FDA-DAM) MMMs also showed increases in permeability for H_2, from 4.30 Barrers to 14.29 Barrers, and for CO_2, from 0.18 Barrers to 3.38 Barrers. The increases in gas permeability could have resulted from changes in the membrane microstructure due to the presence of a higher ZIF-8 loading that reduced the size of the dispersed domains, but increased the quantity of the domains significantly. By comparing Fig. 4.7E to Fig. 4.7H, it can be seen that due to the size reduction in the dispersed domains, the quantity of domains has become larger and the domains are closer to each other as

the ZIF-8 content increased in the PBI/6FDA-DAM blend. These changes in the dispersed domains may have increased the probability of the formation of continuous channels of the dispersed phase through the thickness of the membrane, as was reported previously [42–45]. Any continuous channels formed by the highly permeable and less selective polymer, 6FDA-DAM, would increase the gas permeability and lower the H_2/CO_2 selectivity. Additionally, permeability and selectivity changes for these membranes correlate with the changes in the membrane microstructure due to the higher loadings of ZIF-8. Table 4.1 also shows that the H_2/CO_2 selectivity for the ZIF-8/(PBI/6FDA-DAM) MMMs decreased from 25.2 to 15.9 as the ZIF-8 loading increased from 5 to 10 wt% in the polymer blend membranes. This decrease in selectivity may arise from the formation of voids in the membrane resulting from the aggregation of the ZIF-8 nanoparticle additive. Non-selective voids can be created around ZIF-8 nanoparticles as they aggregate, which also leads to higher permeability and lower selectivity [33,38]. Unfortunately, the ZIF-8 nanoparticle size is similar to the size of the polymer nodules, making it difficult to visualize the aggregation of ZIF-8 nanoparticles in the polymer blend.

The gas separation performance of these membranes (50:50 PBI/6FDA-DAM and ZIF-8/(PBI/6FDA-DAM) MMMs) measured at 35 °C and 3 atm are compared to other polymer membranes in a Robeson's plot shown in Fig. 4.9 [46]. The pure PBI membrane is located below the 2008 upper bound, whereas the 50:50 PBI/6FDA-DAM polymer blend membrane is located on the upper bound mostly due to its improved permeability over pure PBI and its good H_2/CO_2 selectivity. The 5 wt% and 10 wt% ZIF-8/(PBI/6FDA-DAM) MMMs are located above the upper bound due to the combined increase in permeability and the retention or small decrease in selectivity. The overall results suggest that, by adjusting the amount of ZIF-8 added to the 50:50

PBI/6FDA-DAM polymer blend membranes, one may control the gas transport properties of the ZIF-8-compatibilized polymer blend mixed-matrix membranes. The results also show that there is a limit to the amount of ZIF-8 nanoparticles that can be loaded into the polymer blend before other factors (e.g., percolation, void formation) take control or interfere with the properties of the membranes, as was observed for the 20 wt% ZIF-8/(PBI/6FDA-DAM) MMMs, where the separation performance of the membrane decreased significantly due to changes in membrane microstructure and possible void formation due to the aggregation of ZIF-8 nanoparticles.

4.3.3.2 High Pressure, High Temperature Gas Permeation

Gas permeation experiments with tubular membranes were conducted on a custom-built HPHT permeameter at pressures from 5 to 30 atm and at 300 °C. Tubular membranes of PBI, 6FDA-DAM, 50:50 PBI/6FDA-DAM, and the 5 wt% and 10 wt% ZIF-8/(PBI/6FDA-DAM) MMMs were tested for pure H_2 and CO_2 and their 50:50 mixture. As described previously, the tubular membranes adhere tightly to the tubular supports, making the measurement of tubular membrane thickness difficult using SEM. Since all of the tubular membranes were prepared from 8 wt% polymer solutions, their estimated thicknesses, measured with a micrometer, were similar (12-16 μm). Their effective membrane area was also identical since the porous area (13.8 cm^2) is the same for all tubular supports facilitating the comparison of properties such as permeance. As discussed previously, the measured gas permeabilities for tubular immiscible polymer blend membranes may not be completely accurate due to uncertainties in the measurement of the membranes thickness, which may arise from the dip-coating technique employed, the measurement error associated with the micrometer, and the potential infiltration of the porous support by the polymer chains. A more convenient property to compare the gas transport properties

of these membranes is the gas permeance that is calculated using the measured flow rates across the membranes. Gas permeabilities, however, can still be used for coarse comparisons and to evaluate trends. The single gas permeation properties of the tubular membranes for H_2 and CO_2 are summarized in Table 4.2. The calculated H_2/CO_2 ideal selectivity of the tubular PBI membrane at 5 atm and 300 °C (H_2/CO_2 = 22.2) was similar to that reported for PBI hollow fibers (H_2/CO_2 = 21.7) [24]. The results of testing the membranes at 300 °C show that gas permeation increases significantly compared to values at low temperature (35 °C) due to the increased segmental motion of the polymer chains at high temperatures that create larger free volumes in the membranes. The H_2 permeability increased from 1.37 to 38.2 Barrers, from 6.76 to 324 Barrers, from 4.30 to 473 Barrers, and from 7.52 to 1109 Barrers, whereas the CO_2 permeability increased from 0.05 to 1.74 Barrers, from 0.45 to 20.1 Barrers, from 0.18 to 29.4 Barrers, and from 0.48 to 129 Barrers for membranes of PBI, 50:50 PBI/6FDA-DAM, and the 5 wt% and 10 wt% ZIF-8/(PBI/6FDA-DAM) MMMs, respectively. Increased gas permeability for polymer membranes at temperatures higher than 35 °C were also reported previously [18,19]. Since permeability in polymer membranes is explained by the solution-diffusion model, the increased permeability can be explained in terms of increments in gas diffusivity with increasing temperatures as described by Equation (4.4), where D_0 is the pre-exponential factor for diffusivity, E_a is the activation energy for diffusion, R is the universal gas constant, and T is the gas temperature. It can be seen that at high temperature, diffusivity plays a dominant role over solubility and governs the permeation process, which accounts for the large increase in H_2 and CO_2 permeability at 300 °C observed for all the membranes in Table 4.2.

$$D = D_0 \cdot e^{-\frac{E_a}{RT}} \quad \text{(Eq. 4.4)}$$

When comparing the gas permeances and selectivities of the tested membranes (Table 4.2), the gas permeance increased in the order of PBI < 50:50 PBI/6FDA-DAM < 5 wt% ZIF-8/(PBI/6FDA-DAM) MMM < 10 wt% ZIF-8/(PBI/6FDA-DAM) MMM, whereas the H_2/CO_2 selectivity decreased in the order of PBI > 5 wt% ZIF-8/(PBI/6FDA-DAM) MMM > 50:50 PBI/6FDA-DAM > 10 wt% ZIF-8/(PBI/6FDA-DAM) MMM (Fig. 4.10). It can be seen that the permeance increased as the permeable content (6FDA-DAM and ZIF-8) increased in the PBI matrix, regardless of the testing temperature or membrane geometry. For the 50:50 PBI/6FDA-DAM membrane, permeation experiments were conducted with a feed pressure from 30 atm to 5 atm, as well as from 5 atm to 30 atm, to investigate the compression effect by feed pressure. Based on the similarities in gas permeance and H_2/CO_2 selectivity, it was found that the feed pressure does not significantly compress the membrane and impact the gas permeation properties.

Interestingly, 6FDA-DAM membranes tested at 300 °C exhibited an 11% increase in H_2 permeability and a 70% decrease in CO_2 permeability that resulted in an increase in the H_2/CO_2 ideal selectivity from 1.1 at 35 °C to 3.8 at 300 °C. This significant increase in H_2/CO_2 selectivity could be attributed to the decreased CO_2 solubility in the polymer membrane at elevated temperature [47].

Gas mixture (50:50 H_2/CO_2) separation results acquired at 30 atm and 300 °C with PBI, PBI/6FDA-DAM, and 5 and 10 wt% ZIF-8/(PBI/6FDA-DAM) MMMs are shown in Table 4.3 and in Fig. 4.10. Compared to pure gas measurements, all of the membranes except for PBI exhibited a decrease in H_2 permeance but not in CO_2 permeance, which led to a reduction in PBI's H_2/CO_2

selectivity from 27.4 (ideal, PBI) to 17.8 (mixture, PBI) and to 6.5 (mixture, MMM) for the 10 wt% ZIF-8/(PBI/6FDA-DAM) MMM. This phenomenon is commonly seen in gas mixture measurements and typically stems from the effect of penetrant competition, in which CO_2 competes against H_2 for diffusional paths in the membrane [33]. It can also be observed that the trends in gas permeance and selectivities from gas mixture measurements were similar to those from single gas measurements in which the gas permeability increased and H_2/CO_2 selectivity decreased as the permeable content (6FDA-DAM, ZIF-8) increased in the membrane.

The H_2 permeabilities and H_2/CO_2 ideal and mixed gas selectivities of the polymer blend membranes tested at 30 atm and 300 °C are compared in a Robeson plot (Fig. 4.9). It can be seen that all of the polymer blend membranes tested at 300 °C using single gases and a 50:50 H_2/CO_2 gas mixture surpassed the 2008 upper bound due to their high H_2 permeability and high H_2/CO_2 selectivity. Compared to other PBI-based membranes that have been tested at high temperature (230-250 °C), the polymer blend membranes exhibited similar or better H_2 permeability and slightly lower H_2/CO_2 selectivity. A pure tubular PBI membrane that was tested at 3 atm and 250 °C exhibited a high H_2/CO_2 selectivity of 43 [19], however, its H_2 permeability (58 Barrers) is lower than that for the 5 wt% ZIF-8/(PBI/6FDA-DAM) MMM (472 Barrers) that was tested at 300 °C. The 30/70 (w/w) ZIF-8/PBI MMMs that have been tested at 2 atm and 230 °C exhibited a similar H_2 permeability (470 Barrers) but higher H_2/CO_2 selectivity (26.3) [21] as compared to the 5 wt% ZIF-8/(PBI/6FDA-DAM) MMM (472 Barrers, $H_2/CO_2 = 17.4$), which may result from the differences in membrane casting solvent and membrane thermal treatment. It is worth mentioning that the polymer blend membranes in this work were tested at much higher pressure and temperature conditions than those reported PBI-based membranes that were tested at high

temperature (230-250 °C), indicating that the polymer blend membranes are not only thermally stable, but also mechanically robust to withstand the high pressure. To the best of our knowledge, this is the first time that polymer blend membranes have been tested for H_2/CO_2 separation at 30 atm and 300 °C and have exhibited attractive separation properties.

4.4 CONCLUSION

High performance 50:50 PBI/6FDA-DAM immiscible polymer blend membranes and their ZIF-8-containing MMMs were fabricated and tested for H_2/CO_2 separations at industrially relevant conditions of pressure and temperature. SEM images revealed that the addition of ZIF-8 nanoparticles reduced the size and improved the uniformity of the dispersed 6FDA-DAM domains in the PBI matrix. The changes in membrane morphology significantly impacted the gas permeation properties of the membranes. It was observed that smaller dispersed domains led to an increase in gas permeability and a decrease in H_2/CO_2 selectivity probably due to the microstructural change of the dispersed phase in the matrix. Gas permeation experiments at 300 °C and at pressures that ranged from 5 to 30 atm showed that a large increase in gas permeability is attainable at high temperatures with the retention or minimal loss of selectivity. Permeation experiments using a 50:50 H_2/CO_2 mixture at 30 atm and 300 °C showed that the 5 wt% ZIF-8/(PBI/6FDA-DAM) MMMs exhibited promising results for H_2/CO_2 separation. These membranes showed an increase in H_2 permeance and the retention of H_2/CO_2 selectivity, as compared to the polymer blend without ZIF-8 nanoparticles. Overall, the 50:50 PBI/6FDA-DAM polymer blend membranes and their ZIF-8-based MMMs tested at 300 °C surpassed the Robeson's 2008 upper bound for H_2/CO_2 separations, indicating the potential for these membranes to be utilized for the purification of H_2 in the WGSR.

APPENDIX 4A FIGURES AND TABLES

A

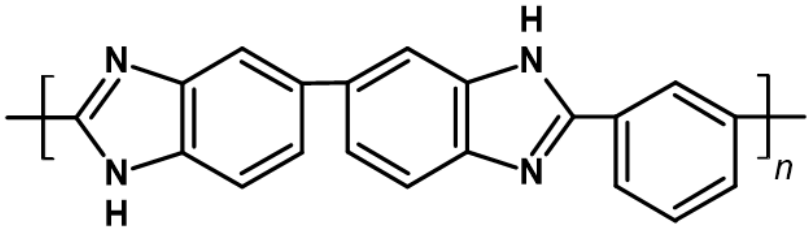

B

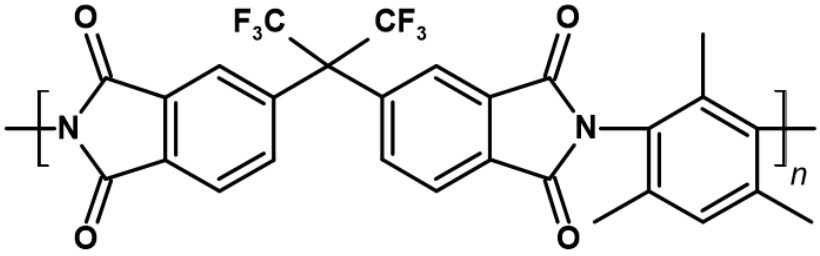

C

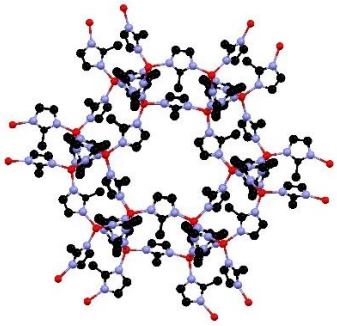

Fig 4.1. Structures of (A) PBI and (B) 6FDA-DAM and of (C) ZIF-8 calculated using the crystallographic data in [27].

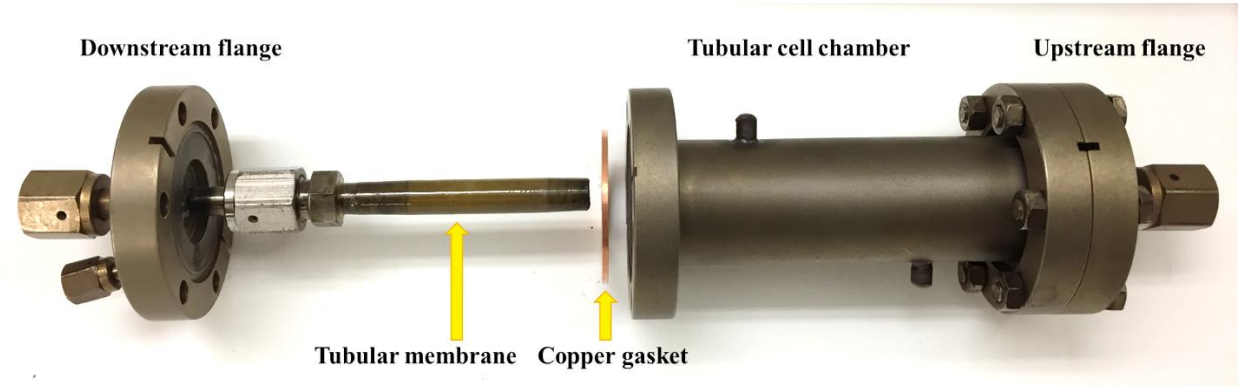

Fig 4.2. Optical image of tubular membrane cell.

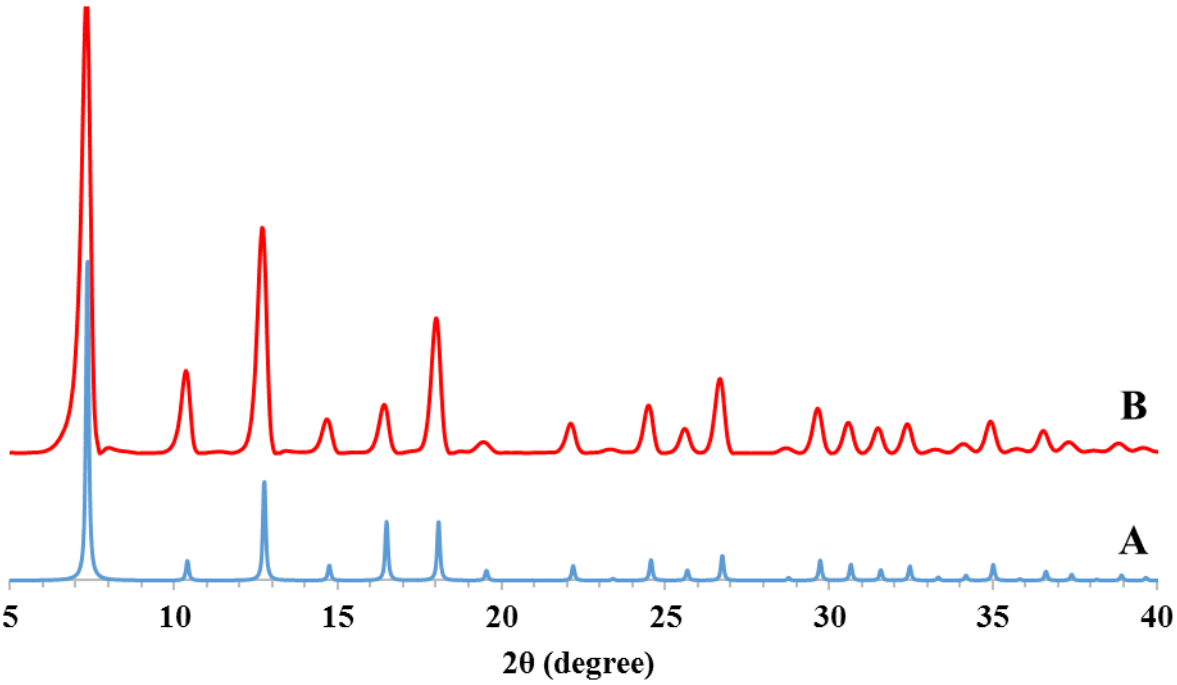

Fig 4.3. XRD patterns of ZIF-8: (A) theoretical calculated using the crystallographic data in [27] and (B) as-synthesized.

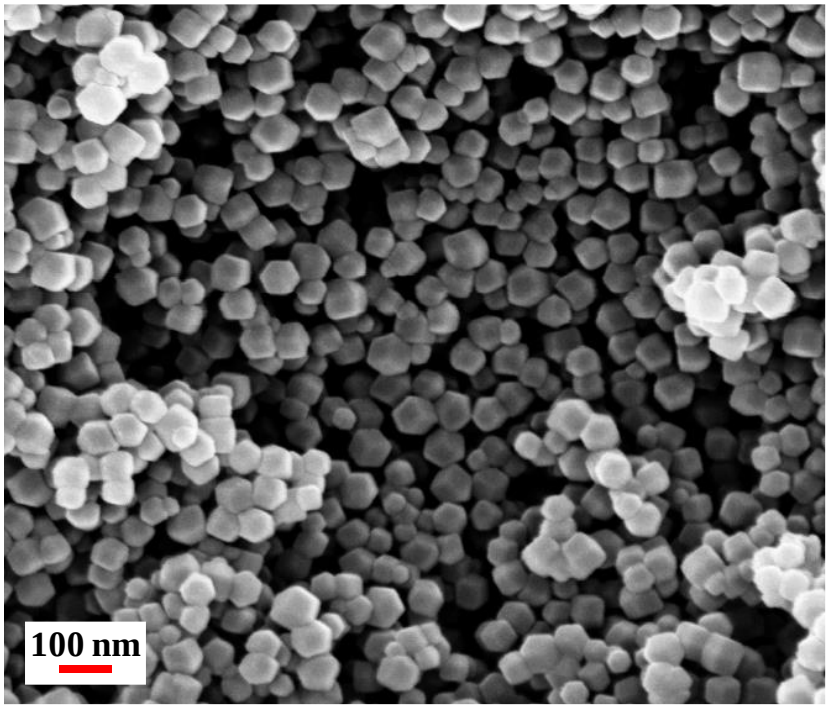

Fig 4.4. SEM image of synthesized ZIF-8 nanoparticles.

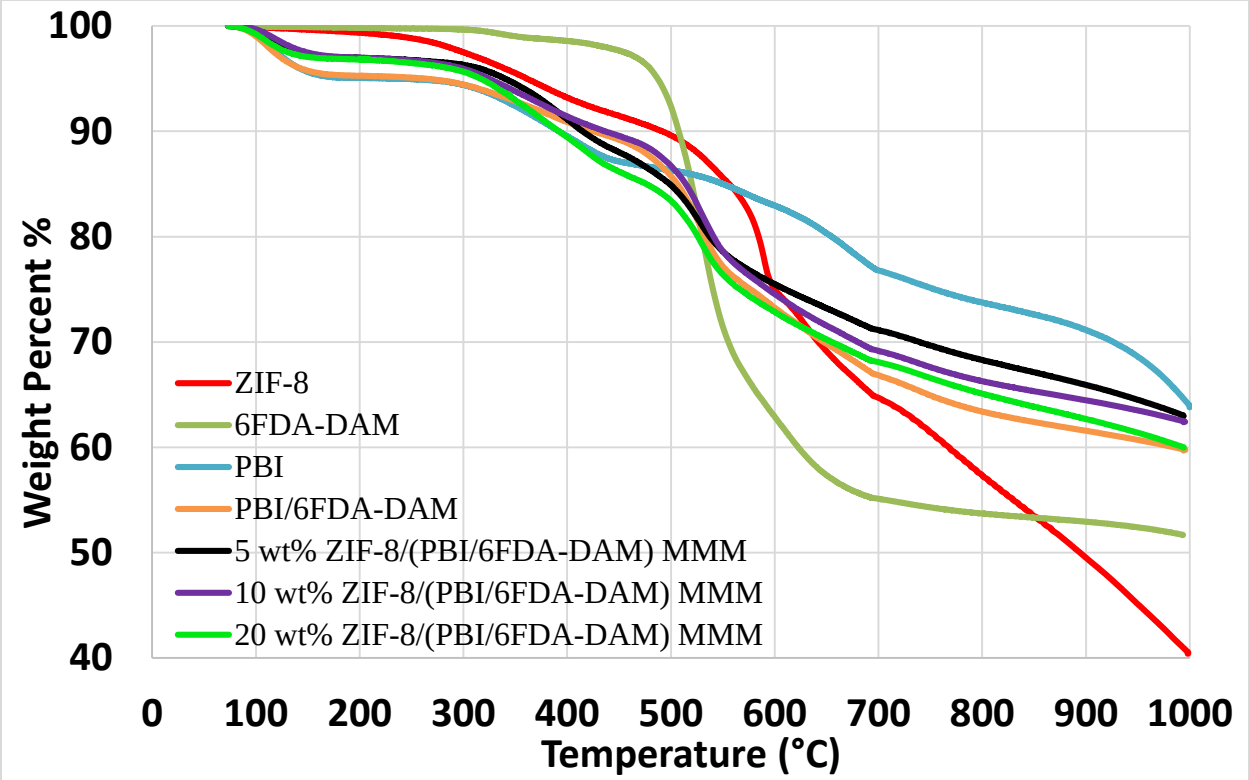

Fig 4.5. Thermogravimetric analysis of ZIF-8, 6FDA-DAM and PBI polymers, PBI/6FDA-DAM polymer blend, and ZIF-8/(PBI/6FDA-DAM) MMMs performed under N_2.

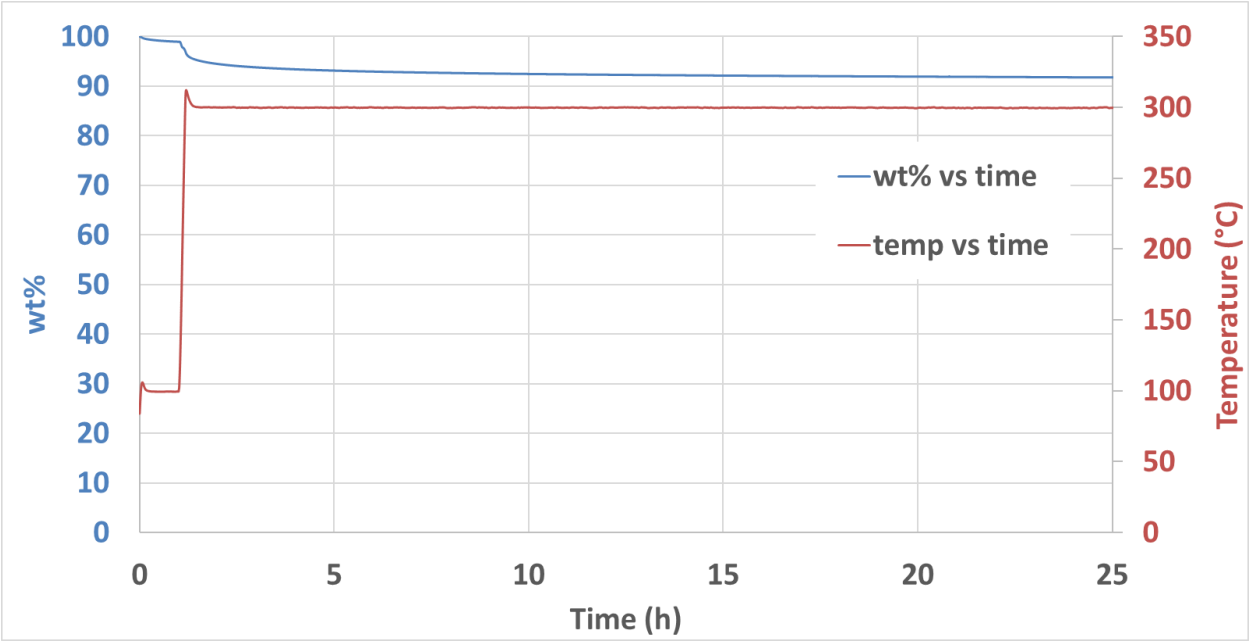

Fig 4.6. Thermal stability (constant temperature TGA) of 5 wt% ZIF-8/(PBI/6FDA-DAM) MMM under N_2 at 300 °C for 24 h.

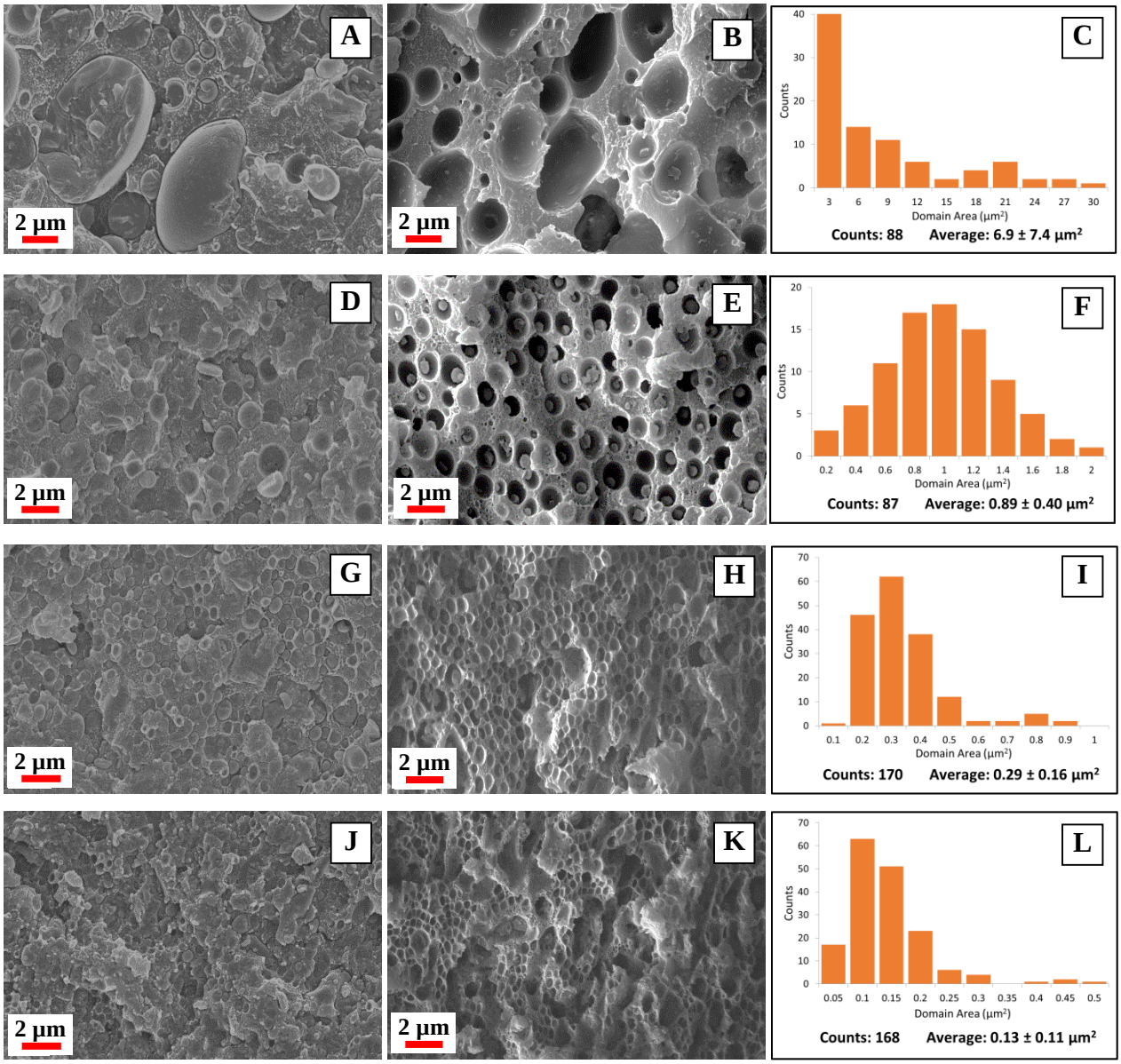

Fig 4.7. SEM images of the cross-sections (A,D,G,J), THF-extracted cross-sections (B,E,H,K), and the histograms of the domain size (C,F,I,L) of the ZIF-8/(PBI/6FDA-DAM) membranes: (A-C) 0 wt%, (D-F) 5 wt%, (G-I) 10 wt%, and (J-L) 20 wt% ZIF-8. The left and right sides of the SEM images represent the air and glass sides of the membranes, respectively, and the membrane casting direction was out of the plane of the page.

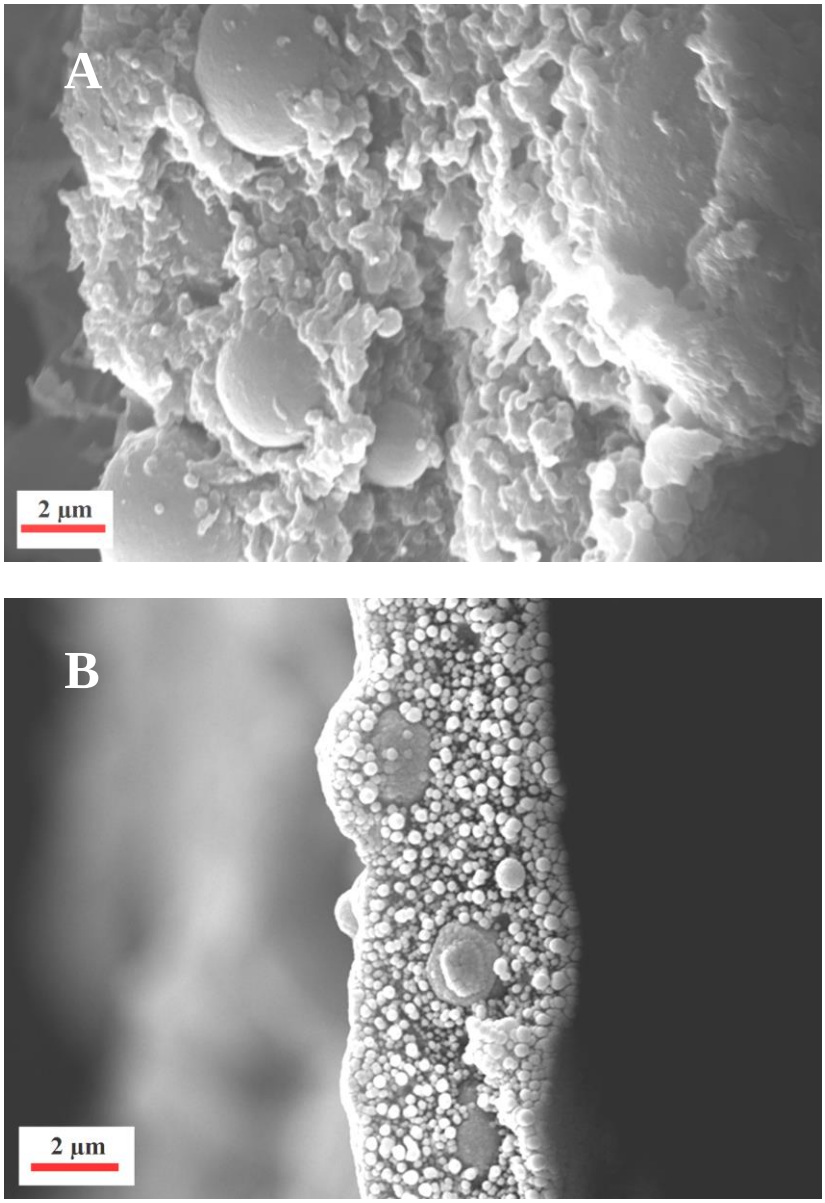

Fig 4.8. SEM images of cross-sections of tubular membranes showing the internal morphology: (A) PBI/6FDA-DAM, (B) 5 wt% ZIF-8/(PBI/6FDA-DAM) MMM.

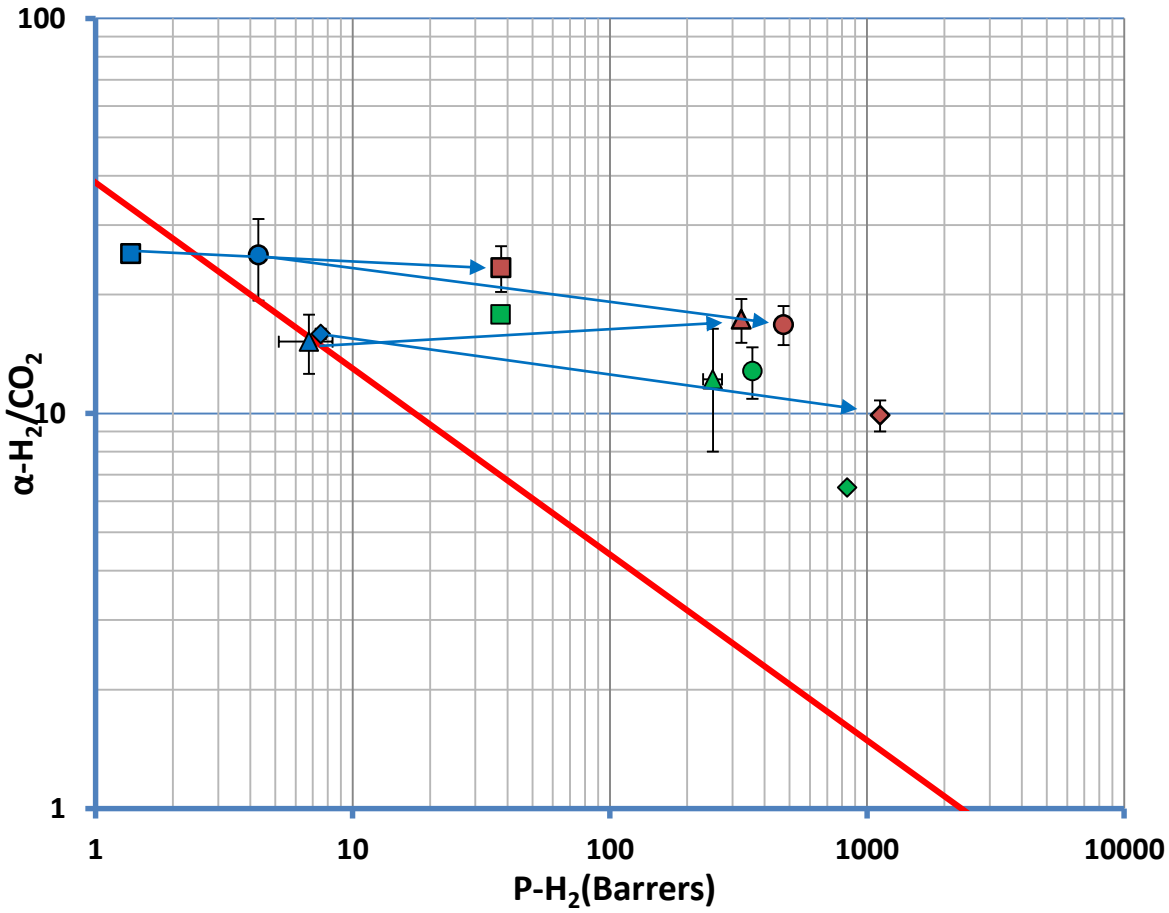

Fig 4.9. H_2 permeability- H_2/CO_2 selectivity Robeson plot for PBI (■), 50:50 PBI/6FDA-DAM (▲), 5 wt% ZIF-8/(PBI/6FDA-DAM) MMM (●), and 10 wt% ZIF-8/(PBI/6FDA-DAM) MMM (◆),tested with pure gases at 3 atm and 35 °C (blue), at 30 atm and 300 °C (orange), and at 30 atm and 300 °C with a H_2:CO_2 (1:1) gas mixture (green). The x error bars represent the standard deviations of H_2 permeability, while the y error bars represent the standard deviations of H_2/CO_2 selectivity. Some error bars are not observed because they are encompassed by the symbols.

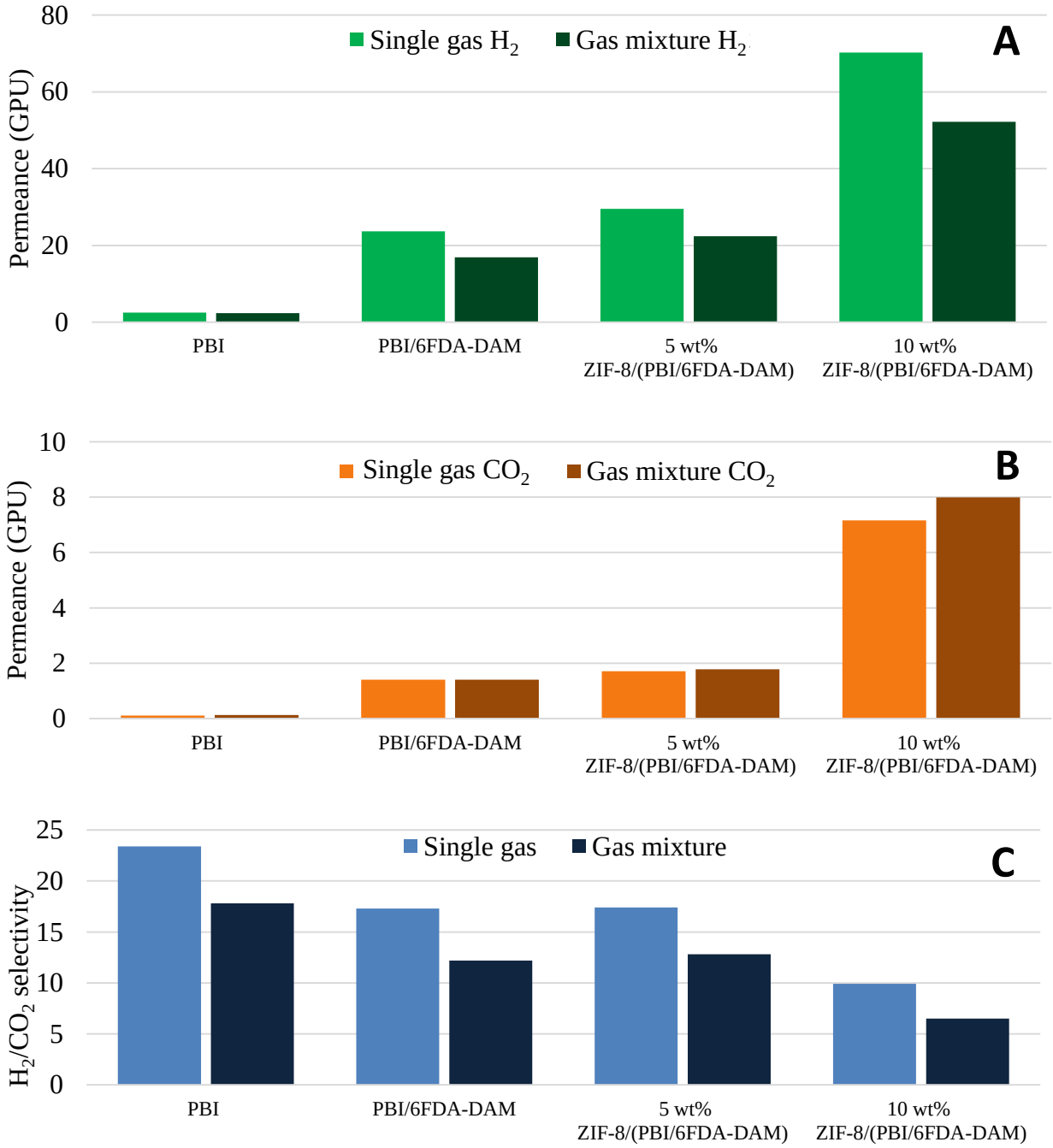

Fig 4.10. Gas permeance of H_2 (A), CO_2 (B), and H_2/CO_2 selectivity (C) of PBI, PBI/6FDA-DAM, and 5 wt% and 10 wt% ZIF-8/(PBI/6FDA-DAM) MMMs tested at 30 atm and 300 °C with pure gases and a H_2/CO_2 (1:1) gas mixture.

.

Table 4.1. H_2 and CO_2 permeabilities and H_2/CO_2 ideal selectivities of PBI, 6FDA-DAM, PBI/6FDA-DAM, and ZIF-8/(PBI/6FDA-DAM) MMMs at 35 °C and 3 atm.

	H_2 permeability (Barrer)	CO_2 permeability (Barrer)	H_2/CO_2 Selectivity
PBI	1.37 ± 0.03	0.05 ± 0.01	27.4 ± 1.1
6FDA-DAM	1020 ± 18.4	943 ± 4.5	1.1 ± 0.1
PBI/6FDA-DAM	6.76 ± 1.61	0.45 ± 0.09	15.2 ± 2.6
5 wt% ZIF-8/(PBI/6FDA-DAM) MMM	4.30 ± 0.15	0.18 ± 0.04	25.2 ± 5.9
10 wt% ZIF-8/(PBI/6FDA-DAM) MMM	7.52 ± 0.35	0.48 ± 0.02	15.9 ± 0.1
20 wt% ZIF-8/(PBI/6FDA-DAM) MMM	14.29 ± 2.30	3.38 ± 1.01	4.3 ± 0.6

Average of 2 membranes.
1 Barrer = 1×10^{-10} $cm^3_{(STP)}$ cm cm^{-2} s^{-1} $cmHg^{-1}$

Table 4.2. Permeance, permeability and selectivity of H_2 and CO_2 measured at 300 °C and at various pressures using single gases for membranes of PBI, PBI/6FDA-DAM, and MMMs with 5 wt%, and 10 wt% ZIF-8 loadings.

Feed pressure (atm)	H_2 permeance (GPU)	H_2 permeability (Barrers)	CO_2 permeance (GPU)	CO_2 permeability (Barrers)	Selectivity
		PBI			
30	2.52 ± 0.14	37.75 ± 1.55	0.11 ± 0.01	1.63 ± 0.28	23.4 ± 3.1
20	2.52 ± 0.13	37.65 ± 1.56	0.11 ± 0.01	1.69 ± 0.33	22.6 ± 3.4
15	2.53 ± 0.13	37.87 ± 1.66	0.11 ± 0.01	1.69 ± 0.30	22.7 ± 3.1
10	2.55 ± 0.12	38.10 ± 1.76	0.12 ± 0.01	1.71 ± 0.30	22.5 ± 2.9
5	2.55 ± 0.12	38.17 ± 1.83	0.12 ± 0.01	1.74 ± 0.33	22.2 ± 3.1
		6FDA-DAM			
30	70.52 ± 0.51	1128.25 ± 8.13	17.74 ± 0.12	283.85 ± 1.95	4.0 ± 0.2
20	70.12 ± 0.63	1121.98 ± 10.05	17.81 ± 0.08	284.93 ± 1.27	3.9 ± 0.5
15	69.88 ± 0.44	1118.15 ± 7.12	18.00 ± 0.11	287.98 ± 1.77	3.9 ± 0.4
10	69.66 ± 0.41	1114.59 ± 6.57	18.33 ± 0.08	293.26 ± 1.22	3.8 ± 0.3
5	71.60 ± 1.82	1145.53 ± 29.08	18.93 ± 0.31	302.86 ± 4.89	3.8 ± 1.2
		PBI/6FDA-DAM (high to low pressure)			
30	23.70 ± 5.00	324.65 ± 2.94	1.40 ± 0.47	18.96 ± 2.60	17.3 ± 2.2
20	23.54 ± 5.09	322.44 ± 4.62	1.43 ± 0.49	19.37 ± 2.76	16.8 ± 2.2
15	23.57 ± 5.11	322.72 ± 4.87	1.45 ± 0.50	19.59 ± 2.85	16.6 ± 2.2
10	23.55 ± 5.09	322.54 ± 4.57	1.47 ± 0.52	19.88 ± 3.02	16.4 ± 2.3
5	23.60 ± 4.59	323.91 ± 2.45	1.48 ± 0.52	20.06 ± 3.04	16.3 ± 2.6
		PBI/6FDA-DAM (low to high pressure)			
5	26.84 ± 3.24	322.10 ± 1.98	1.67 ± 0.44	20.04 ± 2.21	16.1 ± 2.2
10	27.15 ± 3.77	325.74 ± 2.24	1.67 ± 0.45	20.15 ± 2.64	16.3 ± 2.2
15	27.16 ± 4.02	325.89 ± 2.56	1.67 ± 0.52	20.02 ± 2.74	16.3 ± 2.2
20	27.20 ± 4.86	326.42 ± 3.37	1.66 ± 0.72	19.92 ± 3.52	16.4 ± 2.3
30	27.22 ± 4.52	326.72 ± 3.18	1.64 ± 0.33	19.68 ± 1.92	16.6 ± 2.6
		5 wt% ZIF-8/(PBI/6FDA-DAM) MMM			
30	29.52 ± 0.31	472.38 ± 4.89	1.71 ± 0.20	27.31 ± 3.24	17.4 ± 1.9
20	29.31 ± 0.32	469.04 ± 5.17	1.77 ± 0.22	28.35 ± 3.58	16.7 ± 1.9
15	29.35 ± 0.40	469.57 ± 6.45	1.81 ± 0.25	28.87 ± 3.90	16.4 ± 2.0
10	29.29 ± 0.41	468.70 ± 6.56	1.83 ± 0.26	29.25 ± 4.11	16.2 ± 2.0
5	29.57 ± 0.07	473.08 ± 1.08	1.84 ± 0.26	29.38 ± 4.15	16.3 ± 2.3
		10 wt% ZIF-8/(PBI/6FDA-DAM) MMM			
30	70.25 ± 1.79	1123.94 ± 28.59	7.16 ± 0.48	114.51 ± 7.70	9.9 ± 0.9
20	68.96 ± 1.64	1103.41 ± 26.17	7.45 ± 0.81	119.25 ± 12.97	9.3 ± 1.2
15	69.15 ± 1.39	1106.42 ± 22.22	7.54 ± 0.95	120.68 ± 15.21	9.2 ± 1.3
10	69.26 ± 1.24	1108.06 ± 19.76	7.85 ± 0.75	125.60 ± 12.06	8.9 ± 1.0
5	69.31 ± 1.26	1108.93 ± 20.11	8.04 ± 0.70	128.60 ± 11.26	8.7 ± 0.9

Average of 2 membranes

1 Barrer = 1×10^{-10} $cm^3_{(STP)}$ cm cm^{-2} s^{-1} $cmHg^{-1}$

1 GPU = 1×10^{-6} $cm^3_{(STP)}$ cm^{-2} s^{-1} $cmHg^{-1}$

Table 4.3. Permeance, permeability, and selectivity of H_2 and CO_2 acquired at 300 °C and 30 atm using a H_2/CO_2 (50:50) mixture for membranes of PBI, PBI/6FDA-DAM, and ZIF-8(PBI/6FDA-DAM) MMMs with 5 wt%, and 10 wt% ZIF-8 loadings.

	H_2 permeance (GPU)	H_2 permeability (Barrer)	CO_2 permeance (GPU)	CO_2 permeability (Barrer)	H_2/CO_2 ideal selectivity
PBI	2.36 ± 0.01	37.78 ± 0.26	0.13 ± 0.01	2.13 ± 0.03	17.8 ± 0.1
PBI/6FDA-DAM	16.92 ± 2.99	251.58 ± 20.99	1.40 ± 0.91	20.33 ± 11.65	12.2 ± 4.2
5 wt% ZIF-8(PBI/6FDA-DAM) MMM	22.39 ± 0.70	358.18 ± 11.20	1.78 ± 0.32	28.58 ± 5.16	12.8 ± 1.9
10 wt% ZIF-8(PBI/6FDA-DAM) MMM	52.24 ± 1.69	835.73 ± 27.08	7.99 ± 0.46	127.75 ± 7.38	6.5 ± 0.1

Average of 2 membranes
1 Barrer = 1×10^{-10} $cm^3_{(STP)}$ cm cm^{-2} s^{-1} $cmHg^{-1}$
1 GPU = 1×10^{-6} $cm^3_{(STP)}$ cm^{-2} s^{-1} $cmHg^{-1}$

APPENDIX 4B MODEL STUDY

For a dense polymeric membrane that has uniform morphology, the solution-diffusion model (Equation 1) can be used to calculate the permeability of gases from solubility and diffusivity coefficients that can be determined independently [146,147]. The solubility, S, depends on the condensability of the penetrant gas in the polymer, and the diffusivity, D, measures the mobility of the penetrant gas through the membrane [148]. Typically, gas species with higher critical temperatures result in higher solubilities, while gas molecules with smaller kinetic diameters result in higher diffusivity [22]. The ideal selectivity (α) can then be calculated using Equation (2):

$$P = S \cdot D \tag{1}$$

$$\alpha_{a/b} = \frac{P_a}{P_b} \tag{2}$$

The PBI/6FDA-DAM blend flat membranes with polymer weight compositions of 90/10, 70/30, and 50:50 were tested for gas permeation at 3 atm and 35 °C. The gas permeation results calculated using the solution-diffusion model were compared to the predictions generated by other models, including the series model, the parallel model, the Maxwell's model, and the equivalent box (EB) model [149]. Each model corresponds to a specific membrane morphology as shown in Fig. 1. The gas permeabilities of the

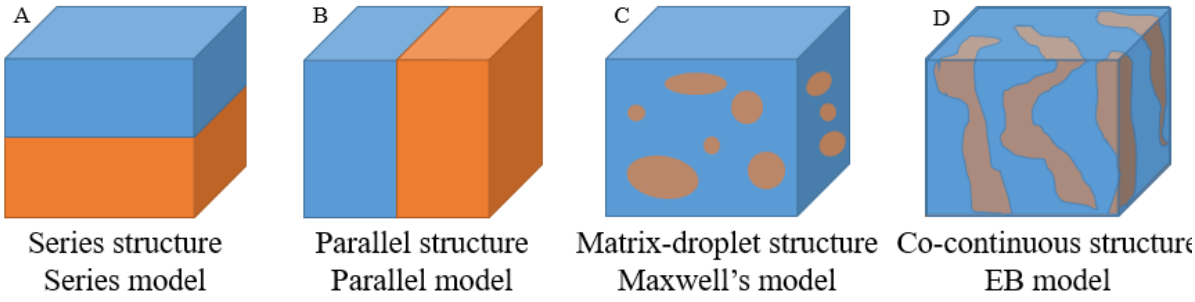

Fig. 1. Proposed models for permeability calculations according to phase dispersed

pure PBI and 6FDA-DAM flat membranes were first measured and then applied in the models to predict gas permeability as a function of the 6FDA-DAM volume fraction (V_1), which was converted from the polymer weight compositions using Equation (3), where m and ρ are the mass and density for polymer 1 and 2 in the blend. The equations and the parameters for each model are summarized in Table 1.

$$V_1 = \frac{(m_1/\rho_1)}{(m_1/\rho_1) + (m_2/\rho_2)} \tag{3}$$

The predictions of the models depend strongly on the orientation and structure of the blend components (Fig. 1). When a highly permeable polymer is blended with a highly selective polymer, the series structure exhibits permeation properties similar to the highly selective polymer. In this case, the highly selective polymer dominantly governs the gas permeation, while the highly permeable polymer works basically as a support. In contrast, the parallel structure exhibits permeation properties similar to the highly permeable polymer due to the existence of a channel formed by the highly permeable polymer. Different from the series and parallel structures, the matrix-droplet (MD) structure, depending on the polymer that forms the matrix, might exhibit high permeability resembling the highly permeable polymer or high selectivity resembling the highly selective polymer. And, because the second polymer is blended as droplets in the matrix, the blend membrane exhibits partial properties of the second polymer. Maxwell's model is commonly used for blend membranes with a MD structure. However, as the volume fraction of the dispersed polymer increases, Maxwell's model becomes inaccurate due to the emergence of percolation of in the dispersed phase or phase inversion [150–152]. The EB model is a combination of the series and parallel models and works appropriately for the co-continuous structure [149]. As the volume fraction of the dispersed polymer increases beyond the percolation threshold, channels formed by the dispersed polymer emerge throughout the membrane, and the permeation properties of the blend membrane become similar to the dispersed polymer.

Table 1

Proposed models [149] for the calculation of permeability, P_b, in immiscible polymer blend membranes.

Model		Parameters
Series	$P_b = \frac{P_1 P_2}{V_1 P_2 + V_2 P_1}$	P_1 and P_2: permeability of polymer 1 and polymer 2 V_1 and V_2: volume fraction of polymer 1 and polymer 2
Parallel	$P_b = P_1 V_1 + P_2 V_2$	
Maxwell's	$P_b = P_m[\frac{P_d + 2P_m - 2V_d(P_m - P_d)}{P_d + 2P_m + V_d(P_m - P_d)}]$	P_m: permeability of matrix polymer P_d: permeability of dispersed polymer V_d: volume fraction of dispersed polymer
Equivalent Box Model (EBM)	$P_b = P_1 V_{1p} + P_2 V_{2p} + {V_s}^2 / [\frac{V_{1s}}{P_1} + \frac{V_{2s}}{P_2}]$ $V_s = V_{1s} + V_{2s}$ $V_{1p} = [(V_1 - V_{1cr})/(1 - V_{1cr})]^{T_1}$ $V_{1s} = V_1 - V_{1p}$ $V_{2p} = [(V_2 - V_{2cr})/(1 - V_{2cr})]^{T_2}$ $V_{2s} = V_2 - V_{2p}$	P_1 and P_2: permeabilities of polymer 1 and polymer 2 V_1 and V_2: volume fractions of polymer 1 and polymer 2 V_{1cr} and V_{2cr}: critical threshold percolation values of polymer 1 and polymer 2 T_1 and T_2: critical universal exponents of polymer 1 and polymer 2 For spherical dispersed domains, $V_{1cr} = V_{2cr} = 0.156$ and $T_1 = T_2 = 1.833$

Immiscible blend membranes with various polymer ratios can result in different morphologies (Fig. 1) that exhibit unique gas permeation properties. Depending on the morphology of the membrane, certain models can be used to interpret and predict the gas permeation properties (Table 1). The experimental H_2 and CO_2 gas permeabilities of PBI/6FDA-DAM blend membranes with different 6FDA-DAM volume fractions were summarized in Table 2. Comparing these experimental results to the predicted values from the models described in Table 1 and shown in Fig. 2 as a function of the 6FDA-DAM volume fraction, it can be seen that the experimental permeability for H_2 is similar to the predictions from Maxwell's model at 6FDA-DAM volume fractions up to 49% (Fig 2A). From Fig. 2B, it was observed that the experimental H_2/CO_2 ideal selectivity (22.4) was similar to the ideal selectivity predicted using Maxwell's model (27.4) at the low 6FDA-DAM volume fraction of 10%. Figure 2B also showed that as the 6FDA-DAM volume fraction in the blend increased to 49%, the experimental H_2/CO_2 ideal selectivity decreased considerably to 15.2 and departed from the predicted value (H_2/CO_2 = 27.2) calculated from Maxwell's model. This drastic decrease in selectivity for immiscible polymer blend membranes can be explained by the percolation theory that suggests once the concentration

Table 2. H_2 permeability and H_2/CO_2 selectivity of 50:50 PBI/6FDA-DAM blend membranes at different polymer blend compositions

PBI/6FDA-DAM weight ratio	6FDA-DAM volume fraction	H_2 permeability (Barrer)	H_2/CO_2 selectivity
PBI	0	1.37	27.4
90/10 PBI/6FDA-DAM	10	2.21	22.4

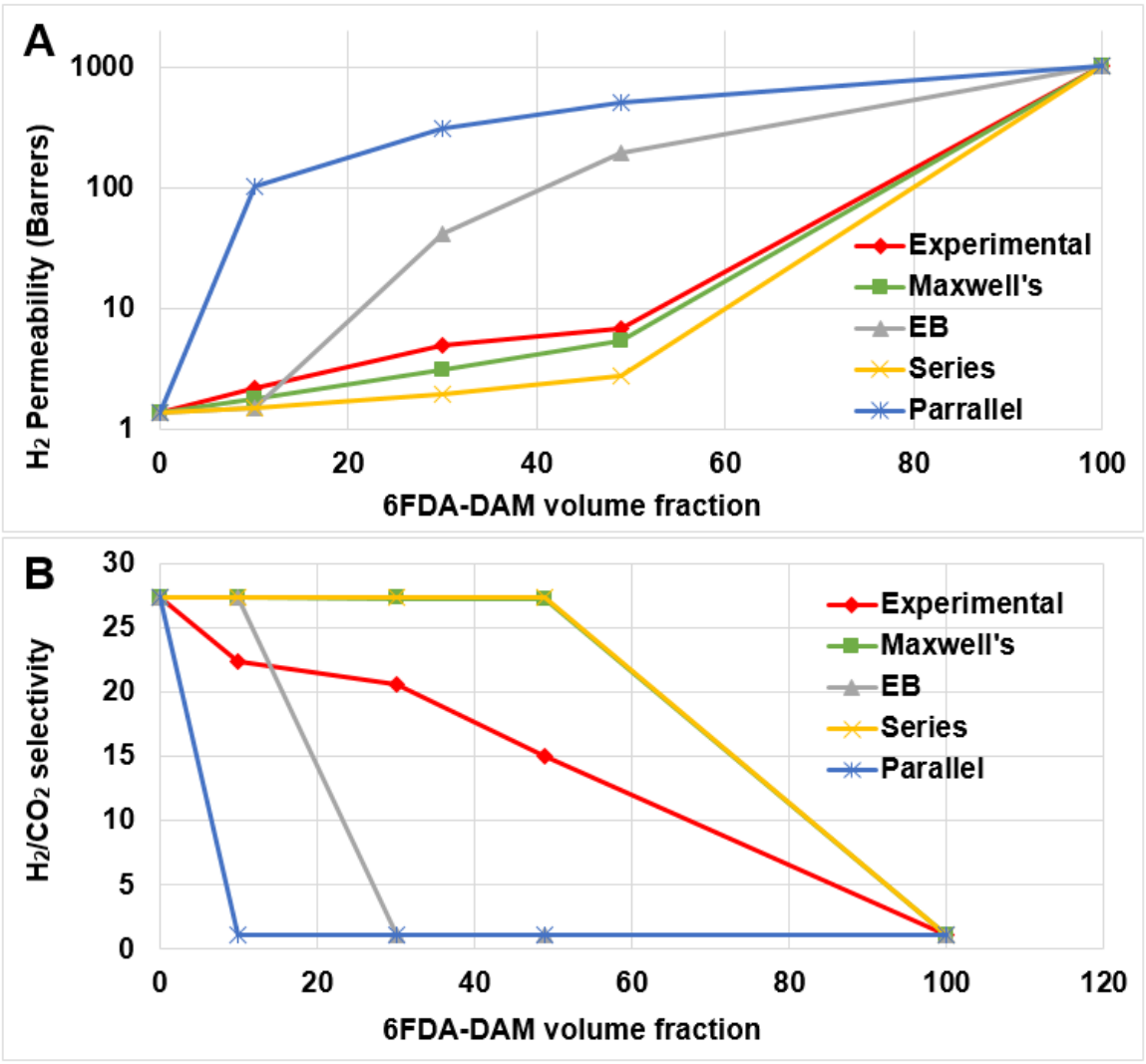

Fig. 2. Experimental and predicted permeabilities of H_2 (A) and H_2/CO_2 selectivities (B)

of the dispersed phase passes a percolation threshold, it starts to form continuous channels throughout the membrane. The experimental H_2/CO_2 selectivity for the 50:50 PBI/6FDA-DAM blend membrane (H_2/CO_2 = 15.2) lied between the predictions of Maxwell's model (H_2/CO_2 = 27.2) and the EB model (H_2/CO_2 = 1.1), as shown in Fig. 2B, and exhibited a deviation of 44% and 1282% from Maxwell's model and the EB model, respectively. These observations assume

that the 50:50 PBI/6FDA-DAM blend membrane morphology is represented primarily as a MD structure. However, further investigation is required to prove the assumption.

REFERENCES

[1] C.W. Forsberg, Future hydrogen markets for large-scale hydrogen production systems, *Int. J. Hydrogen Energy* **2007**, *32*, 431–439.

[2] A. Midilli, M. Ay, I. Dincer, M.A. Rosen, On hydrogen and hydrogen energy strategies I : Current status and needs, *Renew. Sustain. Energy Rev.* **2005**, *9*, 255–271.

[3] S.E. Hosseini, M.A. Wahid, Hydrogen production from renewable and sustainable energy resources: Promising green energy carrier for clean development, *Renew. Sustain. Energy Rev.* **2016**, *57*, 850–866.

[4] S.W. Hasan, M.T. Ghannam, N. Esmail, Heavy crude oil viscosity reduction and rheology for pipeline transportation, *Fuel* **2010**, *89*, 1095–1100.

[5] P. Petit, Hydrogen recovery from ammonia synthesis plant, *Indian J. Cryog.* **1982**, *7*, 155–161.

[6] N. Eliaz, D. Eliezer, D.L. Olson, Hydrogen-assisted processing of materials, *Mater. Sci. Eng. A*. **2000**, *289*, 41–53.

[7] E. Shoko, B. McLellan, A.L. Dicks, J.C.D. da Costa, Hydrogen from coal: Production and utilization technologies, *Int. J. Coal Geol.* **2006**, *65*, 213–222.

[8] A.J. Minchener, Coal gasification for advanced power generation, *Fuel* **2005**, *84*, 2222–2235.

[9] G.J. Stiegel, M. Ramezan, Hydrogen from coal gasification: An economical pathway to a sustainable energy future, *Int. J. Coal Geol.* **2006**, *65*, 173–190.

[10] P. Mondal, G.S. Dang, M.O. Garg, Syngas production through gasification and cleanup for downstream applications - Recent developments, *Fuel Process. Technol.* **2011**, *92*, 1395–1410.

[11] N. Schumacher, A. Boisen, S. Dahl, A.A. Gokhale, S. Kandoi, L.C. Grabow, J.A. Dumesic, M. Mavrikakis, I. Chorkendorff, Trends in low-temperature water-gas shift reactivity on transition metals, *J. Catal.* **2005**, *229*, 265–275.

[12] R. Kumar, Vacuum swing adsorption process for oxygen production–-A historical perspective, *Sep. Sci. Technol.* **1996**, *7*, 877.

[13] C.A. Grande, Advances in pressure swing adsorption for gas separation, *ISRN Chem. Eng.* **2012**, *2012*, 1–13.

[14] P. Bernardo, E. Drioli, G. Golemme, Membrane gas separation: A review/state of the art, *Ind. Eng. Chem. Res.* **2009**, *48*, 4638–4663.

[15] W.J. Koros, R. Mahajan, Pushing the limits on possibilities for large scale gas separation: Which strategies?, *J. Membr. Sci.* **2001**, *181*, 141.

[16] R.W. Baker, Future directions of membrane gas separation technology, *Ind. Eng. Chem. Res.* **2002**, *41*, 1393–1411.

[17] K. Ghosal, B.D. Freeman, Gas separation using polymer membranes: An overview, *Polym. Adv. Technol.* **1994**, *5*, 673–697.

[18] D.R. Pesiri, B. Jorgensen, R.C. Dye, Thermal optimization of polybenzimidazole meniscus membranes for the separation of hydrogen, methane, and carbon dioxide, *J. Membr. Sci.* **2003**, *218*, 11–18.

[19] K.A. Berchtold, R.P. Singh, J.S. Young, K.W. Dudeck, Polybenzimidazole composite membranes for high temperature synthesis gas separations, *J. Membr. Sci.* **2012**, *415–416*, 265–270.

[20] T. Yang, G.M. Shi, T.S.C. Chung, Symmetric and asymmetric zeolitic imidazolate frameworks (ZIFs)/Polybenzimidazole (PBI) nanocomposite membranes for hydrogen purifi cation at high temperatures, *Adv. Energy Mater.* **2012**, *2*, 1358–1367.

[21] T. Yang, T.-S. Chung, High performance ZIF-8/PBI nano-composite membranes for high temperature hydrogen separation consisting of carbon monoxide and water vapor, *Int. J. Hydrogen Energy* **2013**, *38*, 229–239.

[22] T. Yang, Y. Xiao, T.-S. Chung, Poly-/metal-benzimidazole nano-composite membranes for hydrogen purification, *Energy Environ. Sci.* **2011**, *4*, 4171.

[23] S.S. Hosseini, M.M. Teoh, T.S. Chung, Hydrogen separation and purification in membranes of miscible polymer blends with interpenetration networks, *Polymer* **2008**, *49*, 1594–1603.

[24] S.C. Kumbharkar, Y. Liu, K. Li, High performance polybenzimidazole based asymmetric hollow fibre membranes for H_2/CO_2 separation, *J. Membr. Sci.* **2011**, *375*, 231–240.

[25] W. Qiu, L. Xu, C.-C. Chen, D.R. Paul, W.J. Koros, Gas separation performance of 6FDA-based polyimides with different chemical structures, *Polymer* **2013**, *54*, 6226–6235.

[26] N.P. Panapitiya, S.N. Wijenayake, D.D. Nguyen, Y. Huang, I.H. Musselman, K.J. Balkus, Jr., J.P. Ferraris, Gas separation membranes derived from high-performance immiscible polymer blends compatibilized with small molecules, *ACS Appl. Mater. Interfaces* **2015**, *7*, 18618–18627.

[27] K.S. Park, Z. Ni, A.P. Côté, J.Y. Choi, R. Huang, F.J. Uribe-Romo, H.K. Chae, M. O'Keeffe, O.M. Yaghi, Exceptional chemical and thermal stability of zeolitic imidazolate frameworks, *Proc. Natl. Acad. Sci.* **2006**, *103*, 10186–10191.

[28] F. Cacho-Bailo, B. Seoane, C. Téllez, J. Coronas, ZIF-8 continuous membrane on porous polysulfone for hydrogen separation, *J. Membr. Sci.* **2014**, *464*, 119–126.

[29] V. Nafisi, M.B. Hägg, Development of dual layer of ZIF-8/PEBAX-2533 mixed matrix membrane for CO_2 capture, *J. Membr. Sci.* **2014**, *459*, 244–255.

[30] H. Bux, C. Chmelik, R. Krishna, J. Caro, Ethene/ethane separation by the MOF membrane

ZIF-8: Molecular correlation of permeation, adsorption, diffusion, *J. Membr. Sci.* **2011**, *369*, 284–289.

[31] K. Tao, C. Kong, L. Chen, High performance ZIF-8 molecular sieve membrane on hollow ceramic fiber via crystallizing-rubbing seed deposition, *Chem. Eng. J.* **2013**, *220*, 1–5.

[32] C. Zhang, Y. Dai, J.R. Johnson, O. Karvan, W.J. Koros, High performance ZIF-8/6FDA-DAM mixed matrix membrane for propylene/propane separations, *J. Membr. Sci.* **2012**, *389*, 34–42.

[33] M.J.C. Ordoñez, K.J. Balkus, Jr., J.P. Ferraris, I.H. Musselman, Molecular sieving realized with ZIF-8/Matrimid mixed-matrix membranes, *J. Membr. Sci.* **2010**, *361*, 28–37.

[34] N.P. Panapitiya, S.N. Wijenayake, Y. Huang, D. Bushdiecker, D. Nguyen, C. Ratanawanate, G.J. Kalaw, C.J. Gilpin, I.H. Musselman, K.J. Balkus, Jr., J.P. Ferraris, Stabilization of immiscible polymer blends using structure directing metal organic frameworks (MOFs), *Polymer* **2014**, *55*, 2028–2034.

[35] J. Cravillon, S. Münzer, S.J. Lohmeier, A. Feldhoff, K. Huber, M. Wiebcke, Rapid room-temperature synthesis and characterization of nanocrystals of a prototypical zeolitic imidazolate framework, *Chem. Mater.* **2009**, *21*, 1410–1412.

[36] T.L. Grubb, V.L. Ulery, T.J. Smith, G.L. Tullos, H. Yagci, L.J. Mathias, M. Langsam, Highly soluble polyimides from sterically hindered diamines, *Polymer* **1999**, *40*, 4279–4288.

[37] M. Niwa, S. Nagaoka, H. Kawakami, Preparation of novel fluorinated block copolyimide membranes for gas separation, *J. Appl. Polym. Sci.* **2006**, *100*, 2436–2442.

[38] E. V. Perez, K.J. Balkus, Jr., J.P. Ferraris, I.H. Musselman, Mixed-matrix membranes containing MOF-5 for gas separations, *J. Membr. Sci.* **2009**, *328*, 165–173.

[39] H. Hayashi, A.P. Côté, H. Furukawa, M. O'Keeffe, O.M. Yaghi, Zeolite A imidazolate frameworks., *Nat. Mater.* **2007**, *6*, 501–506.

[40] J. Cravillon, C.A. Schröder, H. Bux, A. Rothkirch, J. Caro, M. Wiebcke, Formate modulated solvothermal synthesis of ZIF-8 investigated using time-resolved in situ X-ray diffraction and scanning electron microscopy, *CrystEngComm*. **2012**, *14*, 492–498.

[41] C. Harrats, S. Thomas, G. Groeninckx, *Micro- and Nanostructured Multiphase Polymer Blend Systems: Phase Morphology and Interfaces*, CRC Press LLC, Boca Raton FL, **2006**.

[42] C. Park, W.H. Jo, H.C. Park, Y.S. Kang, Morphological effect of dispersed phase on gas permeation properties through heterophase polymer membrane: theoretical and experimental approaches, *Polymer* **2000**, *41*, 1765–1771.

[43] X.-G. Li, I. Kresse, J. Springer, J. Nissen, Y.-L. Yang, Morphology and gas permselectivity of blend membranes of polyvinylpyridine with ethylcellulose, *Polymer* **2001**, *42*, 6859–6869.

[44] M.H. Kim, J.H. Kim, C.K. Kim, Y.S. Kang, H.C. Park, J.O. Won, Control of phase

separation behavior of PC/PMMA blends and their application to the gas separation membranes, *Polymer* **1999**, 2950–2959.

[45] N. Panapitiya, S. Wijenayake, D. Nguyen, C. Karunaweera, Y. Huang, K. Balkus, Jr., I. Musselman, J. Ferraris, Compatibilized immiscible polymer blends for gas separations, *Materials (Basel)* **2016**, *9*, 643.

[46] L.M. Robeson, The upper bound revisited, *J. Membr. Sci.* **2008**, *320*, 390–400.

[47] W.J. Koros, G.K. Fleming, Membrane-based gas separation, *J. Membr. Sci.* **1993**, *83*, 1–80.

BIOGRAPHICAL SKETCH

Yu (Tony) Huang was born in Nanning, China. He completed his schoolwork at No. 2 High School in Nanning, China in 2000. Tony attended Lewis-Clark State College in Lewiston, Idaho in 2003, and received a Bachelor of Science degree with a major in Chemistry in May 2007. During the following two years, he was employed as a quality control analyst in a plywood company in Nanning, China. In August 2010, he entered the Graduate School of The University of Texas at Dallas.

CURRICULUM VITAE

Yu (Tony) Huang
Department of Chemistry and Biochemistry
The University of Texas at Dallas
800 West Campbell Road, Mail Station 26
Richardson, TX 75080-3021
(972) 883-2901

Educational History

Ph.D.	Chemistry, Department of Chemistry and Biochemistry, The University of Texas at Dallas, Richardson, TX	2016
B.S.	Chemistry, Department of Chemistry Lewis-Clark State College, Lewiston, ID	2007

Professional Experience

◊ Lecturer I — Fall 2016

◊ Research Assistant
Department of Chemistry and Biochemistry, The University of Texas at Dallas, Richardson, Texas — 2011-2016
Supervisor: Professor Inga H. Musselman

◊ Analytical Chemist
Nanning Heng County Lvchen Wood Industry Co., Ltd, China — 2008-2010

Absolute Finish Inc., Lewiston, Idaho — 2007-2008

Teaching Experience

◊ **General Chemistry Lab (Teaching Assistant)** — 2010-2011
Department of Chemistry and Biochemistry,
The University of Texas at Dallas, Richardson, Texas

◊ **Organic Chemistry Lab (Teaching Assistant)** — 2011
Department of Chemistry and Biochemistry,
The University of Texas at Dallas, Richardson, Texas

◊ **Instrumental Analysis Lab (Teaching Assistant)** — 2011-2014
Department of Chemistry and Biochemistry,
The University of Texas at Dallas, Richardson, Texas

◊ **UTD/Plano ISD Summer Program (Mentor)** 2014
Department of Chemistry and Biochemistry,
The University of Texas at Dallas, Richardson, Texas

◊ **NanoExpolrer program (Mentor)** 2015
Department of Chemistry and Biochemistry,
The University of Texas at Dallas, Richardson, Texas

Research Interests

- Gas storage and separations
- Membrane fabrication and characterization
- Instrument construction
- Inorganic nanoparticles synthesis

Achievements in Original Achievement, Investigation, and Research

- Nimanka P. Panapitiya, Sumudu N. Wijenayake, Yu Huang, David Bushdiecker, Do Nguyen, Chalita Ratanawanate, Grace J. Kalaw, Christopher J. Gilpin, Inga H. Musselman, Kenneth J. Balkus, Jr., John P. Ferraris, "Stabilization of immiscible polymer blends using structure directing metal organic frameworks (MOFs)," *Polymer*, Vol. 55 (2014) 2028–2034.

- Sumudu N. Wijenayake, Nimanka P. Panapitiya, Cindy N. Nguyen, Yu Huang, Kenneth J. Balkus, Jr., Inga H. Musselman, John P. Ferraris, "Composite membranes with a highly selective polymer skin for hydrogen separation," *Sep Purif Technol*, Vol. 135 (2014) 190–198.

- Nimanka P. Panapitiya, Sumudu N. Wijenayake, Do D. Nguyen, Yu Huang, Inga H. Musselman, Kenneth J. Balkus, Jr., John P. Ferraris, "Gas separation membranes derived from high-performance immiscible polymer blends compatibilized with small molecules," *ACS Appl. Mater. Interfaces*, Vol. 7 (2015), 18618–18627.

- Nimanka P. Panapitiya, Sumudu N. Wijenayake, Do D. Nguyen, Chamaal Karunaweera, Yu Huang, Inga H. Musselman, Kenneth J. Balkus, Jr., John P. Ferraris, "Compatibilized immiscible polymer blends for gas separations," *Materials*, Vol 9 (2016), 643.

Papers in preparation

- High pressure, high temperature H_2/CO_2 separation using polybenzimidazole/6FDA-DAM immiscible blend membranes

- High pressure, high temperature permeameter for gas permeation measurement